1.0

4.5 2.8 2.5

5.0

6.3 3.2 2.2

1.1 3.6

4.0 2.0

1.8

1.25 1.4 1.6

MICROCOPY RESOLUTION TEST CHART
NATIONAL BUREAU OF STANDARDS-1963-A

AIR FORCE INSTITUTE OF TECHNOLOGY

AIR UNIVERSITY
UNITED STATES AIR FORCE
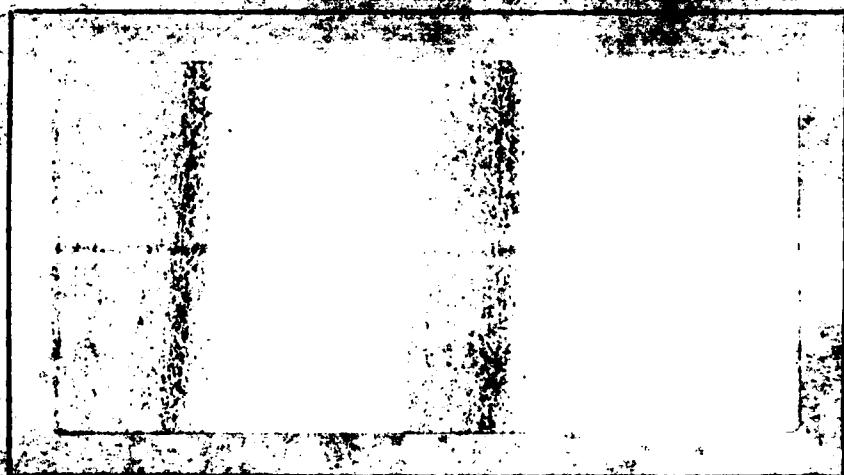
SCHOOL OF ENGINEERING

PATTERSON AIR FORCE BASE, OHIO

83   02   022 161

AFIT/GAE/AA/82D-22

COMPUTER PRƏDICTION OF STORE AERODYNAMIC

LOADING DURING SEPARATION

THESIS

Arthur C. Powell

AFIT/GAE/AA/82D-22   Capt   USAF

FEB 2 2 1983

A

Approved for public release; distribution unlimited

AFIT/GAE/AA/82D-22

COMPUTER PREDICTION OF STORE AERODYNAMIC

LOADING DURING SEPARATION

THESIS

Presented to the Faculty of the School of Engineering

of the Air Force Institute of Technology

Air University

in Partial Fulfillment of the

Requirements for the Degree of

Master of Science

by

Arthur C. Powell, B.S.

Capt   USAF

Graduate Aeronautical Engineering

December 1982

Approved for public release; distribution unlimited.

Preface

The objective of this study is to establish the capability of the Nielsen store separation and trajectory program to predict off-body store loadings. The Nielsen program was developed in the early 1970's and was designed specifically to handle the store trajectory problem.

In order to establish the program capabilities, a computer model of an advanced fighter design was generated. The specific model was chosen because it had been extensively studied in a wind tunnel and aerodynamic data were available for comparison.

A secondary objective is to consolidate, as much as possible, the theory required to understand the program and provide the aircraft computer model for future study. Theory notation was a problem because the theory was developed in three reports with the same symbols used for different quantities in different reports. For this reason a notation section is included for those paragraphs where clarification is required.

The computer program is not included in this report; however, the basic program, with no changes, was used for the analysis.

I would like to express my sincere gratitude for the assistance I received during the course of this study. My primary independent study advisor, Major Michael L. Smith, AFIT/ENY, provided the advice and guidance which allowed me to complete the work. I owe a special debt of gratitude to Mr. Richard Dyer, AFWAL/FIMM, who was the sponsor of the study. I also owe special thanks to Mr. Bart Heath, AFWAL/FIGC, who provided technical guidance on the use of the computer program.

Contents

List of Figures

List of Tables

List of Symbols

a	local body radius
a_n	polar harmonic singularity coefficient
C_m	store pitching-moment coefficient, pitching moment/($q_{\infty S} S_R \ell_R$), positive nose up and taken about store midpoint
C_n	store yawing-moment coefficient, yawing moment/($q_{\infty S} S_R \ell_R$), positive nose to the right and taken about store midpoint
C_N	store normal-force coefficient, normal force/$q_{\infty S} S_R$), positive up
C_Y	store side-force coefficient, side force/($q_{\infty S} S_R$), positive to the right
d	maximum store diameter
F_{iu}, F_{iv}, F_{iw}	backwash, sidewash, and downwash influence coefficients for a wing image vortex; positive in the x_w, y_w, z_w directions
F_u, F_v, F_w	backwash, sidewash, and downwash influence coefficients for a wing or pylon vortex; positive in the x_w, y_w, z_w directions
ℓ	body length
ℓ_R	reference length, taken equal to d
ℓ	store length
m	body contour slope
M_∞	free-stream Mach number
$q_{\infty S}$	ejected store free-stream dynamic pressure
$\vec{q}_\infty$	perturbation velocity vector
r	radial distance in crossflow plane
s_{iv}	semispan of a wing image vortex

$x_{iv,w}, y_{iv,w}, z_{iv,w}$	coordinates of bound-leg midspan of a wing image vortex in x_w, y_w, z_w wing coordinate system in incompressible space
x_s, y_s, z_s	coordinate system in compressible space fixed in separated store with origin at store nose, see figure 10
$x_{s,m}$	x_s location of store moment center
x_w, y_w, z_w	wing coordinate system in incompressible space
x_B, y_B, z_B	fuselage coordinate system, see figures 1 and 2
α	fuselage and store angle of attack
α_ℓ	local angle of attack due to wing twist and camber
Γ	strength of a horseshoe vortex
θ	polar angle, see figure 2
$\vec{\nu}, \vec{\tau}$	vectors normal to and tangential to the crossflow plane contour, see figure 2
ξ, η, ζ	axial, lateral, and vertical displacements, respectively, of the store center of gravity relative to the carriage position on the pylon in the fuselage coordinate system; positive forward, to the right, and downward, respectively
ϕ	angle defined by equation (26)
ϕ_c	complete potential for a body defined by equation (3)
ϕ_e	potential associated with equivalent body of revolution
ϕ_{iv}	dihedral angle of image horseshoe vortex
ϕ_ν	dihedral angle of the νth vortex on the exposed wing panel
ϕ_2	crossflow plane potential associated with the contour of a general body

S	local body cross-sectional area
$S'(x)$	rate of change of body cross-sectional area
S_R	reference area, $\pi d^2/4$
t	time, seconds
u, v, w	incompressible perturbation velocities in x,y,z directions of figure 1; compressible perturbation velocities in x,y,z directions of figure 1
u_i, v_i, w_i	incompressible externally induced perturbation velocities
u_r, u_θ	incompressible perturbation velocities in polar coordinates and associated with ϕ_2
u_x, u_ν, u_τ	incompressible perturbation velocities in x,ν,τ coordinate system
U_x, U_ν, U_τ	incompressible free-stream velocity components in x,ν,τ coordinate system
v_r	incompressible radial velocity in y-z plane of figure 1
V, W	incompressible free-stream velocity components in y and z directions
V_D	velocity inside engine inlet
V_s, W_s	compressible velocities in store body coordinate system, see figure 10
V_∞	free-stream velocity
$\vec{V}_\infty$	free-stream velocity vector in incompressible space
$V_{\infty S}$	separated store free-stream velocity
x, y, z	coordinate system fixed in nose of axisymmetric body in incompressible space, see figure 1; coordinate system fixed in nose of general noncircular body in incompressible space, see figure 2; coordinate system with origin at midspan of the bound leg of a horseshoe vortex in incompressible space

List of Symbols (Cont'd.)

ψ	angle defined by equation (38)
ψ_{iv}	sweep angle of the bound leg of an image horseshoe vortex
ψ_v	sweep angle of the bound leg of a horseshoe vortex on the exposed wing panel
$\Delta\Psi, \Delta\Theta$	changes in yaw and pitch angles, respectively, of store from time = 0 values; positive nose to the right and nose up

Abstract

An advanced fighter design is modeled using the Nielsen store separation and trajectory program with the non-circular fuselage cross section option. The theory required to build the computer model is consolidated for better understanding, with the major points referenced to the appropriate report. The details of the process to generate the computer model are described. The computer model of the aircraft and ogive store is used to predict store forces and moments which are compared with wind tunnel results on the same configuration. The prediction accuracy, at Mach number 0.6, at a store position of three store diameters away from the aircraft, is within ten percent of experiment in the region of interest, which is the area under that portion of the fuselage occupied by the wing.

I. INTRODUCTION

The analysis of what happens to a weapon when it is released from an aircraft is a major concern in weapons development. The weapon must separate from the aircraft without structural interference and it must then follow a predictable path to impact. The prediction of the separation and the initial weapon path is the problem to be addressed. The solution to the problem requires that the forces on the weapon be known. These forces, and the equations of motion predict the path the weapon will follow.

A computer prediction method was developed by Nielsen Engineering and Research, Inc., under contract to the United States Air Force. The work was done during the period 1968 to 1972. The final result was a method for predicting the six degree-of-freedom store separation trajectory at speeds up to the critical speed.

The procedure was developed in three stages. Stage one was a three-degree-of-freedom theory (Ref 1). Stage two was a six-degree-of-freedom program which modified the three-degree-of-freedom program (Ref 2). This second stage included a users' manual for the computer program (Ref 3). The final stage extended the original six-degree-of-freedom approach to handle more general configurations (Ref 4,5).

The final program can model a wing with twist and camber. The wing may have leading and trailing edge sweep, and dihedral. These parameters may vary along the span. Pylons and racks can be modeled

1

although the connectors between store and rack are not modeled. Up to ten stores may be included, either in multiple ejector rack (MER) or triple ejector rack (TER) configuration. The store is modeled as a body of revolution with planar or cruciform empennage. The store is non-powered, but may be given an initial velocity and orientation. The fuselage cross section can be noncircular, but it must have a vertical plane of symmetry. Air inlets may be included and the ratio of the velocity in the inlet to the free stream velocity can be specified. The aircraft must be operating at constant velocity with zero yaw angle and constant angle of attack. The computer program uses a constant, preselected, atmospheric density. This does not restrict the flight path to horizontal only, but the density does not change.

The objective of this report is to validate the Nielsen program by applying it to an advanced fighter design. The store to be separated is a generic store with known characteristics. The fighter and store have been aerodynamically tested in a wind tunnel and these data are used to compare to the computer results.

In the process of building the computer model it was noted that the theory for the model was contained in three different reports. This made the theory very difficult to follow. As a consequence, the theory has been consolidated with each section referenced to the original report. Only those sections essential to the construction of the computer model are included in detail.

The details of the aircraft, store and wind tunnel test conditions are given in Appendix A. For simplicity and data matching, only the aircraft and two stores were modeled. No pylons or racks were included. The aircraft is an advanced fighter design with a non-circular fuselage cross section including flow-through engine inlets. The stores were identical. The store body was a circular cylinder with an ogive nose and cruciform empennage. The computer models were used to generate force, moment, position, and relative velocity data on one store which was placed at various positions under the fuselage. The trajectory option was not used.

At Mach numbers 0.6 and 0.9, one store was placed approximately three store diameters below the fuselage centerline and moved from a position under the fuselage nose to the tail. At Mach number 0.6, the store was placed three feet to the right of centerline and moved from nose to tail. The final position was approximately one store diameter below the centerline. For this case the Mach number was 0.6 and the position was varied from 37.22 feet behind the aircraft nose to the tail. One store remained on the centerline and flush with the fuse-lage.

The data obtained were compared with wind tunnel values on the same configuration. The primary region of interest for store position was the area under the fuselage in the range occupied by the wing. At Mach number 0.6 with the store positioned three diameters below the

fuselage centerline, the predicted results were within ten percent of experimental. Accuracy decreased with lateral movement under the fuselage. The prediction error was 20 percent or greater when the store was moved to a position one store diameter below the fuselage centerline.

II. THEORY-NIELSEN PROGRAM

The three principal tasks in the prediction of a store trajectory are: first, the determination of the nonuniform flow field in the neighborhood of the ejected store; second, the determination of the forces and moments on the store in this flow field; and third, the integration of the equations of motion to determine the store trajectory (Ref 1:1).

Compressibility Correction (Ref 1:4-5)

Nomenclature:

ϕ - potential function in compressible space

ϕ_{xx}, ϕ_{yy}, ϕ_{zz} - $\partial^2\phi/\partial x^2$, $\partial^2\phi/\partial y^2$, $\partial^2\phi/\partial z^2$

x,y,z - coordinate system in compressible space

x',y',z' - coordinate system in incompressible space

It is assumed that the flow field for compressible subcritical flow is governed by a perturbation potential ϕ which satisfies

$$(1-M_\infty^2)\phi_{xx} + \phi_{yy} + \phi_{zz} = 0 \tag{1}$$

The flow field represents a wing-fuselage combination moving at M_∞ with a fuselage angle of attack of α_B. The x, y, z coordinate system is fixed in the fuselage, see figure 1.

The wing fuselage combination is transformed to an equivalent incompressible one. The incompressible flow field for the equivalent

5

body is determined, and then transformed back to the compressible space.

The following transformation is used from the compressible space (x,y,z) to the incompressible space (x',y',z'):

$$x' = \frac{x}{\sqrt{1-M_\infty^2}} \ , \ y'=y \ , \ z'=z \tag{2}$$

Mathematical Models for Determining Flow Field

All of the models described are for the equivalent incompressible configuration, although the primed notation has been dropped. This configuration is determined by the program from the input of the actual aircraft dimensions (Ref 4:2).

Fuselage Potentials (Ref 4:4) The model of bodies with non-circular cross section is based on the equivalence rule which states that the following conditions hold for a general slender body (Ref 6:107-110):

a. Far away from a general slender body, the flow becomes axisymmetric and equal to the flow around the equivalent body of revolution.

b. Near the general slender body, the flow differs from that around the equivalent body of revolution by a two-dimensional constant density crossflow part that makes the tangency condition at the actual body surface be satisfied.

The outer axisymmetric flow is given by the potential ϕ_e which is associated with an equivalent body of revolution. This equivalent body of revolution is axisymmetric, with the same cross sectional area distribution along its longitudinal axis as the actual body.

The inner flow is represented by a two-dimensional potential ϕ_2 which in the limit (outer) becomes $[U_x(x)/2\pi V_\infty]S'(x)\ln r$. The total velocity in the axial direction x of the body is $U_x(x)$. The rate of change of the cross sectional area S with x is $S'(x)$. The radial distance from the body centerline is r, see figure 2.

A solution valid for the entire flow field is given by:

$$\phi_c(r,\theta) = \phi_e(r) + \phi_2(r,\theta) - \frac{U_x(x)}{2\pi V_\infty} S'(x) \ln r \tag{3}$$

The potential ϕ_e and ϕ_2 are determined independently. The potential ϕ_e of the equivalent body is determined from flow modeling of a body of revolution at zero angle of attack with the same cross section area distribution as the actual body. The inner potential ϕ_2 is determined in the crossflow plane and satisfies the flow tangency condition on the actual body contour.

Outer Potential - ϕ_e (Ref 1:9-12)

Nomenclature:

ℓ_R - body length

Q_k - strength of kth point source

Q_k^* - $Q_k/4\pi \ell_R^2 V_\infty$

r^* - r/ℓ_R

U - axial velocity

U^* - U/V_∞

V_r	radial velocity
V_r^*	V_r/V_∞
x^*	x/ℓ_R
x_k	x location of kth point source
x_k^*	x_k/ℓ_R
B_j	body slope at the jth point on the surface
ψ	stream function
ψ^*	$\psi/\ell_R^2 V$

The potential ϕ_e itself is not calculated, although the perturbation velocity field can be determined by knowing the strengths and distribution of three-dimensional point sources along the body longitudinal axis.

The stream function ψ and the axial and radial velocity components, U and V_r, respectively, are given by (Ref 8):

$$\psi^*(x^*,r^*) = \frac{1}{2}r^{*2} - \sum_{k=1}^{N} Q_k^* \frac{1 + (x^*-x^*_k)}{[(x^*-x_k^*)^2 + r^2]^{\frac{1}{2}}} \tag{4}$$

$$U^*(x^*,r^*) = \frac{1}{r^*}\frac{d\psi^*}{dr^*} = 1 + \sum_{k=1}^{N} Q_k^* \frac{(x^* - x_k^*)}{[(x^*-x_k^*)^2 + r^{*2}]^{3/2}} \tag{5}$$

$$V_r^*(x^*,r^*) = -\frac{1}{r^*}\frac{d\psi^*}{dx^*} \sum_{k=1}^{N} \frac{Q_k^* r^*}{[(x^*-x_k^*)^2 + r^{*2}]^{3/2}} \tag{6}$$

8

ℓ_R is a reference length which will be taken as the length of the body (figure 1). U and V_r are due jointly to a free stream velocity V_∞ aligned with the body axis, and a series of N point sources distributed along the body axis.

The quantities Q_k^* and x_k^* are the source strength and location, respectively, of the kth point source and the point (x^*, r^*) designates the field point in cylindrical coordinates.

The flow field about the axisymmetric body is obtained by imposing three conditions on equations (5) and (6). These velocity equations are used to calculate the source strengths rather than the streamline equation because they were found to give a better shape representation. This is due to the fact that they require both body ordinates and surface slopes for their solution.

The first condition requires the flow directions at (N-2) points (x_j^*, r_j^*), $j=1,\ldots,(N-2)$, be specified by angles β_j with respect to the positive x^*-axis:

$$\tan \beta_j = \frac{V_r^*(x_j^*, z_j^*)}{U^*(x_j^*, z_j^*)} \text{ for } j=1,\ldots,(N-2) \tag{7}$$

The locations (x_j^*, r_j^*) where the flow angles β_j are specified lie on the surface of the axisymmetric body being represented and the values of $\tan \beta_j$ correspond to the local body surface slopes $dr^*(x_j^*, r_j^*)/dx^*$.

Writing equation (7) in terms of equation (5) and (6) and rearranging them gives a set of linear algebraic equations in Q_k^*'s.

$$\tan \beta_j = \sum_{k=1}^{N} Q_k^* \frac{r_j^* - \tan \beta_j (x_j^* - x_k^*)}{[(x_j^* - x_k^*)^2 + r_j^{*2}]^{3/2}} \tag{8}$$

The second condition is that the sum of all the source strengths be zero.

$$\sum_{k=1}^{N} Q_k^* = 0 \tag{9}$$

This insures that the surface described by $\psi^*(x^*, r^*) = 0$ will be a closed surface.

The third condition is the existence of a stagnation point at the body nose. $U^* = 0$ at $x^* = r^* = 0$. Substituting this into equation (5), the third condition becomes

$$\sum_{k=1}^{N} \frac{Q_k^*}{x_k^*} = 1 \tag{10}$$

Since the sources are distributed along the positive x^*-axis only, the forward tip of the body is positioned at the origin and the $\psi^* = 0$ surface is the body surface.

When the N source positions, x_k^* are selected, equations (8), (9), and (10) comprise a set of N linear equations in N unknown Q_k^*. Once Q_k^*'s are solved for, equations (5) and (6) can be used to determine the perturbation velocities at any point in the flow field around the body.

<u>Inner Potential - ϕ_2</u> (Ref 4:4-18) The inner potential ϕ_2 is composed of higher order singularities given by polar harmonics and a two-dimensional source term:

$$\phi_2(r,\theta) = \sum_{n=1}^{MH} \frac{a_n \cos n\theta}{r^n(\theta)} + \frac{U_x(x)}{2\pi V_\infty} S'(x) \ln r \qquad (11)$$

where MH is the number of polar harmonics. This assumes flow symmetry about the vertical x-z plane. Side slip is not considered. Two-dimensional polar harmonics are described in greater detail (Ref 7: 40-48, 55-59).

Polar harmonic solutions are obtained at a number of crossflow plane stations along the body longitudinal, x, axis. The x range is the range over which the local flow needs to be calculated. At each crossflow plane station, a number of control points are distributed at equal angular spacings in θ on the body contour over the range, $\theta=0°$ to $\theta=180°$, see figure 2.

The flow tangency condition is applied at the control points resulting in a finite set of simultaneous equations in terms of the unknown polar harmonic coefficients.

To apply the flow tangency boundary condition a coordinate system is set up at each control point, figure 2. The system is set up such that ν is in the direction normal to the contour and τ is tangential to the contour. Figure 2 shows unit vectors associated with those directions. It is assumed (Ref 6) that the shape of the body surface

11

can be expressed as:

$$F(x, \nu, \tau) = 0 \qquad -\ell \leq x \leq 0 \qquad (12)$$

where ℓ is the body length. The unit vector normal to the body surface, not the contour, at the point is given as:

$$\bar{e}_n = \frac{\text{grad } F}{|\text{grad } F|} \qquad (13)$$

where

$$\text{grad } F = \frac{\partial F}{\partial x} \bar{e}_x + \frac{\partial F}{\partial \nu} \bar{e}_\nu + \frac{\partial F}{\partial \tau} \bar{e}_\tau \qquad (14)$$

Let the free-stream velocity, which does not have to be uniform, and the perturbation velocity vector be denoted $\bar{V}_\infty = \bar{V}_\infty(x, \nu, \tau)$ and $\bar{q}_\infty = \bar{q}_\infty(x, \nu, \tau)$, respectively.

The flow tangency boundary condition can now be written in the (x, ν, τ) system

$$[\bar{V}_\infty(x, \nu, \tau) + \bar{q}_\infty(x, \nu, \tau)] \cdot \bar{e}_n = 0 \qquad (15)$$

Expanding $\bar{V}_\infty$, $\bar{q}_\infty$ in terms of their components in the x, ν, and τ directions results in

$$\bar{V}_\infty(x, \nu, \tau) + \bar{q}_\infty(x, \nu, \tau) = (U_x + u_x)\bar{e}_x + (U_\nu + u_\nu)\bar{e}_\nu$$
$$+ (U_\tau + u_\tau)\bar{e}_\tau \qquad (16)$$

Substituting equations (13), (14), and (16) into the boundary equation (15) gives

$$(U_x + u_x) \frac{\partial F}{\partial x} + (U_\nu + u_\nu) \frac{\partial F}{\partial \nu} + (U_\tau + u_\tau) \frac{\partial F}{\partial \tau} = 0 \qquad (17)$$

12

This equation represents the nonlinear flow tangency condition for any body situated in a non-uniform flow.

Equation (17) will now be simplified with no loss of generality. The unit vectors $\bar{e}_n$ and $\bar{e}_\nu$ at a point on the body surface lie in the same longitudinal plane, see figure 2. Since $\bar{e}_\nu$ is perpendicular by definition to $\bar{e}_\tau$, then $\bar{e}_n$ is also at a right angle to $\bar{e}_\tau$. Therefore:

$$\bar{e}_n \cdot \bar{e}_\tau = 0 \tag{18}$$

Using equations (13) and (14), equation (18) becomes:

$$\left(\frac{\partial F}{\partial x}\,\bar{e}_x + \frac{\partial F}{\partial \nu}\,\bar{e} + \frac{\partial F}{\partial \tau} + \bar{e}_\tau\right)\cdot\bar{e}_\tau = 0 \tag{19}$$

Since $F(x,\nu,\tau)$ is a constant and equal to zero on the body surface, it does not vary with respect to the τ direction

$$\frac{\partial F}{\partial \tau} = 0 \tag{20}$$

Taking the differential of $F(x,\nu,\tau)=0$

$$dF(x,\nu,\tau) = \frac{\partial F}{\partial x}\,dx + \frac{\partial F}{\partial \nu}\,d\nu + \frac{\partial F}{\partial \tau}\,d\tau = 0 \tag{21}$$

With equation (20) this becomes:

$$\frac{\partial F}{\partial x} = -\frac{\partial F}{\partial \nu}\,\frac{d\nu}{dx} \tag{22}$$

Substituting equations (20) and (22) into (17) gives the nonlinear flow tangency condition that must be satisfied at points on the surface of a general body.

13

$$[U_x(x) + u_x(x,\nu,\tau)] \frac{d\nu}{dx} = U_\nu(x) + u(x,\nu,\tau) \qquad (23)$$

The problem is to determine $\frac{d\nu}{dx}$ and then write U_ν and u_ν in terms of y and z components along the θ and r directions.

An expression for dν/dx, the streamwise body slope will be derived in accordance with the principles of Ref 6, see figure 3. The body radius r and its derivatives with respect to θ must be single valued and continuous for a given value of θ.

Vector $\bar{\nu}$ is perpendicular to and $\bar{\tau}$ tangential to the body contour at x. Let Δν denote the change measured in the direction of $\bar{\nu}$ of the location of the contour when going in a longitudinal plane from the cross section at x to the one at x-Δx, see figure 2 for definition of x direction. The slope of the body in the longitudinal plane is

$$\frac{d\nu(\theta)}{dx} = \lim_{\Delta x \to 0} \frac{\Delta\nu(\theta)}{\Delta x} \qquad (24)$$

This body slope is approximated by

$$\frac{d\nu(\theta)}{dx} \cong \frac{\Delta r(\theta)\cos}{\Delta x} \qquad (25)$$

$$\Delta r(\theta) = r_{x-\Delta x}(\theta) - r_x(\theta)$$

From figure 3, angle φ between the normal $\bar{\nu}$ and the radial direction r can be expressed in terms of the contour slope m and the polar angle θ:

$$\phi = m - \theta - \frac{\pi}{2} \qquad (26)$$

14

The body contour shape $m(0 \leq m \leq 2\pi)$ is found from

$$m = \lim_{\Delta\theta \to 0} \left[\tan^{-1} \frac{\frac{\Delta y}{\Delta\theta}}{\frac{\Delta z}{\Delta\theta}} \right] = \tan^{-1} \left[\frac{\frac{dr(\theta)}{d\theta} \sin\theta + r(\theta)\cos\theta}{\frac{dr(\theta)}{d\theta} \cos\theta - r(\theta)\sin\theta} \right] \quad (27)$$

The velocities $U_\nu(x)$, $u_\nu(x,\nu,\tau)$, equation (23) will now be written in a more useful form in terms of the free-stream components $V(x)$ and $W(x)$, and the radial and tangential perturbation velocities $u_r(r,\theta)$ and $u_\theta(r,\theta)$.

$$U_\nu(x,r,\theta) = W(x) \cos \left(m - \frac{\pi}{2}\right) + V(x) \sin \left(m - \frac{\pi}{2}\right) \quad (28)$$

$W(x)$, $V(x)$ are the free-stream component contributions in the $\bar{\nu}$ directions, see figure 4.

$$u_\nu(r,\theta) = u_r(r,\theta)\cos\left[\theta - \left(m - \frac{\pi}{2}\right)\right] - u_\theta(r,\theta)\sin\left[\theta - \left(m - \frac{\pi}{2}\right)\right] \quad (29)$$

The inner potential ϕ_2 is the potential that satisfies the flow tangency condition on the actual body surface. This assumes that the effects of the other two terms in equation (3) cancel one another on the body surface. This condition holds true on the surface of the equivalent body and is satisfied approximately on the actual body surface. For the cases studied in Ref 4, the inclusion of the other two terms had a small effect (Ref 4:11). The effects of only the inner potential ϕ_2 will be considered in the boundary condition.

15

The perturbation velocities in equation (29) are related to the crossflow or inner potential ϕ_2 by:

$$\frac{u_r}{V_\infty}(r,\theta) = \frac{\partial \phi_2(r,\theta)}{\partial r}$$

$$\frac{u_\theta(r,\theta)}{V_\infty} = \frac{1}{r(\theta)} \frac{\partial \phi_2(r,\theta)}{\partial \theta} \tag{30}$$

Differentiation of equation (11) gives:

$$\frac{u_r}{V_\infty}(r,\theta) = \sum_{n=1}^{MH} \frac{na_n \cos_n \theta}{r^{n+1}(\theta)} + \frac{U_x(x)}{2\pi V_\infty} \frac{S'(x)}{r(\theta)} \tag{31}$$

$$\frac{u_\theta}{V_\infty}(r,\theta) = -\sum_{n=1}^{MH} \frac{na_n \sin_n \theta}{r^{n+1}(\theta)} \tag{32}$$

Substitute equations (31) and (32) into (29). Using this result and equation (28), the flow tangency condition given by equation (23) becomes:

$$\frac{U_x(x)}{V_\infty} \frac{d\nu(\theta)}{dx} = \frac{W(x)}{V_\infty}\cos\left(m - \frac{\pi}{2}\right) +$$

$$\left[\frac{U_x(x)}{2\pi V_\infty} \frac{S'(x)}{r(\theta)} - \sum_{n=1}^{MH} \frac{na_n \cos_n \theta}{r^{n+1}(\theta)}\right]\cos\left[\theta - \left(m - \frac{\pi}{2}\right)\right] \tag{33}$$

$$+ \sum_{n=1}^{MH} \frac{na_n \sin_n \theta}{r^{n+1}(\theta)} \sin\left[\theta - \left(m - \frac{\pi}{2}\right)\right]$$

The perturbation term $u_x(x,\nu,\tau)$ is omitted since it is small compared to $U_x(x)$. The rate of change with x of the body cross-sectional area $S'(x)$ can be written in terms of the equivalent body radius and thus the source term in equation (33) can be written

$$\frac{U_x(x)}{2\pi V_\infty} \frac{S'(x)}{r(\theta)} = \frac{U_x(x)}{2\pi V_\infty} \frac{1}{r(\theta)} \frac{d}{dx}(\pi R_{eq}^2) = \frac{U_x(x)}{V_\infty r(\theta)} R_{eq} \frac{dR_{eq}}{dx} \quad (34)$$

where R_{eq} is the radius of the equivalent axisymmetric body.

Equation (33) is rewritten by transposing and factoring terms and is applied at MC control points. The result is a set of MC flow tangency equations in MH unknown polar harmonic coefficients a_n

$$\sum_{n=1}^{MH} \left[\frac{na_n}{r^{n+1}(\theta_i)} \left\{ - \cos n\theta_i \cos\left[\theta_i - (m_i - \frac{\pi}{2})\right] \right. \right. \quad (35)$$

$$\left. \left. + \sin n\theta_i \sin\left[\theta_i - (m_i - \frac{\pi}{2})\right] \right\} \right] = \frac{U_x(x)}{V_\infty} \frac{d\nu(\theta_i)}{dx} - \frac{W(x)}{V_\infty} \cos(m_i - \frac{\pi}{2})$$

$$- \frac{U_x(x)}{2\pi V_\infty} \frac{S'(x)}{r(\theta_i)} \cos\left[\theta_i - (m_i - \frac{\pi}{2})\right]$$

$$i = 1,2,\ldots,MC \quad , \quad MC<MH$$

The problem now is to find the best possible values for a set of unknown $a_1, a_2, \ldots a_{MH}$ for a set of MC linear equations. Instead of the exact solution of MH=MC, a set of MC equations will be satisfied in the least-square sense. Minimize the quantity

17

$$E = \sum_{i=1}^{MC} \delta_i^{\,2} \qquad (36)$$

where $\delta_i^{\,2}$ represents equation (35). (Equation (35) [A]=[B], [A] - [B] = δ_i) Using the procedure (Ref 9:177-178) to minimize E by setting the partial derivatives equal to zero.

$$\frac{\partial E}{\partial a} \; , \; \frac{\partial E}{\partial a_2} \; , \; \ldots, \; \frac{\partial E}{\partial a_{MH}} \qquad (37)$$

and letting

$$\psi_i = \theta_i - m_i + \frac{\pi}{2} \qquad (38)$$

gives the result

$$\sum_{j=1}^{MH} \left[ja_i \sum_{i=1}^{MC} - \frac{\cos_j\theta_i\cos\psi_i + \sin_j\theta_i\sin\psi_i}{r^{j+1}(\theta_i)} \; \frac{n}{r^{n+1}(\theta_i)} \right. \qquad (39)$$

$$\left. (-\cos n\theta_i \cos\psi_i + \sin n\theta_i \sin\psi_i) \right]$$

$$= \sum_{i=1}^{MC} \left[\frac{U_x(x)}{V} \frac{d\nu(\theta_i)}{dx} - \frac{W(x)}{V} \cos(m_i - \frac{\pi}{2}) \right.$$

$$\left. - \frac{U_x(x)}{2\pi V_\infty} \frac{S'(x)}{r(\theta_i)} \cos\psi_i \right] \frac{n}{r^{n+1}(\theta_i)} \; (-\cos n\theta_i \cos\theta_i + \sin n\theta_i \sin\psi_i)$$

$$n=1,2,\ldots,MH$$

18

This represents a set of MH equations in inknowns a_1, a_2,....,a_{MH} which are to be solved simultaneously. The numbers MC and MH must be specified, and their determination requires judgement. The choosing of MC and MH will be discussed in detail in a later section, in which the input to the trajectory program is determined. The details are in (Ref 4:15-18).

Fuselage Mounted Air Inlets (Ref 4:18-20) Air inlets include the entire region from the mouth to the engine exhaust. The portion of the inlet that is a solid boundary is treated as part of ϕ_2, the inner fuselage potential.

In the section where the contour is not a solid boundary, figure 5, the body slope boundary condition used in the polar harmonic calculation is determined in a different way. The inlet is first considered to have a solid boundary. Control points are laid out on the range $0° \leq \theta \leq 180°$ of the crossflow contour. With each control point is associated a stream-wise body slope and upwash if angle of attack is considered. For the control points lying on the contour which is not a solid boundary the streamwise slopes θ_3 depend on the inlet to free-stream velocity ratio, designated V_D/V_∞. For $V_D/V_\infty = 1$, streamlines are parallel to the axis of the inlet, and for lesser values they point downward. To account for the change in streamline direction caused by blockage, the streamwise slopes calculated for the solid boundary to give

$$\theta_3 = (1 - \frac{V_D}{V_\infty}) \left. \frac{d\upsilon(\theta)}{dx} \right|_{solid\ boundary} \tag{40}$$

19

The term $\frac{d\nu(\theta)}{dx}$ in the flow tangency condition in equation (33) is replaced by θ_3. The rate of change of cross-sectional area $S'(x)$ must also be determined. For a $V_D/V_\infty = 0.5$ only one half of the inlet cross-sectional area is added to the fuselage. This adjusts the area distribution to reflect the inlet velocity ratio.

The outer potential θ_e is also adjusted to reflect the inlet velocity ratio. Its cross-sectional area distribution is modified by excluding a portion of the inlet area based on V_D/V_∞.

Wing-Pylon Flow Model (Ref 4:20-24) The fuselage is first represented by the potential flow methods previously described. The influence of the fuselage on the exposed wing panels is then determined. This is done by a vortex lattice with unknown vortex strengths which is laid out on the exposed wing panels and pylon. An image vortex lattice of the wing is constructed inside the fuselage. The wing-pylon loading is computed in terms of the vortex strengths with the inclusion of the fuselage influence on the exposed wing panels and pylon. The inclusion of the image vortices inside the fuselage approximately satisfies the condition of no flow through the surface and accounts for nearly all of the wing-fuselage interference. The crossflow plane theory for the imaging scheme is described in (Ref 4:20-23) and (Ref 9).

The vortex lattice is set up only on the portion of the wing outside the equivalent body of revolution for the noncircular fuselage. If the body of revolution radius varies over the region of influence of the wing, the maximum radius is used. Each horseshoe vortex that

is outside the body of revolution is then imaged inside. Velocities normal to the equivalent body are exactly zero in the wing chordal plane and are very small at all other locations on the body of revolution surface near the wing-body junction. For noncircular bodies the actual fuselage surface is generally close to the equivalent body surface so that to a good approximation the same conditions hold for the actual fuselage surface.

Vortex Lattice (Ref 4:20-25) Figure 6 shows the vortex lattice arrangement. The wing panels and pylons are divided into trapezoidal area elements. A horseshoe vortex is placed in each area element such that the spanwise bound leg lies along the element quarter chord and its trailing legs along the sides of the element. The trailing legs lie in the plane of the area element. The area elements in each chordwise row have equal chords and spans. In the spanwise direction, the area element width need not be equal to allow for closer spacing where large spanwise loading gradients exist. For a wing with breaks in sweep and/or dihedral, the area elements are arranged spanwise so that the breaks lie on the line formed by one of the sides of a chordwise row of elements. The wing-pylon junction is also made to lie along a common boundary between two adjacent rows of elements. On the wing, the flow tangency boundary condition is applied at a set of control points given by the midpoint of the 3/4 chord line of each area element located in the wing chordal plane. This is the planar approximation. On the

camberless pylon, the flow tangency condition is applied at control points situated in its chordal plane determined by halving the thickness envelope.

Figure 7 illustrates the boundary condition. The velocities normal to the wing consist of a component of the free-stream, perturbation velocities u, v, and w induced by the wing-pylon horseshoe vortex system, and perturbation velocities u_i, v_i, and w_i induced by the distribution of sources accounting for thickness superimposed on the vortex lattice. This thickness distribution will be well described in the next section. With M control points on the left wing panel and MP on the left pylon, the boundary condition on the left wing panel is given by

$$\sum_{n=1}^{M} \frac{\Gamma_n}{4\pi V_\infty} \left[(F_{w_{\nu,n}} + F_{iw_{\nu,n}})\cos\phi_\nu - (F_{v_{\nu,n}} + F_{iv_{\nu,n}})\sin\phi_\nu \right]$$

$$+ \sum_{n=M+1}^{M+MP} \frac{\Gamma_n}{4\pi V_\infty} (F_{w_{\nu,n}}\cos\phi_\nu - F_{v_{\nu,n}}\sin\phi_\nu) \tag{41}$$

$$= (\alpha + \alpha_{\ell_\nu})\cos\phi_\nu + \frac{v_{i,\nu}}{V_\infty}\sin\phi_\nu - (\frac{u_{i,\nu}}{V_\infty}\alpha_{\ell_\nu} + \frac{w_{i,\nu}}{V_\infty})\cos\phi_\nu$$

$$\nu = 1,2,\ldots,M$$

With the camberless pylon at zero incidence, the pylon boundary condition is written for MP control points

$$- \sum_{n=1}^{M} \frac{\Gamma_n}{4\pi V_\infty} \left(F_{v_{\nu,n}} + F_{iv_{\nu,n}} \right) - \sum_{n=M+1}^{M+MP} \frac{\Gamma_n}{4\pi V_\infty} F_{v_{\nu,n}} = \frac{v_{i,\nu}}{V_\infty} \tag{42}$$

$$\nu = M+1, \ M+2, \dots, M+MP$$

The wing angle of attack is α and α_ℓ is the local angle of attack due to wing camber and twist. Both angles are assumed small.

The right-hand side of equation (41) represents the free-stream component and the externally induced perturbation velocities normal to the wing chordal plane. The right-hand side of equation (42) consists only of an external perturbation velocity normal to the pylon chordal plane since there is no pylon incidence. The first summation on the left-hand side of the equations represents the perturbation velocities induced by vorticity on the left and right wing panels. The second summation represents the velocities induced by vorticity on the left and right pylons.

The functions F_u, F_v, F_w, are influence coefficients relating the perturbation velocity components, induced at some point by a horseshoe vortex, to its circulation, and the coordinates of the point relative to the vortex. Functions F_{iw} and F_{iv} relate the perturbation velocity components, induced at some point by a wing image horseshoe vortex, to its circulation and the coordinates of the point relative to the bound-leg midpoint of the image horseshoe vortex.

23

Using the Biot-Savart Law (Ref 11:156-160) the perturbation velocities induced at a point by a horseshoe and image horseshoe vortex are

$$u(x,y,z) = \frac{\Gamma}{4\pi V_\infty} [F_u(x,y,z,s,\psi,\phi) + F_{iu}(x,y,z,s_{iv},\psi_{iv},\phi_{iv})]$$

$$v(x,y,z) = \frac{\Gamma}{4\pi V_\infty} [F_v(x,y,z,s,\psi,\phi) + F_{iv}(x,y,z,s_{iv},\psi_{iv},\phi_{iv})]$$

$$w(x,y,z) = \frac{\Gamma}{4\pi V_\infty} [F_w(x,y,z,s,\psi,\phi) + F_{iw}(x,y,z,s_{iv},\psi_{iv},\phi_{iv})] \tag{43}$$

The influence functions depend only upon the coordinates (x,y,z) of the point at which the velocity is to be computed relative to the horseshoe vortex/image horseshoe vortex, the vortex span, s, the image vortex semispan s_{iu}, bound-leg sweep angle ψ, ψ_{iu}, and dihedral angle ϕ, ϕ_{iu}. The analytical expressions for the influence coefficients are given (Ref 2:12-14), and are subject to equation (13), (Ref 2:14) to account for the images of the horseshoe vortices laid out on the right wing panel.

Equations (41) and (42) represent a set of M + MP simultaneous equations in which the unknowns are the M + MP values of circulation strength Γ. These can be solved for a given angle of attack, twist or camber distribution, and a specified set of externally induced perturbation velocities u_i/V_∞, v_i/V_∞, and w_i/V_∞ caused by wing and pylon

24

thickness effects and from other aircraft components such as fuselage, rack and stores.

Thickness Model, Wing and Pylon (Ref 4:25) Wing and pylon thickness are accounted for by laying out thickness strips on the exposed panels. These strips are made of a three-dimensional source distribution.

The three-dimensional source method is similar to that used by Fernandes (Ref 12). Figure 8 and 9 show the coordinate and angle system for the wing and pylon.

The incompressible velocity potential due to a surface of sources, with chord $|X_b-X_a|$ and span $|Y_b-Y_a|$, on the wing may be obtained (Ref 6; Ref 13).

$$\frac{\Delta\phi}{V_\infty} = \frac{1}{2\pi} \int_{X_b}^{X_a} \int_{Y_b}^{Y_b} \frac{\tan \phi_t \, dX_1 \, dY_1}{[(X_1-X)^2+ (Y_1-Y)^2 + (Z_1-Z)^2]^{\frac{1}{2}}} \qquad (44)$$

for a surface located at Z_1=constant and local incidence angle ϕ_t measured from the positive x direction. The integration is performed over the span and chord of the surface and coordinates X, Y, Z locate the field point at which the velocity potential is determined. The integration is simplified and performed. This gives $\Delta\phi/V_\infty$ for one strip. This is differentiated to give the perturbation velocities due to one thickness strip. The same method is applied to the pylon (Ref 2: 15-20)

The perturbation velocities induced by the thickness envelopes of the wing and pylons are computed at the control points associated with the vortex lattice area elements on the wing-pylon combination. The velocities are obtained by adding the result of summing equations over all wing source strips to the result of summing equations over all pylon source strips. The final sums are then added to the set of externally induced perturbation velocities that appear in the flow tangency boundary condition. All interference effects induced by the wing on the pylon and vice-versa are accounted for and will be reflected in the resulting circulation strength distribution on the wing-pylon combination (Ref 2:15-20).

Store and Rack Flow Models (Ref 4:26) The store model uses the same technique as the axisymmetric fuselage model. The model accounts only for the volume distribution of the axisymmetric body, by a distribution of three-dimensional point sources along the longitudinal axis of the store.

The rack model is approximated by an axisymmetric body with three short pylons attached. The body is modeled by a source distribution while the short pylon is neglected (Ref 2:20).

Force and Moment Calculation (Ref 4:26-27)

Calculation of the forces and moments on a store requires specification of the nonuniform velocity field in which the store is immersed. This field, as seen with respect to the store, must be

26

determined at each point in time. The field includes the free-stream velocity, the perturbation velocities induced by the parent aircraft and the angular velocities due to the store's pitch, yaw, and roll motions. The velocity distribution along the body axis is required to calculate the body forces, and the velocity distribution over the tail fin surfaces is required for the empennage forces and moments.

Velocity Field (Ref 2:21-26)

Nomenclature:

p, q, r	- rotational velocities about x,y,z axes
r	- radial distance in y-z plane
u_s, v_s, w_s	- sum of all perturbation velocities
$U_{\infty s,x}, V_{\infty s,y}, W_{\infty s,z}$	- free-stream velocity components as seen by store, figure 10
U_s, V_s, W_s	- total velocities as seen by store
$x_{s,m}$	- x location of store moment center
ξ, η, ζ	- inertial coordinate system fixed in fuselage nose, positive forward along longitudinal axis, positive laterally to the right, and positive vertically downward

The x_s, y_s, z_s coordinate system to be used is shown in figure 10. The coordinate system is fixed in the store, with the origin at the store nose. The velocities U_s, V_s, W_s are total velocities as seen by a point on the store and each is composed of three components: free-stream, perturbation due to parent aircraft, and damping due to store motion.

$$U_S = U_{\infty S, x_S} + u_S$$

$$V_S = V_{\infty S, y_S} + v_S + r(x_S - x_{S,m})$$

$$W_S = W_{\infty S, z_S} + w_S + q(x_S - x_{S,m})$$

(45)

A reference system must now be established to represent the equations of motion used in the trajectory calculation. Figure 11 shows the ξ, η, ζ system which is an inertial system fixed in the aircraft which is in rectilinear flight at uniform velocity. The positive ξ axis is forward along the fuselage longitudinal axis, the η axis is positive to the right, and the ζ axis is positive downward. The origin is fixed in the nose of the aircraft.

In figure 11, the origins of the two systems have been drawn to coincide in order to show the angles used to determine the orientation of the store with respect to the inertial (ξ, η, ζ) axis. The Euler angles relate the two coordinate systems (Ref 14:100-103).

$$\begin{bmatrix} \xi \\ \eta \\ \zeta \end{bmatrix} = [A] \begin{bmatrix} x \\ y \\ z \end{bmatrix}$$

(46)

with A given by equation (28)(Ref 2:22).

For a parent aircraft moving at velocity V_∞, and flying at angle of attack α_f, the velocity of the inertial coordinate system relative

28

to a point in space is

$$\bar{V}_\infty = V_\infty \cos\alpha_f \bar{e}_\xi + \bar{V}_\infty \sin\alpha_f \bar{e}_\zeta \qquad (47)$$

The velocity of the store moment center relative to the moving inertial system is

$$\bar{V}_m = \dot{\xi}\bar{e}_\xi + \dot{\eta}\bar{e}_\eta + \dot{\zeta}\bar{e}_\zeta \qquad (48)$$

The velocity of the store relative to a point in space is

$$\bar{V}_{\infty S} = \bar{V}_\infty + \bar{V}_m \qquad (49)$$

Since the velocity components needed in equation (45) are with respect to a point fixed in the store and moving with the store, equation (49) becomes

$$\bar{V}_{\infty S} = -(V_\infty \cos\alpha_f + \dot{\xi})\bar{e}_\xi - \dot{\eta}\bar{e}_\eta \qquad (50)$$

$$- (V_\infty \sin\alpha_f + \dot{\zeta})\bar{e}_\zeta$$

The components in the x,y,z coordinate system of figure 10 are then

$$\begin{bmatrix} U_{\infty S,x} \\ V_{\infty S,y} \\ W_{\infty S,z} \end{bmatrix} = [A]^T \begin{bmatrix} -(V_\infty \cos\alpha_f + \dot{\xi}) \\ -\dot{\eta} \\ -(V_\infty \sin\alpha_f + \dot{\zeta}) \end{bmatrix} \qquad (51)$$

29

where

$$U_{\infty s, x_s} = -U_{\infty s, x} \tag{52}$$

$$V_{\infty s, y_s} = V_{\infty s, y}$$

$$W_{\infty s, z_s} = -W_{\infty s, z}$$

It is essential to remember that the second term in each equation, equation (45), is comprised of the perturbation velocities induced by the fuselage, wing, pylon, rack, and other stores. These velocities, determined in the previous sections, apply to the equivalent incompressible configuration. At each point in the trajectory the points at which the velocities are required must be located in the incompressible space. The velocities calculated using specific equations for each component are defined in the coordinate system of each component. Prior to transforming these back to the compressible space they must be summed in the fuselage coordinate system since this is the coordinate system in which the compressibility correction was applied (Ref 4:26-27). This is the (ξ, η, ζ) system of Figure 11.

Let $u_\xi', v_\eta', w_\zeta'$ be the sums in the ξ, η, ζ directions. From the section on compressibility correction

$$u_\xi = \frac{u_\xi'}{\beta^2} \ , \ v_\eta = \frac{v_\eta'}{\beta} \ , \ w_\zeta = \frac{w_\zeta'}{\beta} \tag{53}$$

The velocity components in the x,y,z direction of figure 10 are

$$
\begin{bmatrix} u \\ v \\ w \end{bmatrix} = [A]^T \begin{bmatrix} u_\xi \\ v_\eta \\ w_\zeta \end{bmatrix}
\tag{54}
$$

and finally, the components in the coordinate system of figure 10 are

$$
u_S = -u \;,\; v_S = v \;,\; w_S = -w
\tag{55}
$$

The velocities to be used in the force and moment calculations are nondimensionalized by the store free-stream velocity. Thus, equation (45) becomes

$$
U_S^{\;*} = \frac{U_S}{V_{\infty_S}} = V^*_{\infty S, x_S} + u_S^{\;*}
\tag{56}
$$

$$
V_S^{\;*} = \frac{V_S}{V_{\infty_S}} = V^*_{\infty S, z_S} + v_S^{\;*} + \frac{r(x_S - x_{S,m})}{V_{\infty_S}}
$$

$$
W_S^{\;*} = \frac{W_S}{V_{\infty_S}} = W^*_{\infty S, z_S} + w_S^{\;*} + \frac{q(x_S - x_{S,m})}{V_{\infty_S}}
$$

where from equation (49) or (50)

$$
V_{\infty_S} = [(V_\infty \cos\alpha_f + \dot{\xi})^2 + \dot{\eta}^2 + (V_\infty \sin\alpha_f + \dot{\zeta})^2]^{\frac{1}{2}}
\tag{57}
$$

At any point in time during the trajectory, the forces and moments are determined by removing the store from the flow field, determining

31

the velocities at a series of points which the store longitudinal axis and tail fins occupied, and then immersing the store in this flow field.

Buoyancy Forces and Moments (Ref 2:27-29) The buoyancy forces and moments are calculated with the assumption that the flow in planes perpendicular to the axis of the store obeys Laplace's equation and that the upwash and sidewash velocities vary along the store length. The potential is constructed on this basis, then integration of the body pressures obtained from the unsteady Bernoulli equation yield both the buoyancy forces and the slender-body forces. The final expression for the buoyancy normal-force coefficient is given by equation (63) of reference 1. The derivation is carried out in Appendix I of that reference with the final expression which contains both buoyancy and slender-body terms given by equation (I-14).

The expression used to calculate the coefficients are

$$(C_N)_{BY} = \frac{2\pi}{S_R} \int_0^{\ell_s} a^2 \frac{dW_s^*}{dx_s} dx_s \qquad (58)$$

$$(C_Y)_{BY} = \frac{2\pi}{S_R} \int_0^{\ell_s} a^2 \frac{dV_s^*}{dx_s} dx_s \qquad (59)$$

The expressions for pitching moment and yawing-moment coefficients with the moment taken about $x_{s,m}$ (see figure 10), are

$$(C_m)_{BY} = \frac{2\pi}{S_R \ell_R} \int_0^{\ell_s} (x_{s,m} - x_s) a^2 \frac{dW_s^*}{dx_s} dx_s \qquad (60)$$

32

$$(C_n)_{BY} = \frac{2\pi}{S_R \ell_R} \int_0^{\ell_s} (x_{s,m} - x_s) \, a^2 \frac{dV_s^*}{dx_s} \, dx_s \tag{61}$$

Slender-Body Forces and Moments (Ref 2:28) The slender-body forces and moments are derived in section 6.21 of reference 1. The expressions are:

$$(C_N)_{SB} = \frac{2\pi}{S_R} \int_0^{x_{s,o}} \frac{d}{dx_s} (a^2 W_s^*) dx_s \tag{62}$$

$$(C_Y)_{SB} = \frac{2\pi}{S_R} \int_0^{x_{s,c}} \frac{d}{dx_s} (a^2 V_s^*) dx_s \tag{63}$$

$$(C_m)_{SB} = \frac{2\pi}{S_R \ell_R} \int_0^{x_{s,o}} (x_{s,m} - x_s) \frac{d}{dx_s} (a^2 W_s^*) dx_s \tag{64}$$

$$(C_n)_{SB} = \frac{2\pi}{S_R \ell_R} \int_0^{x_{s,o}} (x_{s,m} - x_s) \frac{d}{dx_s} (a^2 V_s^*) dx_s \tag{65}$$

The integrals above are assumed valid until the separation location is reached. At that point, the viscous forces become important.

There are no definite rules for picking $x_{s,o}$, the upper limit of integration where the integrals are valid. However, the problem is discussed in section 6.2, and 8.2 of reference 1. From that reference, a formula is given which relates $x_{s,o}/\ell_s$, which is the location on the body where potential flow is no longer applicable, to $x_{s,1}/\ell_s$

$$\frac{x_{s,o}}{\ell_s} = 0.378 + 0.527 \frac{x_{s,1}}{\ell_s} \tag{66}$$

33

where $x_{s,1}/\ell_s$ is the location on the body of the maximum negative rate of change of cross-sectional area. This can be used to estimate the value of $x_{s,o}$.

Viscous Crossflow Forces and Moments (Ref 2:29-30) From the assumed separation location to the base of the store a viscous crossflow calculation is used in place of the slender body calculation. The expressions are derived in section 6.2.2 of reference 1.

$$(C_N)_{CF} = \frac{2C_{d_c}}{S_R} \int_{x_{s,o}}^{\ell_s} a \; V_c^* \; W_s^* dx_s \qquad (67)$$

$$(C_Y)_{CF} = \frac{2C_{d_c}}{S_R} \int_{x_{s,o}}^{\ell_s} a \; V_c^* \; V_s^* dx_s \qquad (68)$$

$$(C_m)_{CF} = \frac{2C_{d_c}}{S_R \ell_R} \int_{x_{s,o}}^{\ell_s} (x_{s,m} - x_s) a \; V_c^* \; W_s^* dx_s \qquad (69)$$

$$(C_n)_{CF} = \frac{2C_{d_c}}{S_R \ell_R} \int_{x_{s,o}}^{\ell_s} (x_{s,m} - x_s) a \; V_c^* \; V_s^* dx_s \qquad (70)$$

where $\quad V_c^* = [(V_s^*)^2 + (W_s^*)2]^{\frac{1}{2}} \qquad (71)$

$$C_{d_c} = \frac{\text{drag per unit length}}{q_{\infty_s} 2a} \qquad (72)$$

Empennage Forces and Moments   A method of calculating the forces
and moments associated with planar or cruciform empennages is presented
in section 5.3, reference 2. The details are not essential to the
construction of the trajectory program input and will not be presented
here.

Equations of Motion (Ref 4:27; Ref 2:33-38)

The complete derivation of the equations of motion of a rigid body
with mass and inertia asymmetries is presented in Appendix II (Ref 2:131-
145). Generally, a store body will have axes of geometrical symmetry
about which the store forces and moments are determined. By mass asym-
metry it is meant that the store center of mass does not have to lie at
the origin of this coordinate system. By inertia asymmetry it is
meant that the principal axes of inertia of the store do not coincide
with the geometric axes of symmetry so that the tensor of inertia
possesses off diagonal terms, the products of inertia.

The derivation of the equations of motion used two previously dis-
cussed coordinate systems, see figure 11. The x,y,z coordinate system
is fixed in the store and rotates with the store. The x-axis is posi-
tive forward, y-axis positive to the right, and the z-axis positive
downward. These axes coincide with the geometric axis of symmetry with
the origin at the point about which the moments and products of inertia
and the aerodynamic moments are calculated. The x,y,z coordinate system

is used because the time derivatives of the moments and products of
inertia do not appear in the rotational equations of motion. The
equations of motion are given in Appendix II (Ref 2:136, 144) by equa-
tions (II-15) and (II-40).

The x,y,z coordinate system does not allow the store position
and orientation to be determined relative to the host aircraft. The
ξ,η,ζ system is used for this purpose, with the assumption that the
parent aircraft is flying at constant velocity, constant angle of
attack, and constant flight path angle relative to the horizontal. The
ξ,η,ζ system can be regarded as inertial because it is non-rotating,
and the store motion relative to the moving system calculated.

The ξ,η,ζ system is fixed at the nose of the parent aircraft with
the ξ-axis positive forward, η-axis positive to the right, and ζ posi-
tive vertically downward.

The orientation of the store with respect to the ξ,η,ζ system is
accomplished through Euler angles Ψ,Θ,Φ (Ref 14:100-107). The time
histories of these angles are determined by expressing them as store
rotational velocities p,q,r, see figure 11. The differential equations
expressing this are

$$\dot{\Psi} = (q\sin\Phi - r\cos\Phi)/\cos\Theta$$

$$\dot{\Theta} = (q\cos\Phi - r\sin\Phi) \tag{73}$$

$$\dot{\Phi} = p + q\sin\Phi\,\tan\Theta + r\cos\Phi\,\tan\Theta$$

These equations along with equations (II-16) through (II-18), and (II-41) through (II-43) are the final differential equations which are to be integrated to determine the store position and orientation relative to the inertial system fixed in the fuselage (Ref 2:136-144).

In the equations, $\ddot{\xi}, \ddot{n}, \ddot{\zeta}$ are the accelerations of the store moment center in the inertial coordinate system. The velocities in this system are $\dot{\xi}, \dot{n}, \dot{\zeta}$ and the quantities $\dot{x}_o$, $\dot{y}_o$, $\dot{z}_o$ are these velocities resolved into the store body coordinate system using $[A]^T$, previously defined. The location of the store center of mass relative to the store moment center, in store body coordinates, is $\bar{x}$, $\bar{y}$, $\bar{z}$. The rotational velocities in the store body coordinate system are $\dot{p}$, $\dot{q}$, $\dot{r}$. The quantities I_{xx}, I_{yy}, I_{zz} are the moments of inertia and I_{yz}, I_{xz}, I_{xy} are the products of inertia.

The remaining parameters in the equations of motion are the store mass, m, the forces F_x, F_y, F_z; the moments, M_x, M_y, M_z. The forces and moments act on the store and are positive in the positive x,y,z,p, q,r directions.

$$F_x = mg_x - q_{\infty S} \, S_R \, C_A$$

$$F_y = mg_y + q_{\infty S} \, S_R \, C_Y \qquad\qquad (74)$$

$$F_z = mg_z - q_{\infty S} \, S_R \, C_N$$

where g_x, g_y, g_z are the components of the gravitational acceleration in the store body coordinate system (Ref 2:36). The second terms in equation (74) are the aerodynamic forces acting on the store. The axial-force coefficient, C_A, is specified by the user and is positive in the negative x direction. The sideforce and normal force coefficients, C_Y and C_N are calculated by the computer program using the methods developed in the section on force and moment calculation. The parameters q_{∞_S} and S_R are the dynamic pressure and reference area used in nondimensionalizing the forces.

$$q_{\infty_S} = \tfrac{1}{2}\rho_\infty V_{\infty_S}^{\;2} \tag{75}$$

$$S_R = \pi a_{max}^2 \tag{76}$$

The density q_∞ is assumed constant at the value for the aircraft flight altitude at time t=0, and V_{∞_S} is given by equation (56). The maximum store body radius is used for a_{max}.

The moments about the store moment center are

$$M_x = q_{\infty_S} S_R \ell_R C_\ell + m(g_z \bar{y} - g_y \bar{z})$$

$$M_y = q_{\infty_S} S_R \ell_R C_m + m(g_x \bar{z} - g_z \bar{x}) \tag{77}$$

$$M_z = q_{\infty_S} S_R \ell_R C_n + m(g_y \bar{x} - g_x \bar{y})$$

The coefficients C_ℓ, C_m, C_n are calculated by the computer. The reference length ℓ_R is the maximum store diameter

$$\ell_R = 2a_{max} \tag{78}$$

The second terms in the moment equations are the moments produced by the gravitational force when the location of the store center of mass does not coincide with the center of moments.

The final specifications required before the equations of motion can be integrated are the initial conditions. These are the position of the store center of moments (ξ, η, ζ), the translational velocity of this point $(\dot{\xi}, \dot{\eta}, \dot{\zeta})$, the angular velocity about the store axes (p, q, r) and initial orientation angles Ψ, Θ, Φ. With these specifications the equations can be integrated with the aerodynamic forces and moments being recalculated at each point in the trajectory.

The mathematical model for determining the flow field around an aircraft fuselage-wing combination and associated stores has been developed. This model has been used to establish the forces and moments on a separated store, and using these forces, the equations of motion can now be integrated to predict the store trajectory.

The equations and relationships have been programmed into a source and trajectory program (Ref 5). The input for each of these programs will now be described and developed.
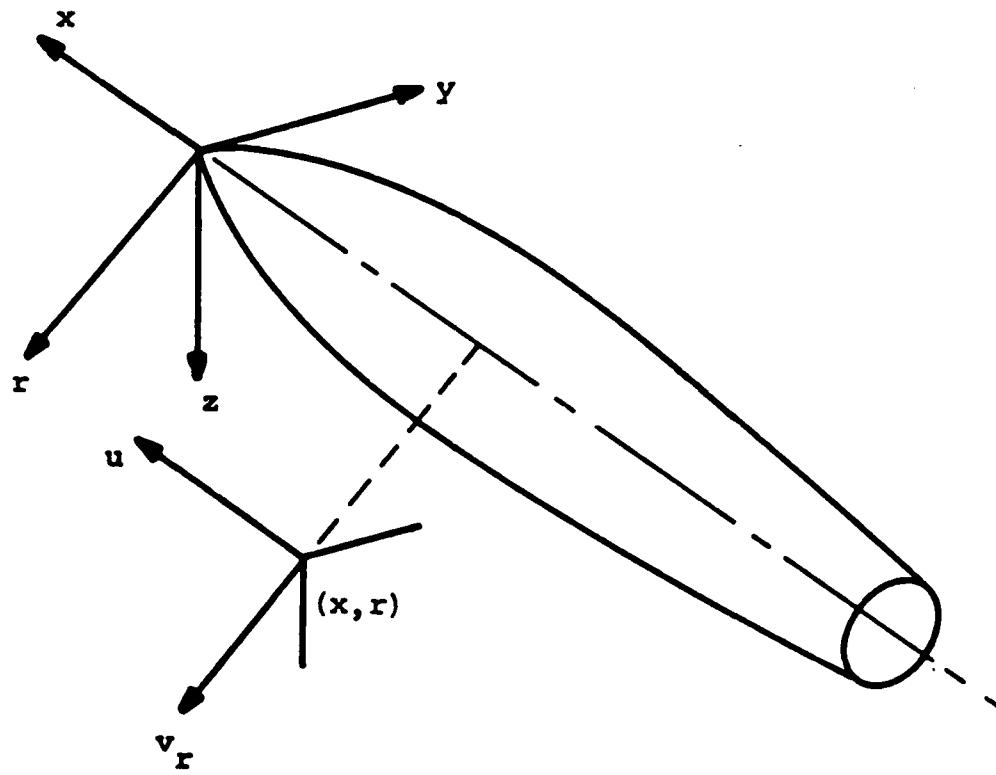
Figure 1. Coordinate System for an Axisymmetric Body
(Ref 4: 37)
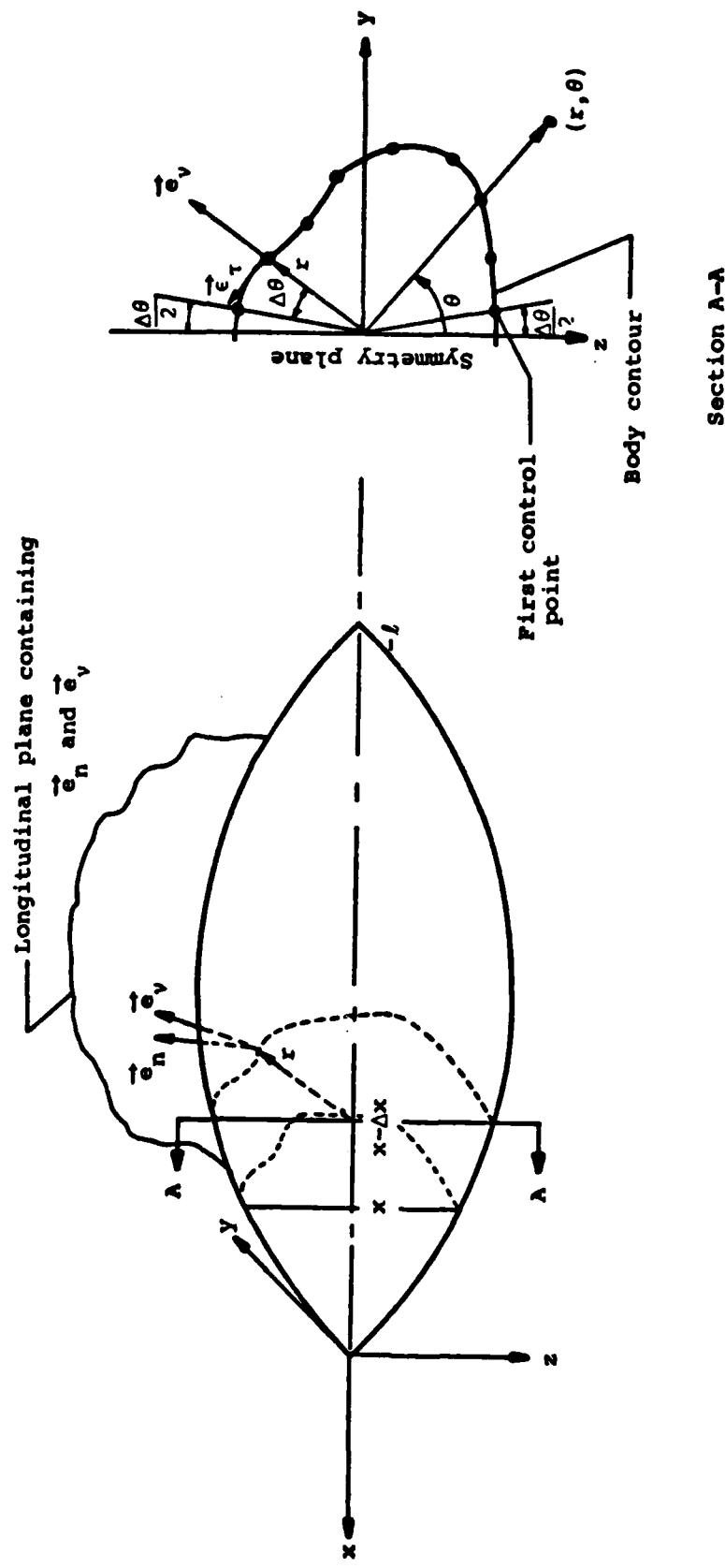
Figure 2. Coordinate Systems for a General Slender Body

(Ref 4: 38)

41

$$\phi = m - \theta - \frac{\pi}{2}$$
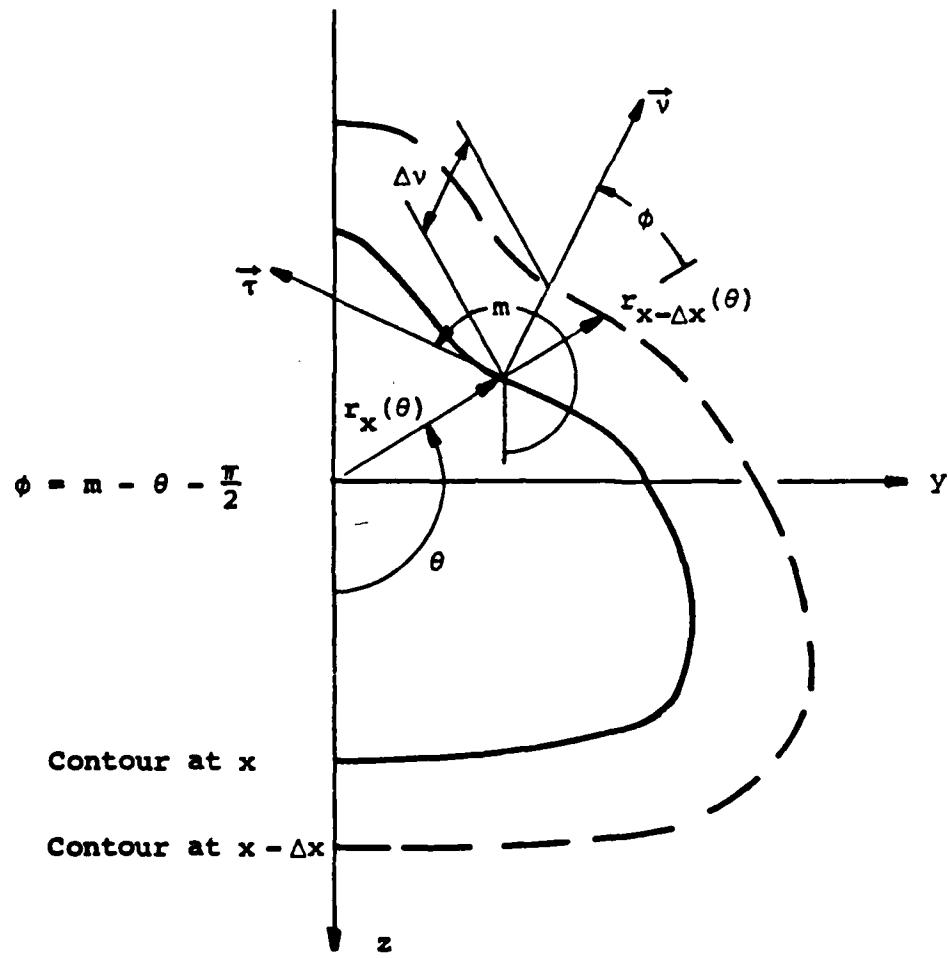
Figure 3.   Streamwise Body Slope

(Ref 4: 9)

42
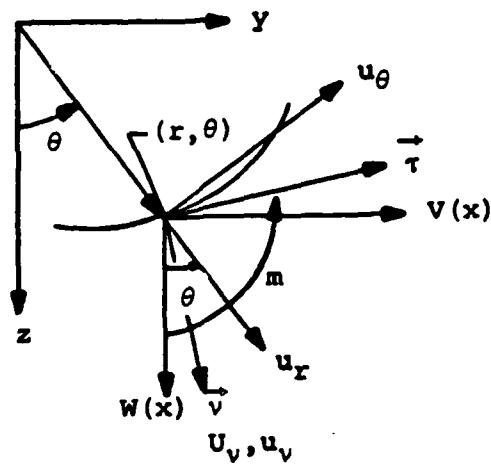
Figure 4. Coordinate Systems for Streamwise Body Slope

(Ref 4: 10)
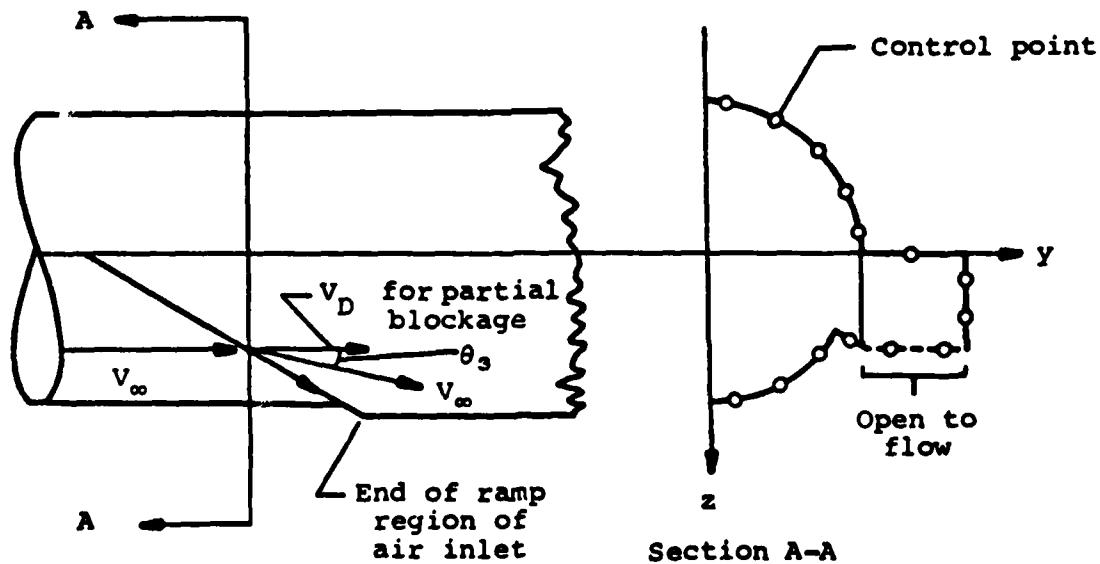
Figure 5. Engine Inlet Crossflow Plane

(Ref 4: 18)

43

HORSESHOE VORTEX

CONTROL POINT

AREA ELEMENT

M_∞
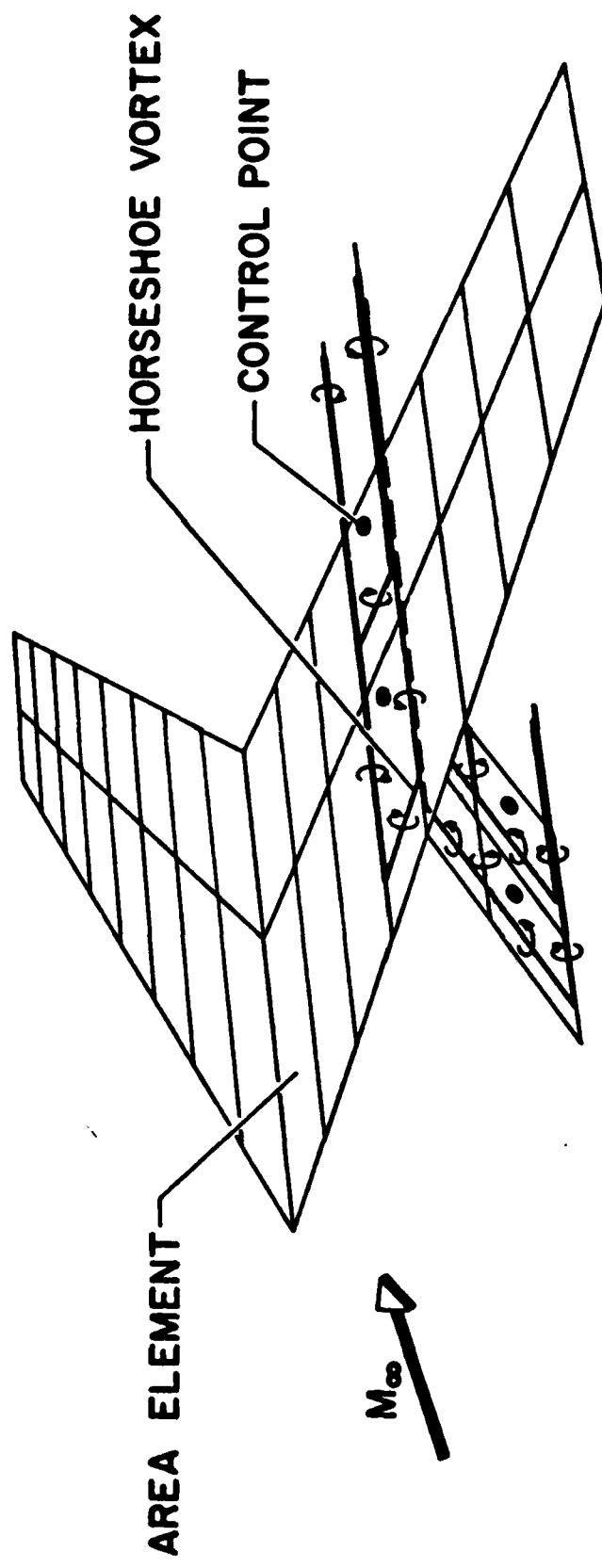
Figure 6. Vortex Lattice Model

(Ref 2: 60)
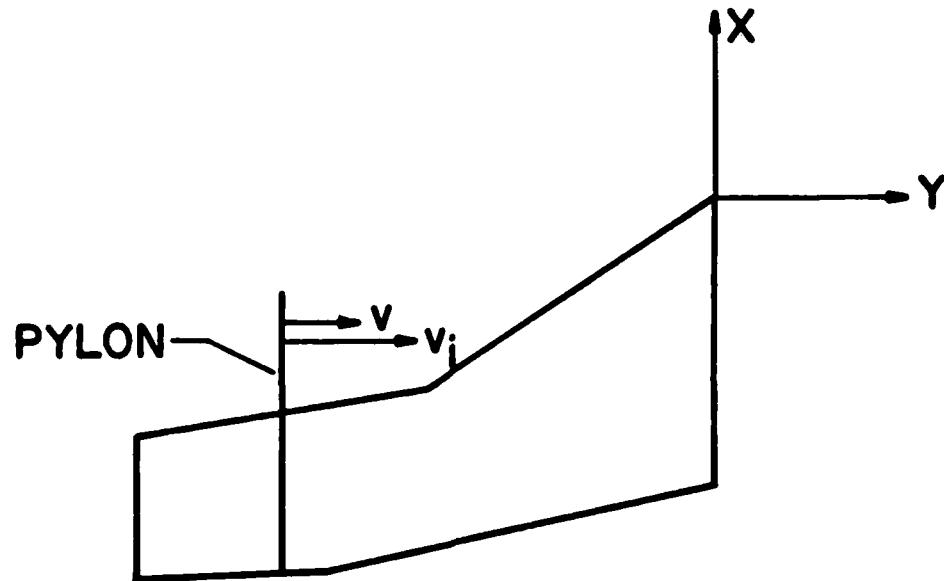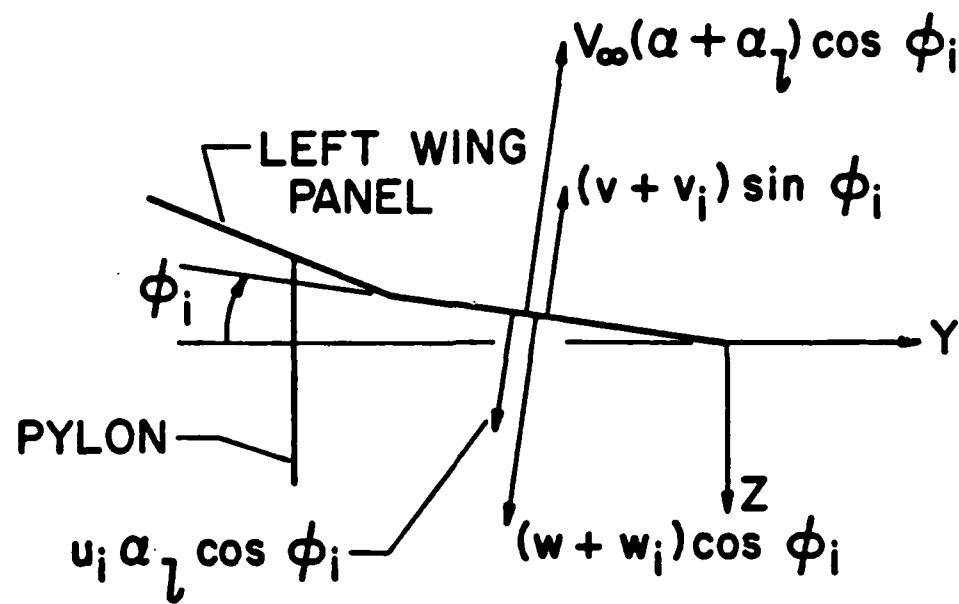
Figure 7. Flow Tangency Boundary Conditions

(Ref 2: 61)
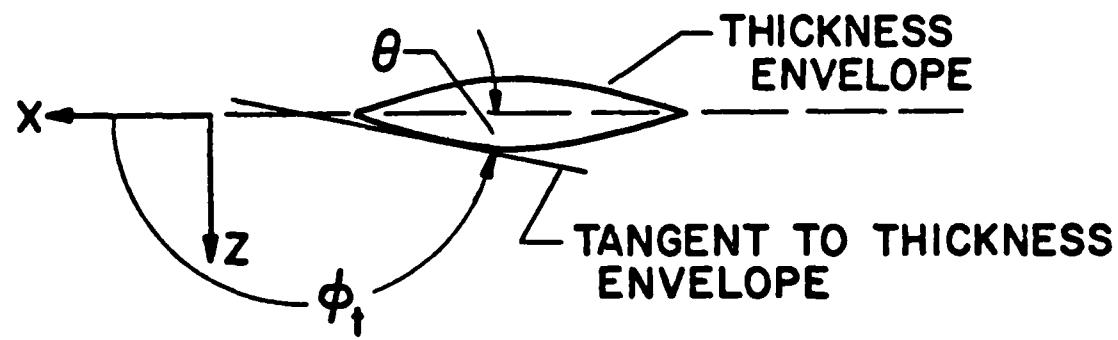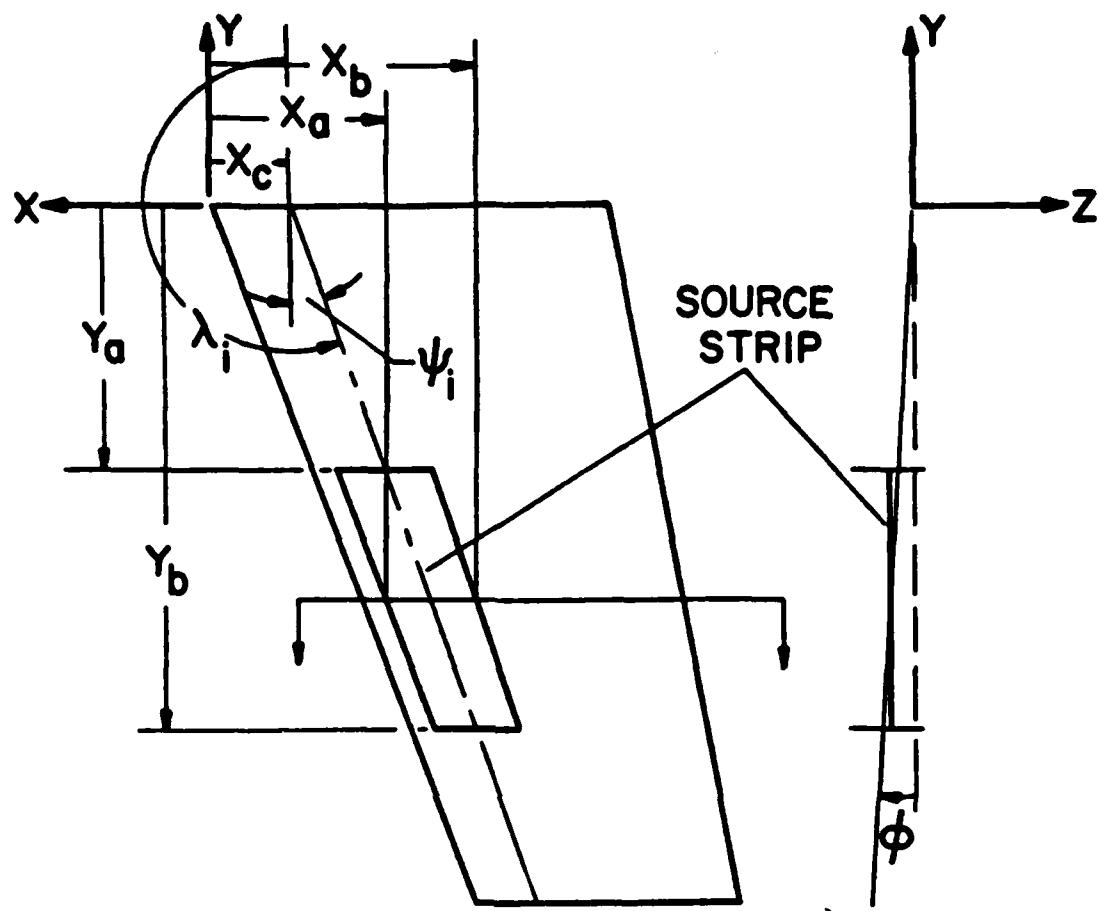
Figure 8. Coordinate System for Wing Thickness

(Ref 2: 62)
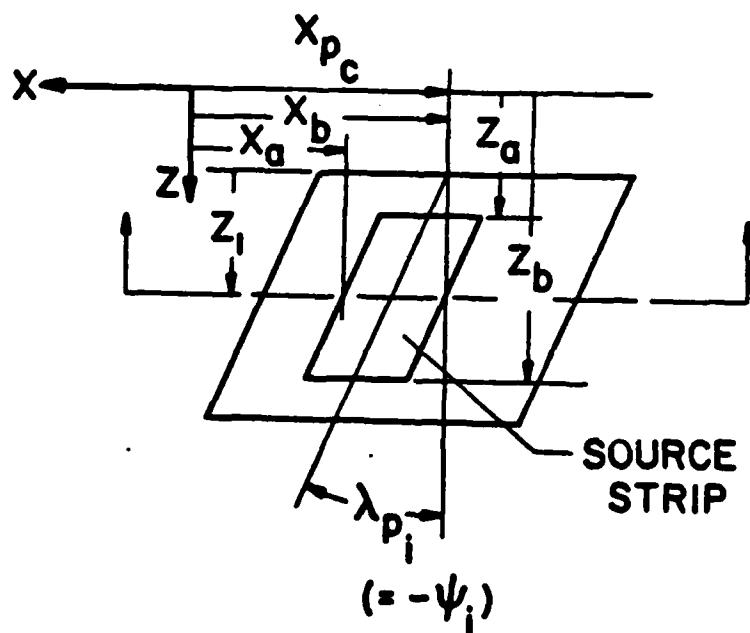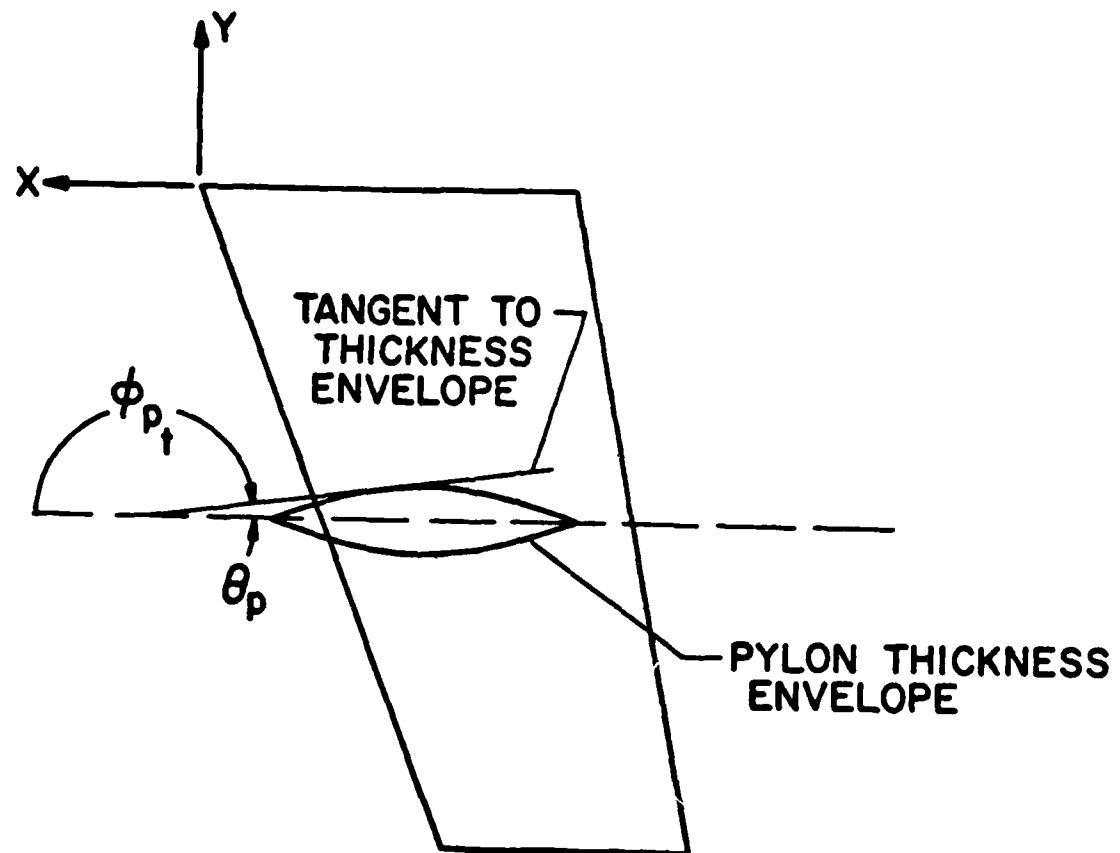
Figure 9. Coordinate System for Pylon Thickness (Ref 2: 63)

47
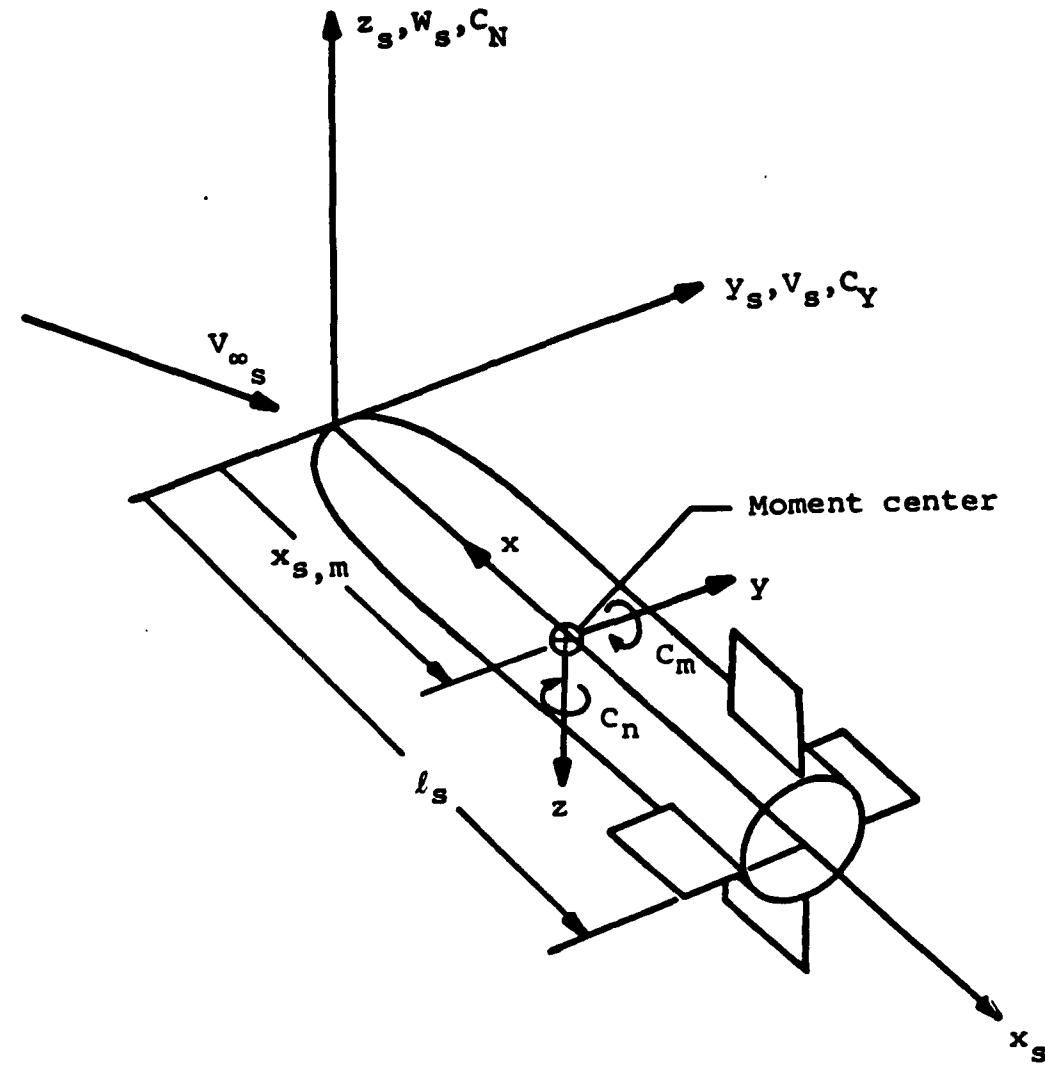
Figure 10. Coordinate System Fixed in Ejected Store

(Ref 4: 64)

48
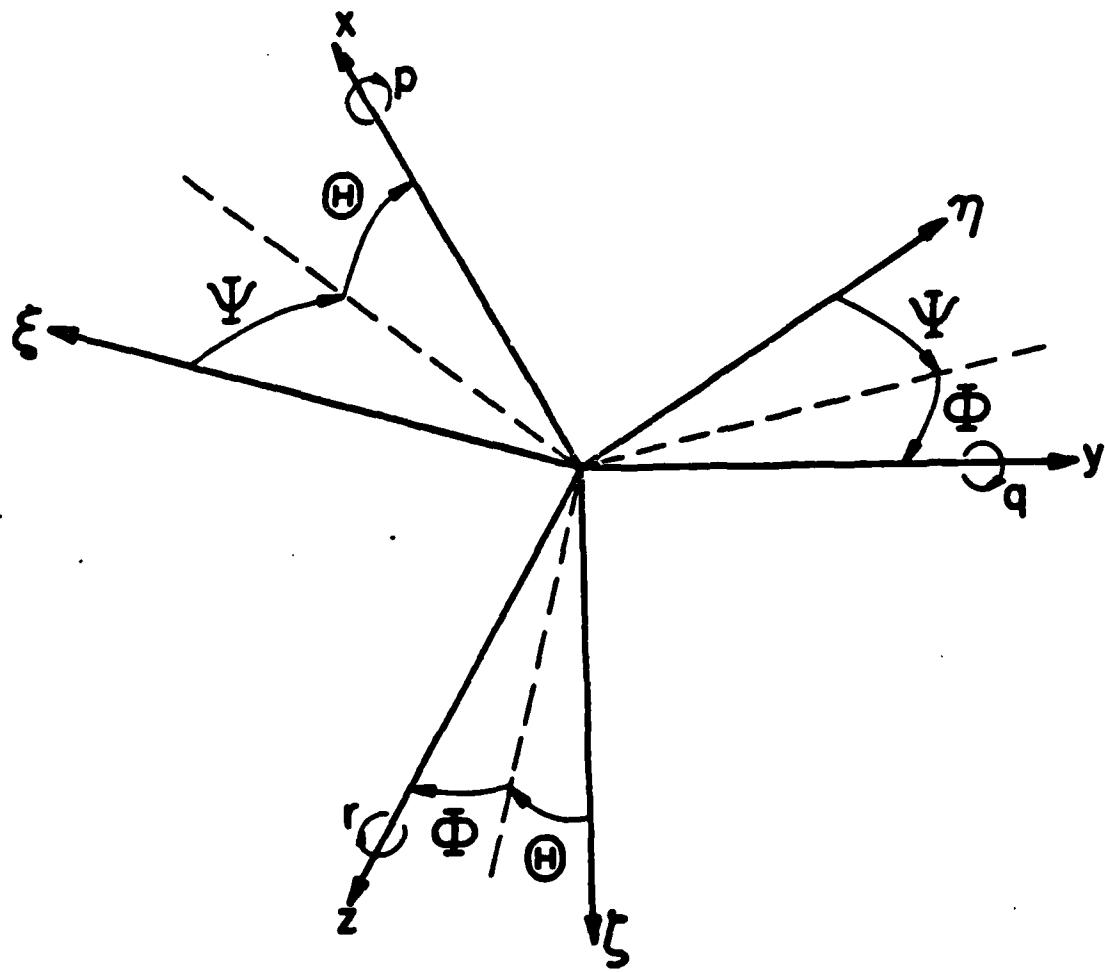
Figure 11. Coordinate Systems for Trajectory

(Ref 2:66)

49

III. NEILSEN PROGRAM APPROACH

The Neilsen approach uses two separate computer programs, a source program and the trajectory program (Ref 5:4-8). The two programs are used with no direct exchange of information during a run. The source program does provide an input to the trajectory program, but the user must provide the information exchange.

The source program is used to represent an axisymmetric body as a distribution of sources along the axis of the body. This representation is used for the fuselage, store, and pylon volume effects on the overall flow field around the aircraft. The program calculates and prints the source strengths and locations. These quantities are used as input data to the trajectory program.

The trajectory program calculates the trajectory of the dropped store by accounting for the effects of the other aircraft components on the store, and integrating the equations of motion. The program contains options to allow for a circular or noncircular fuselage, no fuselage, pylons, racks, and up to ten stores. This report will deal only with a noncircular cross-section fuselage, with one store on the fuselage and one store separated. There is no rack or pylon. This configuration was chosen to compare with available wind tunnel data.

The input for each program will be discussed in detail in Appendix B and Appendix C. Those items which do not apply will be referenced to the proper users manual. Details of the preparation are included to allow future users to concentrate on those items which cause the most difficulty.

IV. Source Program Input and Analysis

The program input (Ref 5:9-16) is initiated by the user representing the body as an equivalent body of revolution (EBR). The surface of the EBR is then approximated by a series of polynomials which represent the EBR x,r distribution. At this point the source program is run with a user specified finite source distribution. The program calculates the shape of the EBR from the source strengths and the output is presented so that the user may compare calculated values of the surface to the polynomial representation of the surface. There is no set procedure for specifying the source distribution; trial and error, and experience are the only tools available. Once the proper representation is determined, the source strengths and locations are input into the trajectory program.

The source program input was developed for the fuselage and store at M = 0.6 and M = 0.9. The fuselage input will be described in detail. The input was determined in distinct steps:

1. Cross-section area distribution for fuselage

2. Inlet velocity ratio

3. Cross-section area distribution of EBR

4. Polynomial to represent EBR

5. Develop input deck

6. Run source program

Cross-Section Area

Cross-section data were available at 22 fuselage stations. Data on more stations would have improved the program accuracy in representing the body. The area at each station is converted to an EBR area and radius. This provides one point on a curve which must then be represented by a given polynomial. The accuracy of the polynomial is directly related to the number of data points.

Inlet Velocity Ratio

As previously stated, the inlet velocity ratio is used to adjust the area distribution to reflect the change in streamwise flow caused by blockage due to the presence of the inlet. For an inlet velocity ratio of 0.5 only one-half of the inlet cross-sectional area is added to the area of the body. For an inlet velocity ratio of 1.0, none of the cross-sectional area is added. This correction is made on the right and left nacelle.

The inlet ratio was determined from experimental data (Ref 15) to be $V_D/V_\infty = 0.862$. This was calculated by knowing the theoretical capture area of the duct, the exit area of the nozzle, and experimental flow data. By assuming a constant mass flow through the duct, the velocity at the duct inlet was determined. This duct inlet velocity divided by the free-stream velocity gives the required inlet velocity ratio. Reference 5 uses an inlet velocity ratio of 0.5 with no explanation of how the number was determined. This value could be used

if no experimental data were available. Note: the inlet velocity ratio must be greater than or equal to zero, but less than or equal to 1.0.

A capture area, including both nacelles, of 1068 in^2 was used. With an inlet velocity ratio of 0.862, the area at each fuselage station was reduced by 921 in^2.

Cross-Sectional Area Distribution of EBR

The cross-sectional area, corrected for inlet velocity ratio was determined for each fuselage station. This area was then converted to an EBR radius, Table 2, Appendix A.

$$R_{EBR} = \left[\frac{A_{total}}{\pi}\right]^{1/2} \tag{79}$$

The information on the last station was taken from the engineering drawing.

Polynomial to Represent EBR

The EBR is represented by a series of polynomials describing the curve of r/ℓ plotted versus x/ℓ, figure 12. All coordinates are non-dimensionalized with respect to the body length.

The equation used to describe the EBR is given by

$$r/\ell = C_1 + C_7 \sqrt{C_2(x/\ell)^2 + C_3(x/\ell)^2 + C_4} + C_5(x/\ell)^2 + C_6(x/\ell)^2 \tag{80}$$

(Ref 5:11)

Combinations of coefficients C_1 thru C_7 are used to describe the desired curve. For this case, let $r/\ell = y$ and $x/\ell = x$. The following curves can be represented by

$$y = C_1 + C_7\sqrt{C_2 x^2 + C_3 x + C_4} + C_5 x + C_6 x^2 \qquad (81)$$

Straight line

$$y = C_1 \qquad\qquad C_1 \text{ through } C_7 = 0$$

$$y = C_1 + C_5 x \qquad\qquad C_2 = C_3 = C_4 = C_6 = C_7 = 0$$

Circle

$$y = C_1 + C_7\sqrt{C_2 x^2 + C_3 x + C_4} \qquad C_6 = C_5 = 0$$

Parabola

$$y = C_1 + C_5 x + C_6 x^2 \qquad\qquad C_2 = C_3 = C_4 = C_7 = 0$$

Ellipse

$$y = C_7\sqrt{C_2 x^2 + C_4} \qquad\qquad C_1 = C_3 = C_5 = C_6 = 0$$

$$C_2 < 0$$

Hyperbola

$$y = C_7\sqrt{C_2 x^2 + C_4} \qquad\qquad C_1 = C_3 = C_5 = C_6 = 0$$

$$C_2 < 0$$

54

The source program allows for seven polynomials (NSECT) to be used to describe an EBR. This includes a polynomial to close the body, or model the wake. The wake was modeled (Ref 5;13,16) for the ogive store with the same polynomial as the nose. For the present case a straight line was used to close the fuselage body (EBR).

Observation of the EBR plot, figure 12, indicated that straight lines or parabolas would be sufficient to model the EBR. A least square curve fit was used to determine the coefficients, Table 3, Appendix A.

Source Program Input

The development of the source program input is given in Appendix B. The two variables in the input deck are NRAT and PERCR. NRAT is the number of segments which the body will be divided for the specification of the source distribution. PERCR is the source spacing for each NRAT segment. PERCR is input as a fraction of the local body radius of the segment.

Source Program Analysis

The output of the source program is given in figure 29, Appendix B. The data from this program were input into the trajectory program.

The value of NRAT was chosen, see figure 12, which left the values of PERCR as the only variables in the source program. It is recommended (Ref 5:13) that an initial run be made with PERCR = 1.0. The value of PERCR should then be decreased until the proper shape is calculated or

a maximum number of 100 sources is reached. Computation in the trajectory program is a function of the number sources which must be used to model the fuselage, stores, and racks. The maximum of 100 sources is applied to each component modeled.

The accuracy of the program generated shape was judged by analysis of the output section (figure 29): SHAPE CALCULATED FROM SOURCE DISTRIBUTION AND POLYNOMIALS. For each x/ℓ specified, a value of R/L (S.D.) and R/L (POLY) is calculated. A guideline was established for judging the acceptable error between R/L (S.D.) and R/L (POLY). Except for the nose and tail, the error must be less than two percent.

Runs were made with PERCR equal to 1.0, 0.8, 0.6, 0.4. The value of 0.4 gave more than 100 sources. Results were outside the guidelines for all of these values. By reference to figure 12, it was noted that the body radius in segments one and two was small compared to the others. Also the accuracy did not vary with values of PERCR. PERCR was held at 1.0 in these segments while the others were varied. PERCR was reduced in a random manner in segments three, four, and five until values of 0.9, 0.3, and 0.4 respectively were found to give the best results.

The computer execution time for the fuselage source program with 73 sources was 0.96 seconds. For the ogive store with 59 sources, the execution time was 0.779 seconds. These values were taken from runs

56

on the CYBER 750 system and are typical values for runs with varying
numbers of sources.
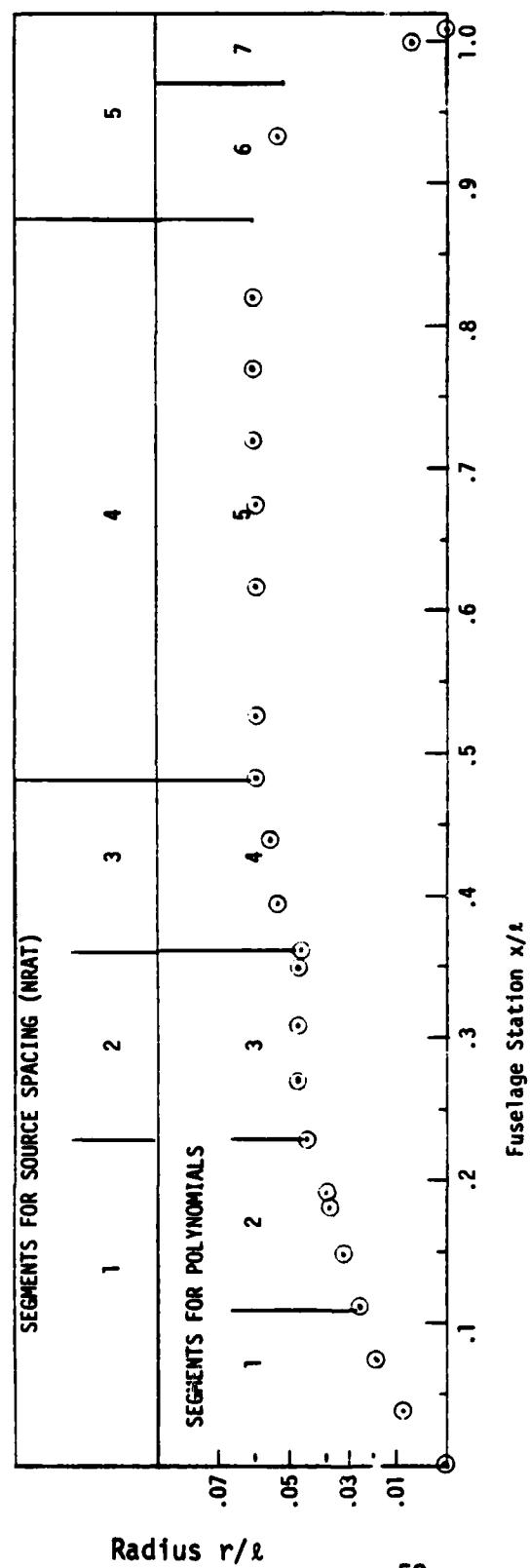
Figure 12. Equivalent Body of Revolution

V. TRAJECTORY PROGRAM - INPUT AND ANALYSIS

Selection of the Number of Polar Harmonic Coefficients

The trajectory program has numerous parameters that must be either calculated or set before the program can be run. Most parameters are set by the flight condition or geometry of the complete vehicle. The only parameter which must be picked on the basis of the trajectory program output is the number of polar harmonic coefficients input, item 13, (see Appendix C). Other parameters affect the output, but they are set by the given problem. The polar harmonics must be chosen by the user, and very few details were given, (Ref 4) for the selection.

Recall that MH was defined as the number of polar harmonic coefficients, and MC was the number of control points. Some basic guidelines were given for the selection of MH (Ref 4:15-18). The value of MH should be such that $MH \leq 0.9MC$. The calculated coefficients should converge. The value of the sidewash velocity diverges at a certain value of MH, and the best value of MH occurs just prior to this divergence. The least error occurs when $MH \ll MC$. The run time and cost increase with the value of MH.

The sidewash criteria for selection was not used because it required another computer program to calculate the values for analysis. The convergence of the coefficients was of no value because the coefficients converged at all stations for all values of MH. Different

values of MH gave different coefficients but no analysis of the con-
vergence could be made because of the random nature of the numbers.

The value of MH = 15 was selected by using the example given in
reference 4 and 5, along with analysis of the computer output for
different values of MH. It was noted that the two examples in refer-
ence 4, where coefficient convergence was used as a criteria, gave MH:

$$MH = 14 \quad \text{for} \quad MC = 32$$
$$MH = 14 \quad \text{for} \quad MC = 24$$

For the case of this report, a value of MH = 14 for MC = 30 should be
close. The sidewash velocity criteria was used (Ref 4) to give a value
of MH = 32 for MC = 14.

The above results indicate that the value of MH should occur at
about 0.5 MC and at a value of MH just prior to some kind of velocity
divergence. If the velocity field diverges, the forces and moments on
the store should also show some kind of divergent trend. This was the
approach taken.

A store location was chosen and a trajectory program run was made
with values of MH from 4 through 27. The results were plotted for C_N
and C_M versus MH, see figures 13 and 14. The values of C_N and C_m both
show a divergent trend at approximately MH = 17. Comparison with ex-
perimental data revealed that C_m matched best at MH = 10, while C_N

60

matched best at MH = 17. A value of MH = 15 was selected to give re-
sults within 3% of experimental for both C_N and C_m. The divergence
beyond MH = 17 was the key to the selection, with values of MH = 15,
16, 17 giving good results.

This method is a very gross use of the computer output to select
a parameter within the program. It uses a store which is approximately
10 feet long to analyze the contribution of several fuselage stations
to the flow field. A better approach would be to introduce a very
small store and analyze the forces and moments on it. This approach
would take a large amount of computer time and money, and up to 30
runs for each station of interest.

The gross approach was used at two other store positions. The
results indicated new values of MH for these positions. This new
information was introduced into the input; however, the final result,
with the new values of MH, was no more accurate than for the run with
all MH = 15. The original position analyzed was a critical position
in that the solution at that point gave the best results for all points.
At present, the selection of the proper position for analysis can be
based only on experience and trial and error.

Number of X_B Stations for Polar Harmonics

An attempt was made to increase the accuracy of the program in the
region behind the wing. The number of stations where polar harmonic

solutions were created was increased in this region. Six extra stations were added: however, no increase in accuracy was achieved.

Free-Stream Position of the Store

Confidence in the program model of the store was achieved by moving the store to a free-stream position 10,000 feet ahead of the aircraft. The values for C_N and C_m for angles of attack of 0°, 2°, 4° were all within 10% of experimental values.

Trajectory Integration

The trajectory option was exercised although no wind tunnel data were available for comparison. The stores were loaded on the fuselage centerline in tandem, with the aft store separated. Both stores were in positions which matched experimental positions. The program would not run until the initial position of the store being separated was moved 0.25 feet below the fuselage. The error messages indicated arguments too large for calculation. The program still over-predicted the forces and moments when the store was close to the fuselage.

The required theory to predict store trajectories was established in Chapter II. The required input for the computer model was generated and the program was used to predict the forces and moments on a separated store at various positions under the aircraft model. The results of this prediction will now be compared with experimental data from wind tunnel tests on the same configuration.
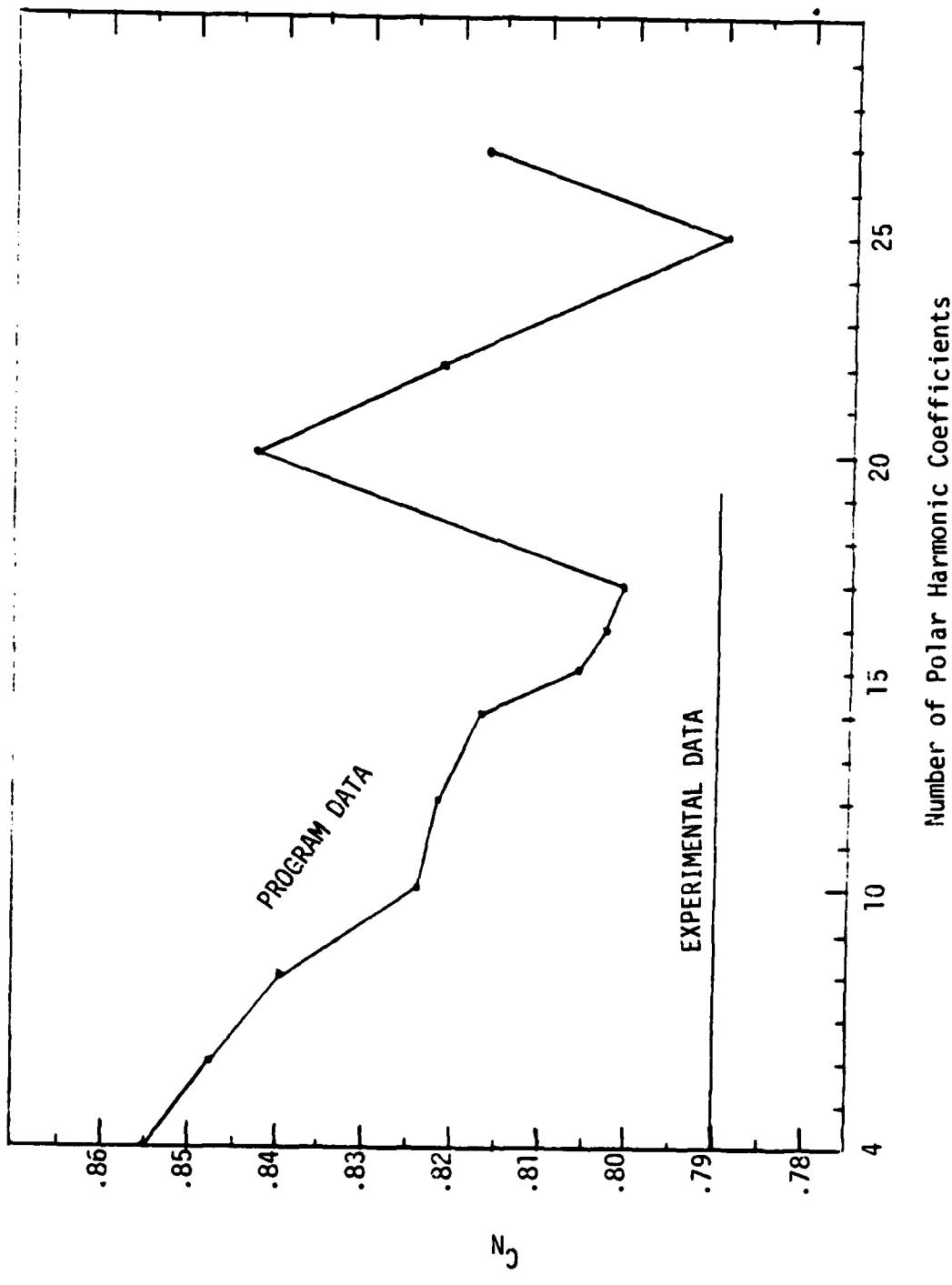
Figure 13. Polar Harmonic Study - C_N

Number of Polar Harmonic Coefficients
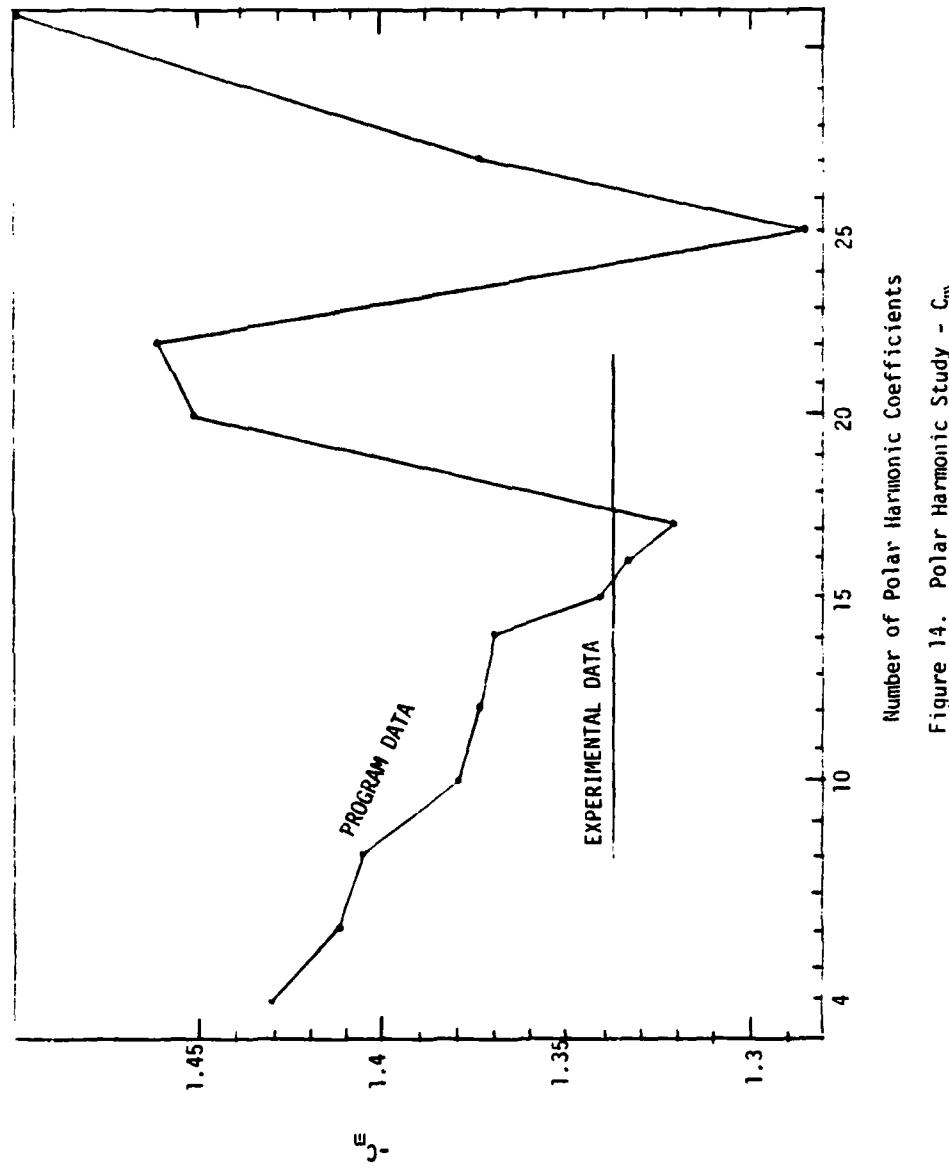
Figure 14. Polar Harmonic Study - C_m

64

VI. COMPARISON WITH WIND TUNNEL RESULTS

The comparison must begin with consideration of the basic differences between the actual model and the Nielsen Program model. The program does not model the canard or tail. Only the wing-fuselage combination is considered. The program does not allow some of the fuselage detail to be modeled. An example is the gap between the inlets and the fuselage. The polar harmonic solutions for the near field use the exact fuselage cross-section, but the number of available stations is limited.

The store model would also be a problem if the store was other than axisymmetric. Only the aircraft fuselage can be modeled with a non-circular cross-section. The store is modeled as an equivalent body of revolution regardless of its shape. The procedure for modeling a non-axisymmetric store would be the same procedure as described in Chapter IV for the fuselage.

Reference Dimensions

The data comparison cannot be made until all force and moment coefficients are non-dimensionalized with respect to the same reference areas, or lengths.

The basic forms for the coefficients are

$$C_N = \frac{\text{Normal Force}}{q_\infty S_R} \tag{82}$$

$$C_m = \frac{\text{Pitching Moment}}{q_\infty S_R \ell_R}$$

The terms q_∞ and S_R were the same for experimental and program data. The value of ℓ_R was not the same. The experimental data were based on a ℓ_R equal to the store length, 127.5 inches. For the program ℓ_R is equal to the maximum store diameter, 15 inches. The experimental data were corrected for the difference in ℓ_R.

$$C_m = \frac{\text{Pitching Moment}}{q_\infty S_R \ell_R} \left(\frac{127.5 \text{ in}}{15.0 \text{ in}} \right) \tag{83}$$

$$C_m = \begin{bmatrix} \text{original} \\ \\ C_m \end{bmatrix} (8.5)$$

The data for comparison were generated by moving the store under the fuselage with the store CG as a reference. Table 1 gives the store position data.

Table 1

Store Positions

Run Sequence	Mach	$-x_{Ref}$ inches (feet)	y_{Ref} (feet)	z_{Ref}(feet) Below FRL	Figures
1	0.6	18.12(1.51) - 648(54)	0.0	6.07	15,16
2	0.6	18.12(1.51) - 648(54)	3.0	6.07	17,18,19,20
3	0.6	447(37.22) - 648(54)	0.0	3.82	21,22
4	0.9	18.12(1.51) - 648(54)	0.0	6.07	23,24

Run Sequence 1 Figures 15 and 16 were the primary sequence for comparison. The Mach number was 0.6 and the store was positioned under the fuselage centerline with a separation of approximately three store diameters. The polar harmonics of the fuselage were optimized for this position.

The program accuracy in the region of the optimum polar harmonics was within ten percent of wind tunnel data with less than 3% error in C_N and C_m occurring at x=-33 feet. C_m showed less accuracy in the area ahead of the wing. The results diverge from experimental values at x=-51 feet. This will be discussed in a later paragraph. The computer execution time for run sequence 1 was 27 seconds on the CYBER 74 system. This is a typical value for all run sequences.

Run Sequence 2 Figures 17 through 20 considered a y variation with the same z position as run sequence 1. The Mach number was again 0.6. The store was positioned under the fuselage, but offset three feet from centerline.

The C_N and C_m predictions were within 15 percent of wind tunnel data in the region of polar harmonics. The values of C_Y were accurate, but the values were very small. The yawing moment, C_n, was underpredicted, but this is consistent with the near zero values of C_Y.

The store position is in the region where interference is the greatest, the edge of the fuselage. The canard, which is not modeled

67

would affect the experimental data ahead of the wing, and the wing would create interference at the wing-fuselage junction.

Run Sequence 3 Figures 21 and 22 were used to consider a store position close to the fuselage, approximately one store diameter clearance. Wind tunnel results were available aft of $x = -37.22$ feet. The C_N results were within 22 percent of wind tunnel results until $x = -51$ feet, where a spike in the data occurs. The C_m results were less than 50 percent accurate.

The program accuracy decreased when the store was placed close to the fuselage. This was expected because of the potential flow model used by the program. The model does not consider any viscous effects in a region where the interference effects are important.

Run Sequence 4 Figures 23 and 24 were made to test for the upper Mach number limit of the program. The store position was the same as in run sequence 1. The Mach number was 0.9, which is above the critical Mach number, but was the only high Mach number where data were available for comparison.

A Mach number of 0.9 required a new run from the source program, although the same inlet velocity ratio was used. This induced an error in the results because the flow through the inlet would not be the same. The magnitude of this error could not be estimated, and a complete new model was not generated.

The polar harmonics were not changed. The area of the fuselage in the wing region was optimized for a Mach number of 0.6. This region is the region of interest; however, the area upstream might not be correctly represented due to the unknown flow pattern created by the higher than critical Mach number.

The predicted values for C_N show the trends of the wind tunnel results; however, the accuracy was not as good as the lower Mach number case. The C_m results show the proper trends, but the curve is shifted. This shift occurs in the region ahead of the wing, and is probably due to the unknown flow field caused by the high Mach number. The program was not designed to handle this Mach number, but it does give results that can be used for comparison.

The data spike previously mentioned occurs in all run sequences at $x = -51$ feet. The wind tunnel results show an upward trend. This trend is overpredicted by the program. The trend in the experimental data is a natural result of some disturbance in the flow field around the fuselage. This flow field is affected by the components of the aircraft and loaded store. The store position is in the downwash region of the wing and the region directly under the horizontal tail. Both are possibilities for the cause of the experimental results; however, the tail is not modeled by the program. The fuselage is relatively wide which may also account for the interference. With the flow around the

69

fuselage as the possible cause, its effects would be increased in the program results due to the lack of a horizontal tail.

An unsuccessful attempt was made to isolate the cause of the spike. The program does not model the tail; therefore, these effects could not be eliminated. The effects of the store which remained on the aircraft were eliminated by removing the store from the model. The effects of the inlet region on the downstream flow were eliminated by using a z direction traverse at various x positions under the fuselage. Any disturbance from the inlet region should be felt along a line, at an angle, downstream of the inlet. This line should be predicted by the two traverses. No correlation could be made from the results.
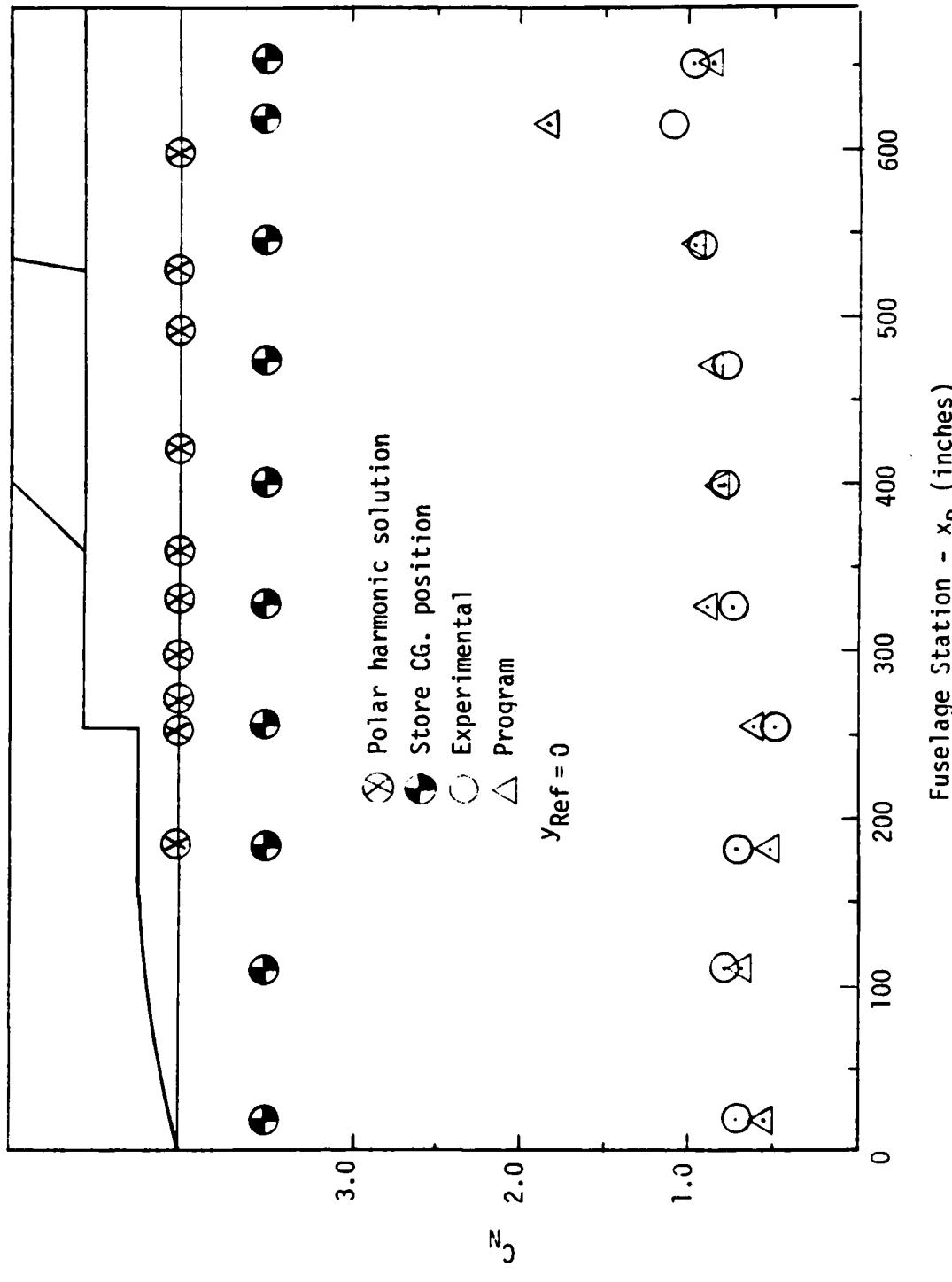
Figure 15. Run Sequence 1, C_N, Mach=0.6, z_{Ref}=6.07 feet

71
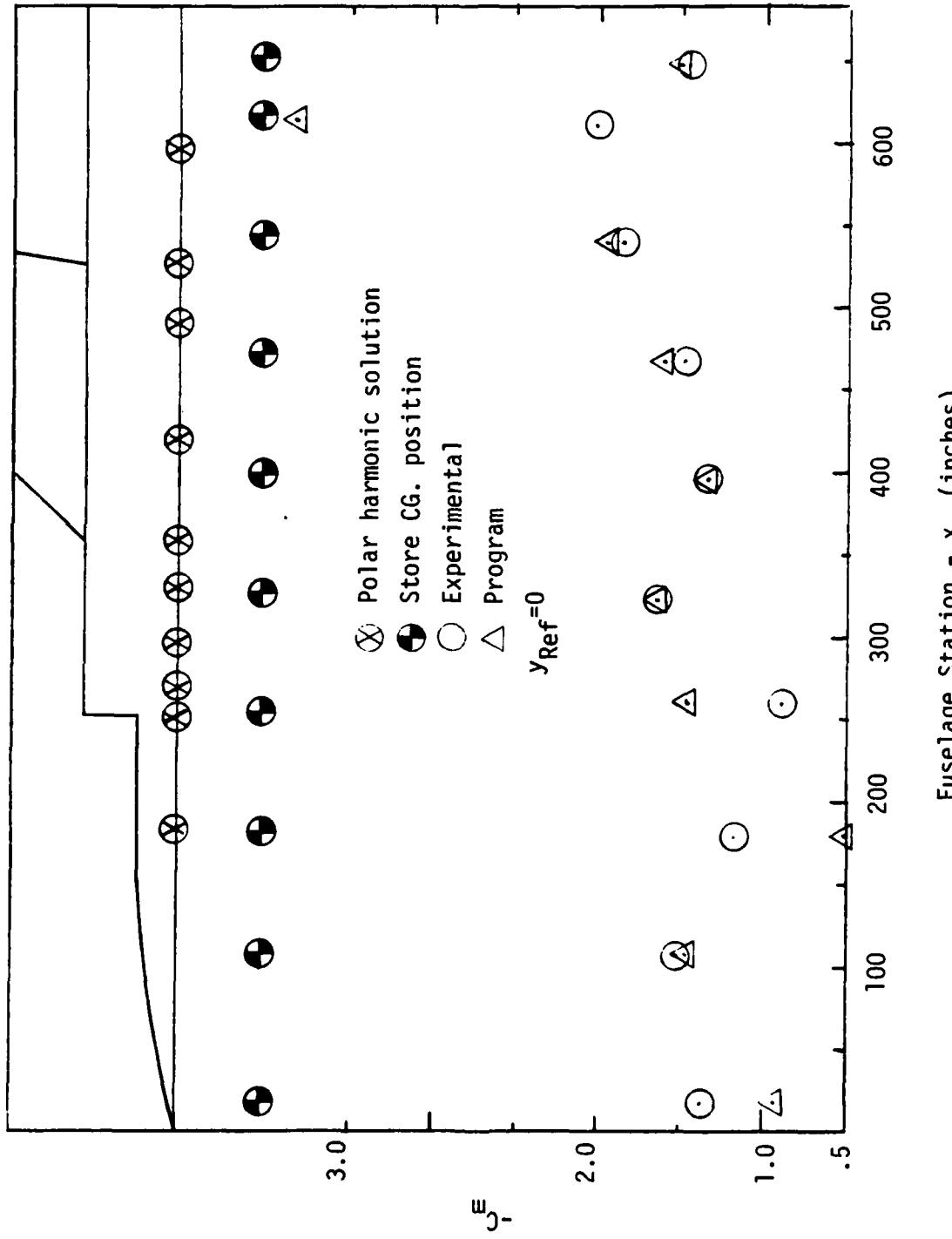
Figure 16. Run Sequence 1, C_m, Mach=0.6, z_{ref}=6.07 feet

72
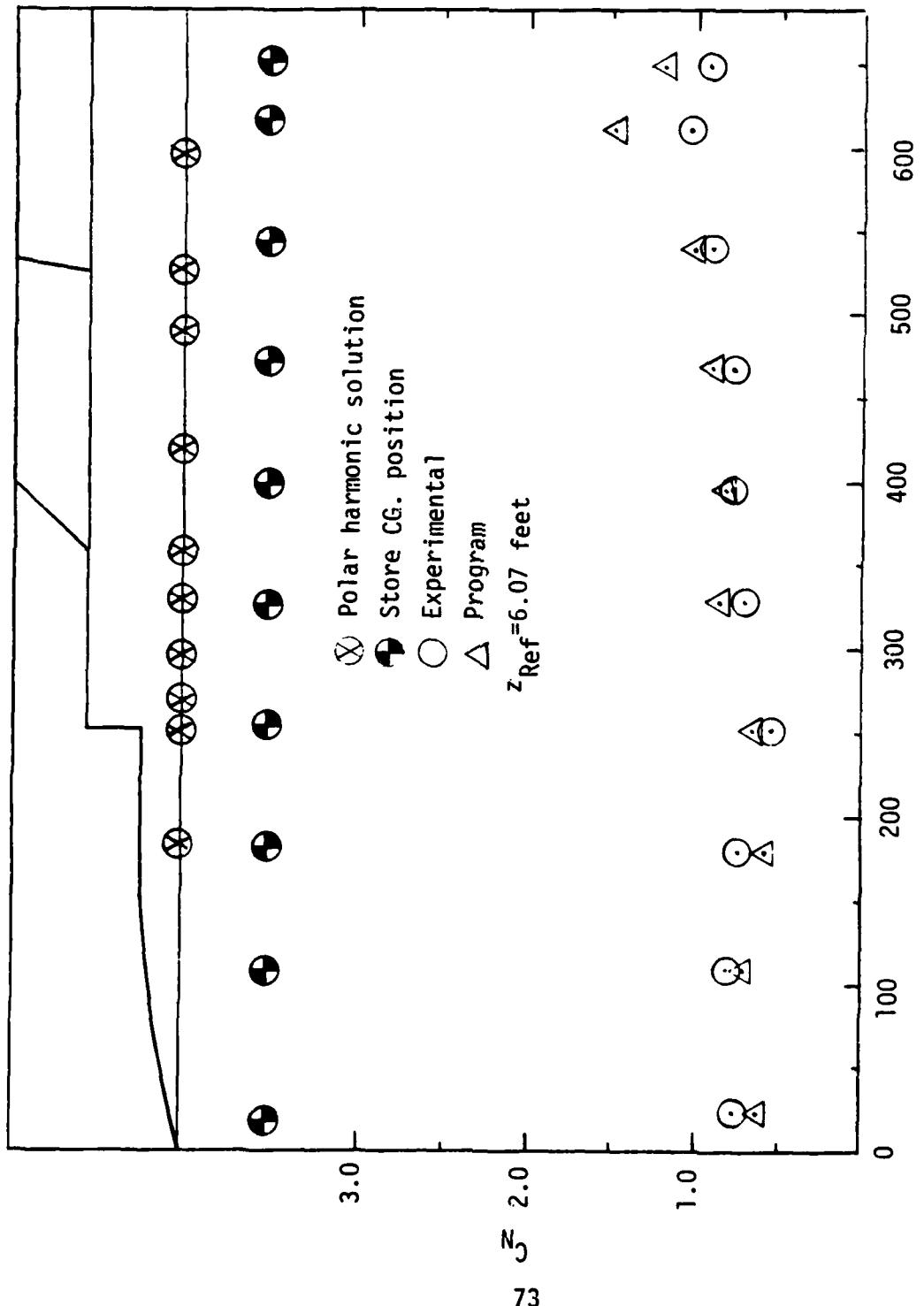
Figure 17. Run Sequence 2, C_N, Mach=0.6, y_{Ref}=3 feet

73
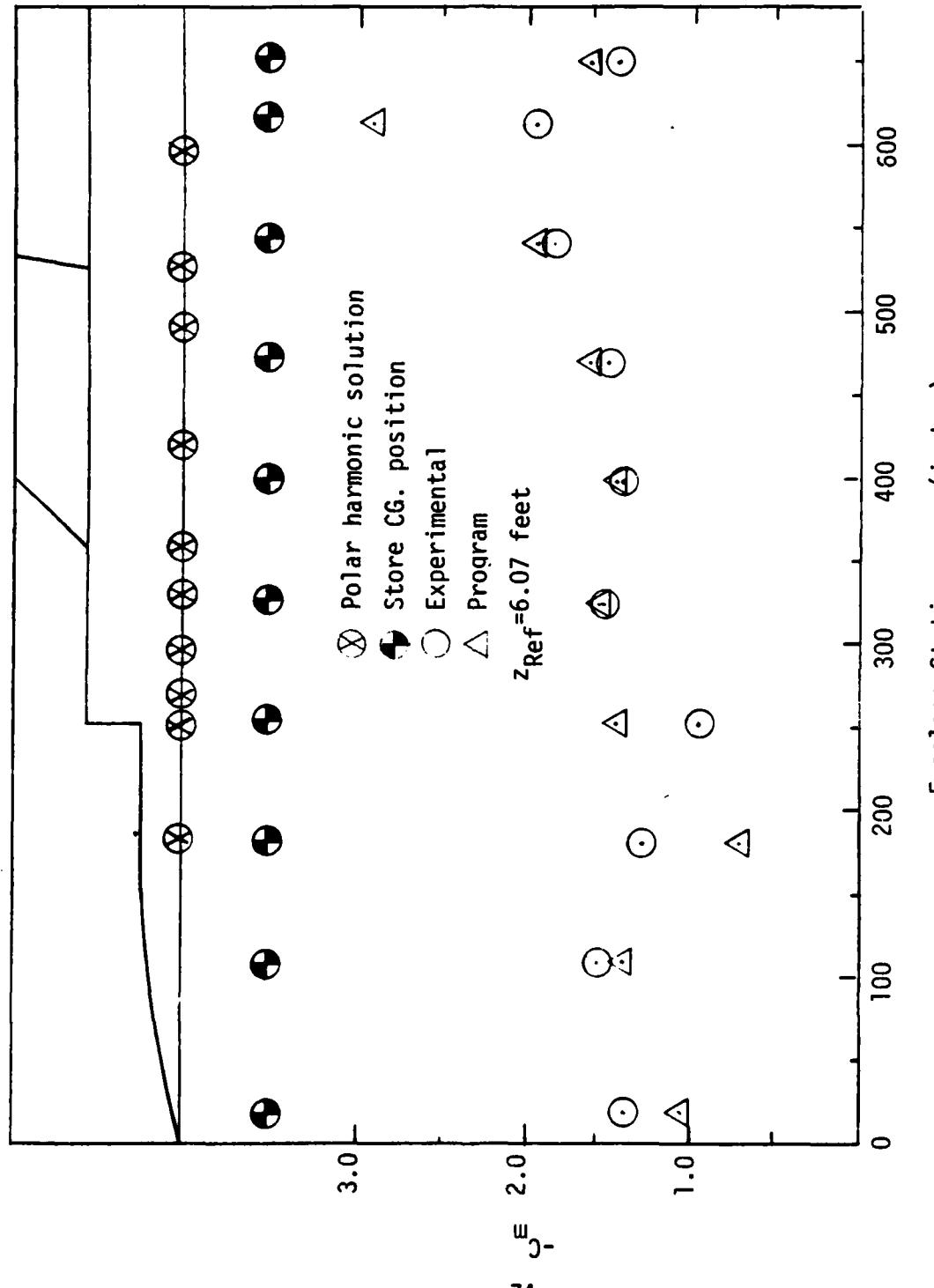
Figure 18. Run Sequence 2, C_m, Mach=0.6, y_{Ref}=3 feet

⊗ Polar harmonic solution
◐ Store CG. position
◯ Experimental
△ Program

z_{Ref}=6.07 feet

Fuselage Station - x_B (inches)

$-C_m$
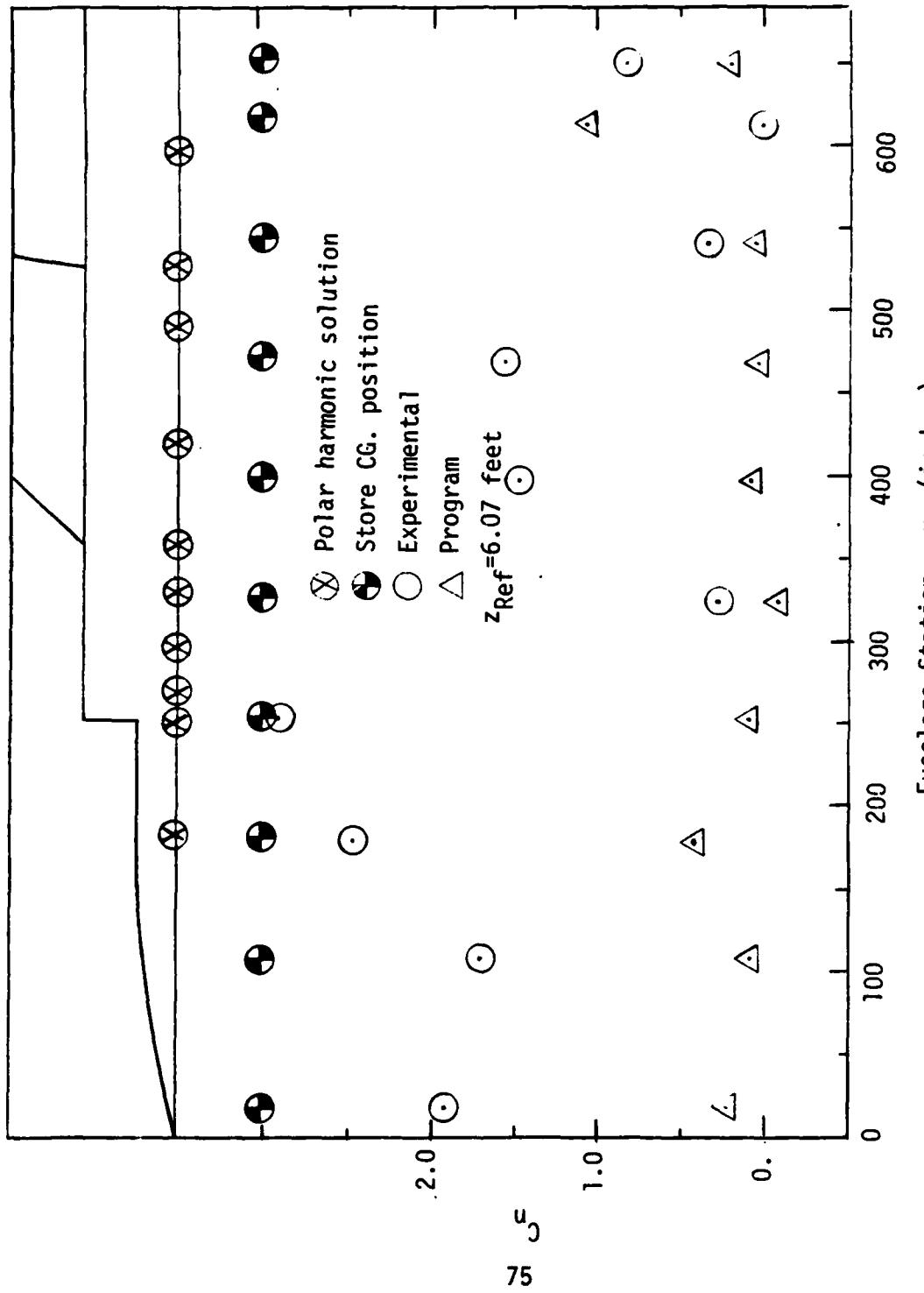
Figure 19. Run Sequence 2, C_n, Mach=0.6, y_{Ref}=3 feet
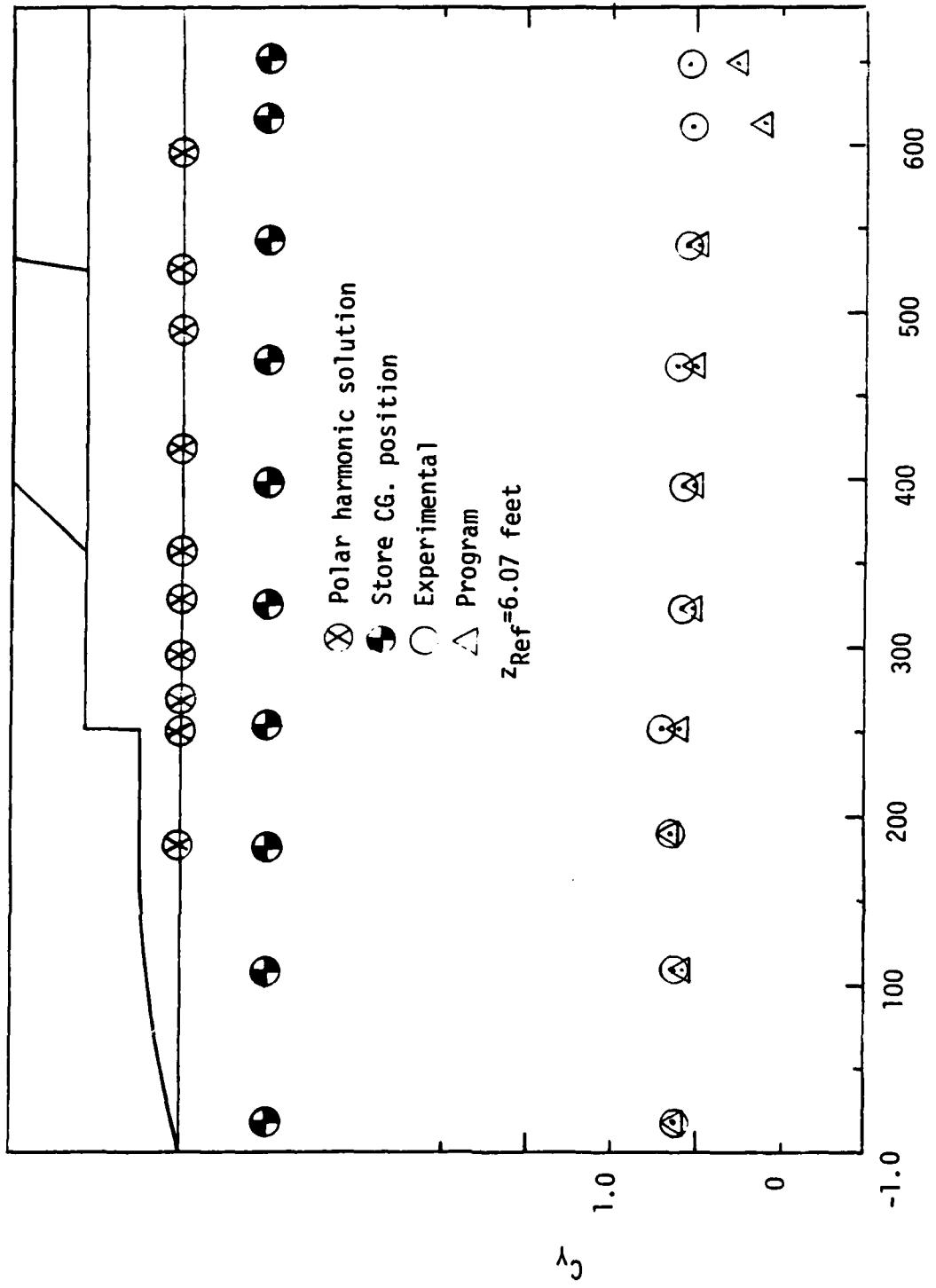
Figure 20. Run Sequence 2, C_Y, Mach=0.6, y_{Ref}=3 feet

Fuselage Station - x_B (inches)

$\bigotimes$ Polar harmonic solution
$\bigoplus$ Store CG. position
$\bigcirc$ Experimental
$\triangle$ Program
z_{Ref}=6.07 feet

C_Y
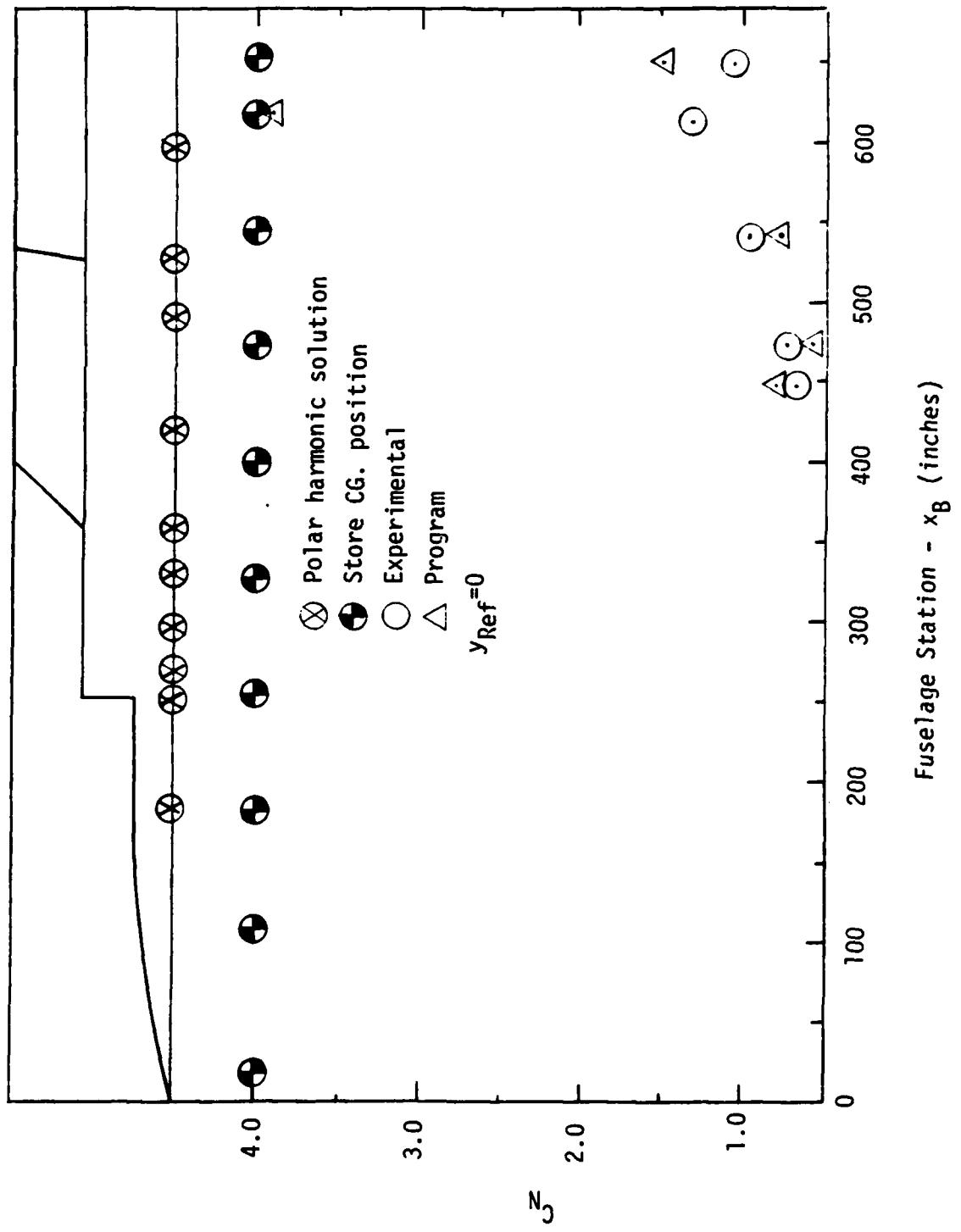
Figure 21. Run Sequence 3, C_N, Mach=0.6, z_{Ref}=3.82 feet

Fuselage Station - x_B (inches)

$\otimes$ Polar harmonic solution
$\oplus$ Store CG. position
$\bigcirc$ Experimental
$\triangle$ Program

y_{Ref}=0

C_N

77
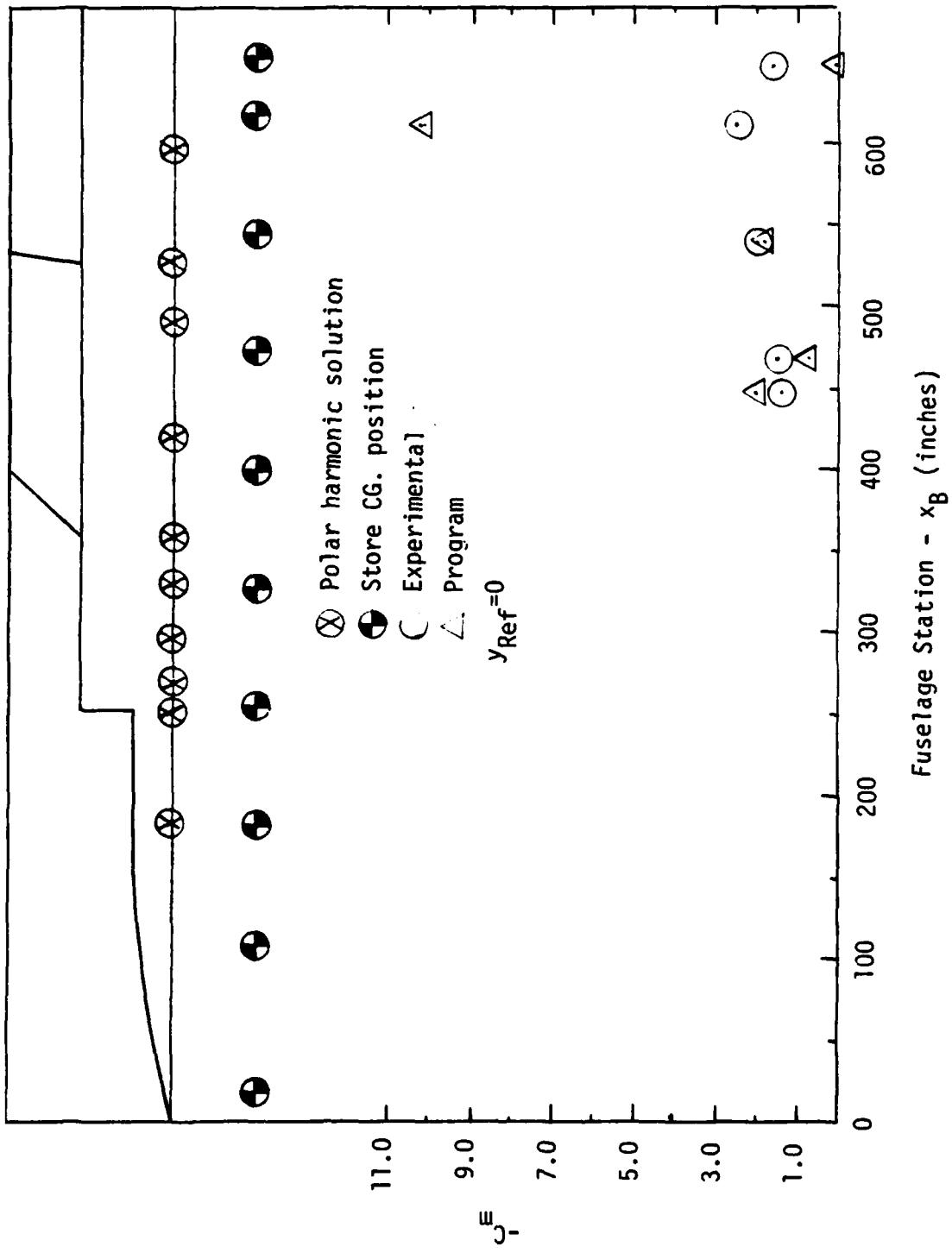
Figure 22. Run Sequence 3, C_m, Mach=0.6, z_{Ref}=3.82 feet
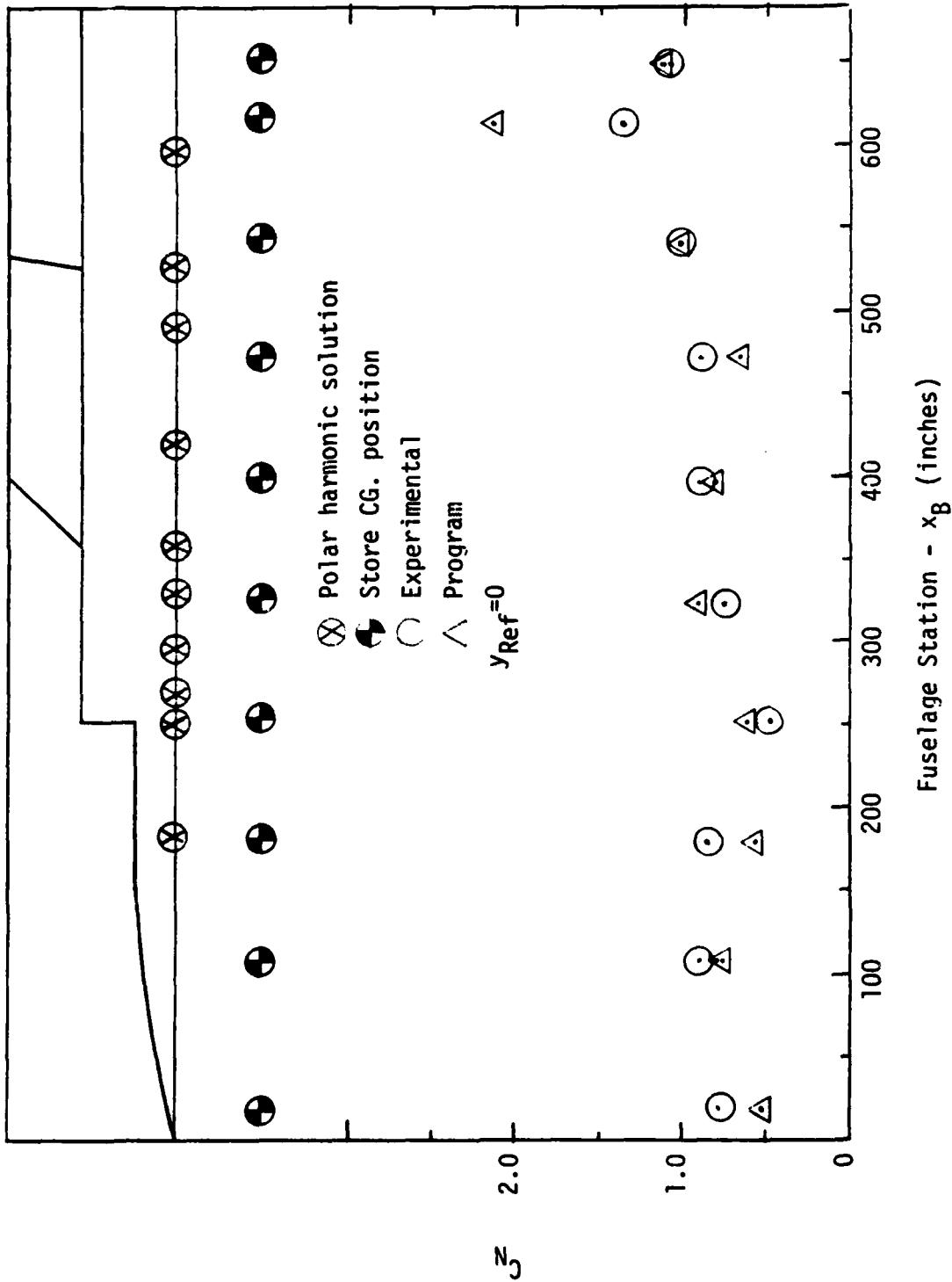
Figure 23. Run Sequence 4, C_N, Mach=0.9, z_{Ref}=6.07 feet
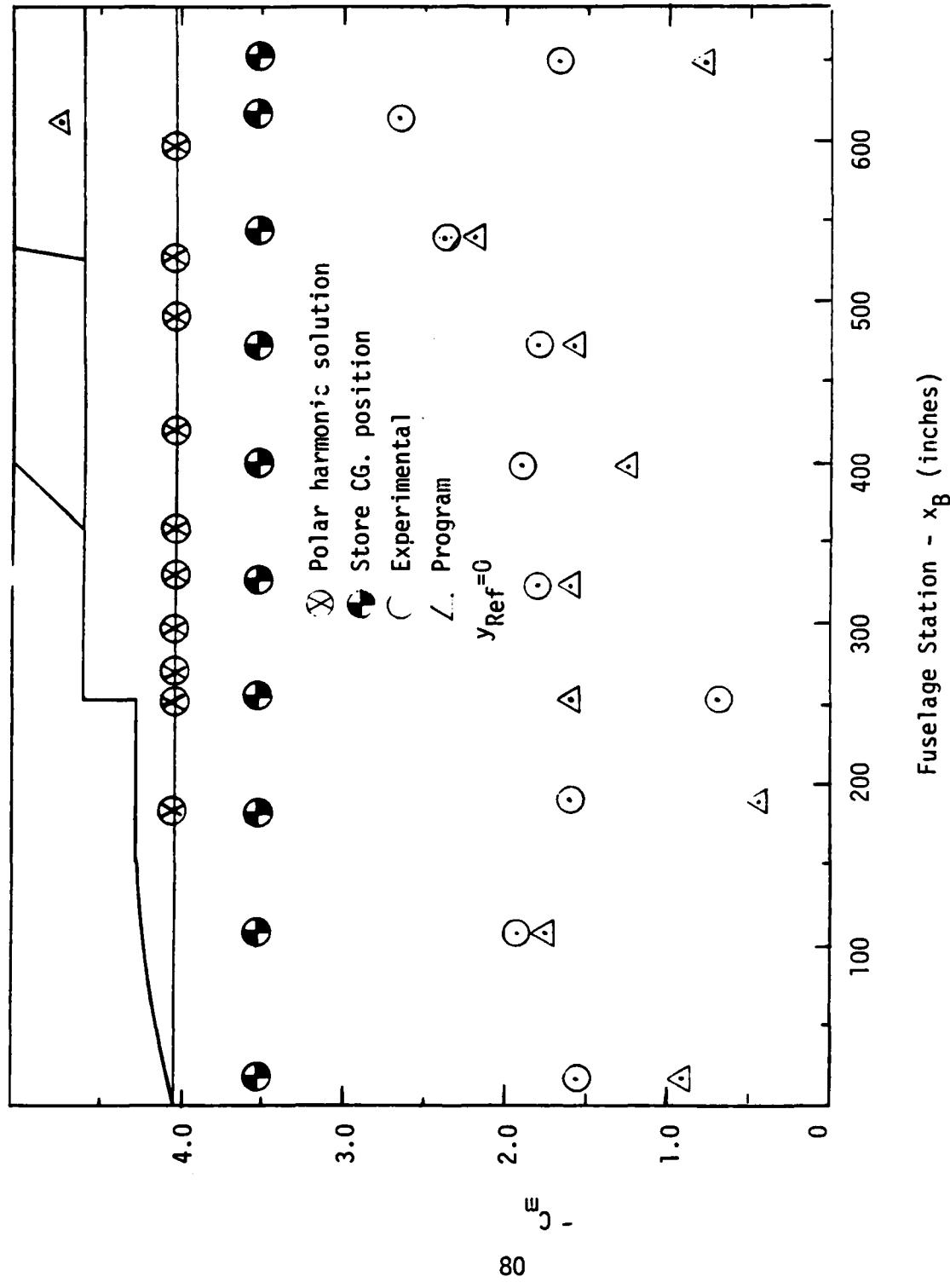
Figure 24. Run Sequence 4, C_m, Mach=0.9, z_{Ref}=6.07 feet

VII. CONCLUSIONS AND RECOMMENDATIONS

An advanced fighter design was successfully modeled using the Nielsen store separation and trajectory program. This model was used to determine the loads on a single store at various positions under the aircraft fuselage. Results of the program prediction were compared with wind tunnel values.

The computer model was a potential flow model, with a variation to account for a non-circular crosssection fuselage. Only the wing, fuselage, and two stores were modeled; however, the program could be used to analyze up to ten stores with appropriate pylons and racks.

As a result of generating the computer model and using it to predict the forces and moments on a store, the following conclusions were reached:

1. The Nielsen program can predict the forces and moments on a separated store. For the region of interest, where the program is optimized, the prediction accuracy was within ten percent of wind tunnel results. The region of interest, at Mach number 0.6, was under that portion of the fuselage centerline which is occupied by the wing. For the same region of interest, but Mach number 0.9, the prediction accuracy decreased. For this case, results are only within 28% of experimental values.

2. The generation of the program input requires considerable knowledge and experience. Flow regions of interest must be selected for optimization. This requires a knowledge of possible store carriage requirements as well as store free fall characteristics. Parameter values within the program input must be selected with very little guidance given for how the selection should be made.

3. The program is easy to use once the model is generated. Various store positions and trajectories can be studied with few changes required in the input.

The Nielsen approach to the store trajectory problem has been exercised, and the following areas were identified for further study:

1. The selection of the optimum number of polar harmonic coefficients to describe the non-circular fuselage is a major area of interest. The methods for selection have been discussed and an extension of these methods was used to select the numbers for this report. Other models should be generated and analyzed to increase confidence in the process.

2. In order to build confidence in the program it should be used to model other aircraft; however, caution should be exercised when using the program to generate

data on an unknown aircraft design. The model should

be generated for a low subcritical Mach number. This

model should then be applied to a store of known char-

acteristics and at a store position away from the air-

craft. The store should then be studied at numerous

positions to determine the limits of the program at

that Mach number. Other Mach numbers should be ana-

lyzed in the same manner to determine the Mach number

limits. This procedure should be used to build con-

fidence in the program prior to analysis of a store of

interest. For this report, confidence in the program

was achieved by comparison with experimental results.

3. The effort required to generate the model input could

be cut by writing additional programs. The automated

calculation of crossflow coordinates and slopes for

the polar harmonic coefficients would save time. A

program to plot the source generated shape and the real

shape would help to visualize the accuracy of the source

program. The programs would save time and effort, but

not necessarily increase program accuracy.

The Nielsen approach to the store separation and trajectory problem

can provide the information required to determine what happens to a

END

FILMED
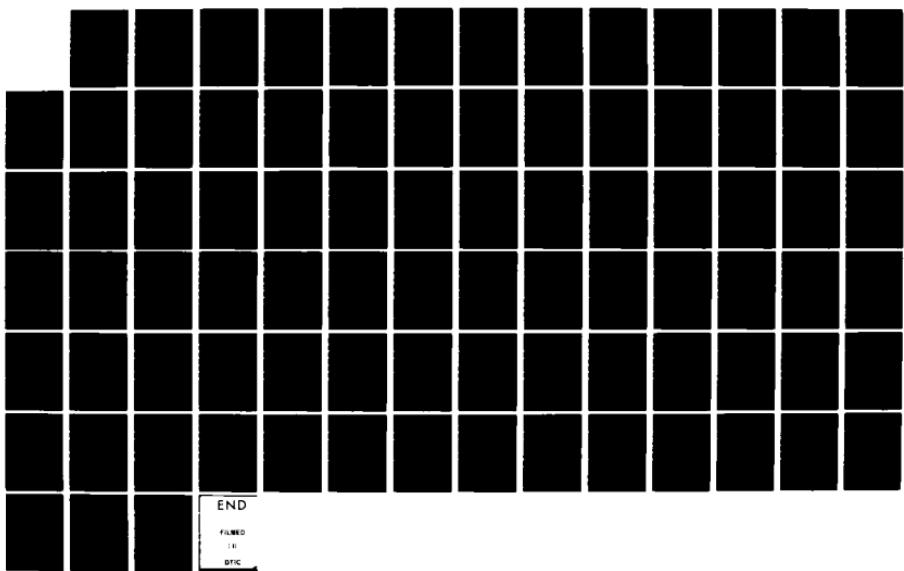
DTIC
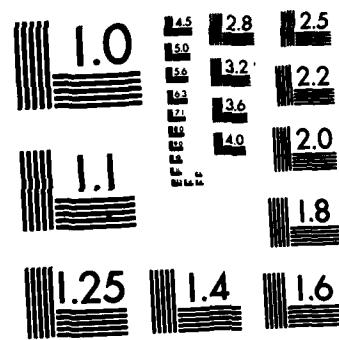
MICROCOPY RESOLUTION TEST CHART

NATIONAL BUREAU OF STANDARDS-1963-A

weapon when it is released from an aircraft. The program input, once generated, is easy to use and minimum changes are required to study various store positions and trajectories.

BIBLIOGRAPHY

1. Goodwin, F.K., Nielsen, J.N., and Dillenius, M.F.E., <u>A Method for Predicting Three-Degree-of-Freedom Store Separation Trajectories at Speeds up to the Critical Speed</u>, Tech. Rept., AFFDL-TR-71-81, July 1971.

2. Goodwin, F.K., Dillenius, M.F.E., and Nielsen, J.N., <u>Prediction of Six-Degree-of-Freedom Store Separation Trajectories at Speeds up to the Critical Speed, Vol. I - Theoretical Methods and Comparisons with Experiment</u>, Tech. Rept., AFFDL-TR-72-83, Vol. I, 1972.

3. Goodwin, F.K. and Dillenius, M.F.E., <u>Prediction of Six-Degree-of-Freedom Store Separation Trajectories at Speeds up to the Critical Speed, Vol. II - Users Manual for the Computer Program</u>, Tech. Rept., AFFDL-TR-72-83, Vol. II, 1973.

4. Dillenius, M.F.E., Goodwin, F.K., and Nielsen, J.N., <u>Extension of the Method for Predicting Six-Degree-of-Freedom Store Separation Trajectories at Speeds up to the Critical Speed to Include a Fuselage with Noncircular Cross Section, Vol. I - Theoretical Methods and Comparisons with Experiment</u>, Tech. Rept., AFFDL-TR-74-130, Vol. I, 1974.

5. Dillenius, M.F.E. Goodwin, F.K., <u>Extension of the Method for Predicting Six-Degree-of-Freedom Store Separation Trajectories of Speeds up to the Critical Speed to Include a Fuselage with Noncircular Cross Section, Vol. II - Users Manual for the Computer Programs</u>, Tech. Rept., AFFDL-TR-74-130, Vol. II, 1974.

6. Ashley, H. and Landahl, M., <u>Aerodynamics of Wings and Bodies</u>, Addison-Wesley Publishing Co., Inc., Reading, Mass., 1965.

7. Nielsen, J.N., <u>Missile Aerodynamics</u>, McGraw-Hill Book Co., Inc., New York, NY, 1960.

8. Vallentine, H.R., <u>Applied Hydrodynamics</u>, Plenum Press, New York, NY, 1967.

9. Wylie, C.R., Jr., <u>Advanced Engineering Mathematics</u>, McGraw-Hill Book Co., Inc., New York, NY, 1960, pp 177-178.

BIBLIOGRAPHY (Cont'd.)

10. Milne-Thomson, L.M., Theoretical Hydrodynamics, Fifth ed., The
    MacMillan Company, New York, NY, 1968, pp 364-368.

11. Glauert, H., The Elements of Airfoil and Airscrew Theory, MacMillan
    Press, 1943, Chapter 12, pp 156-160.

12. Fernandes, F.D., A Method for Predicting Interference Forces and
    Moments on Aircraft Stores at Subsonic Speeds, Paper presented
    at Aircraft/Stores Compatibility Symposium, Eglin Air Force Base,
    Florida, November 19-21, 1969.

13. Liepmann, H.W. and Roshko, A., Elements of Gasdynamics, John Wiley
    & Sons, Inc., New York, 1957, Chapter 9, pp 248-251.

14. Etkin, B., Dynamics of Flight, John Wiley & Sons, Inc., New York,
    NY, 1959, pp 100-103.

15. Data Package: A Wind Tunnel Test of Advanced Aircraft Configura-
    tions and Various Weapons at Mach Numbers From 0.6 to 1.6, (U),
    Confidential Report, AEDC-TSR-79-P69, D.A. Vore, November 1979,
    (Unclassified Tabulated Data Used).

16. Texas Instruments Incorporated, Learning Center, Sourcebook for
    Programmable Calculators, McGraw-Hill Book Co., New York, NY,
    1979.

17. Abbott, I.H. and VonDoenhoff, A.E., Theory of Wing Sections, Dover
    Publications, Inc., New York, NY, 1959.

18. USAF Stability and Control Datcom, Air Force Flight Dynamics Lab-
    oratory, Flight Control Division, Wright-Patterson Air Force
    Base, Ohio, October 1960, revised April 1978.

Appendix A

Wind Tunnel Data

DIMENSIONS IN INCHES
FULL SCALE (MODEL SCALE)
BASIC CONFIGURATION CODE:

SHORT BODY, FLOW-THRU NACELLE

392.7 (19.64)

677 (33.85)
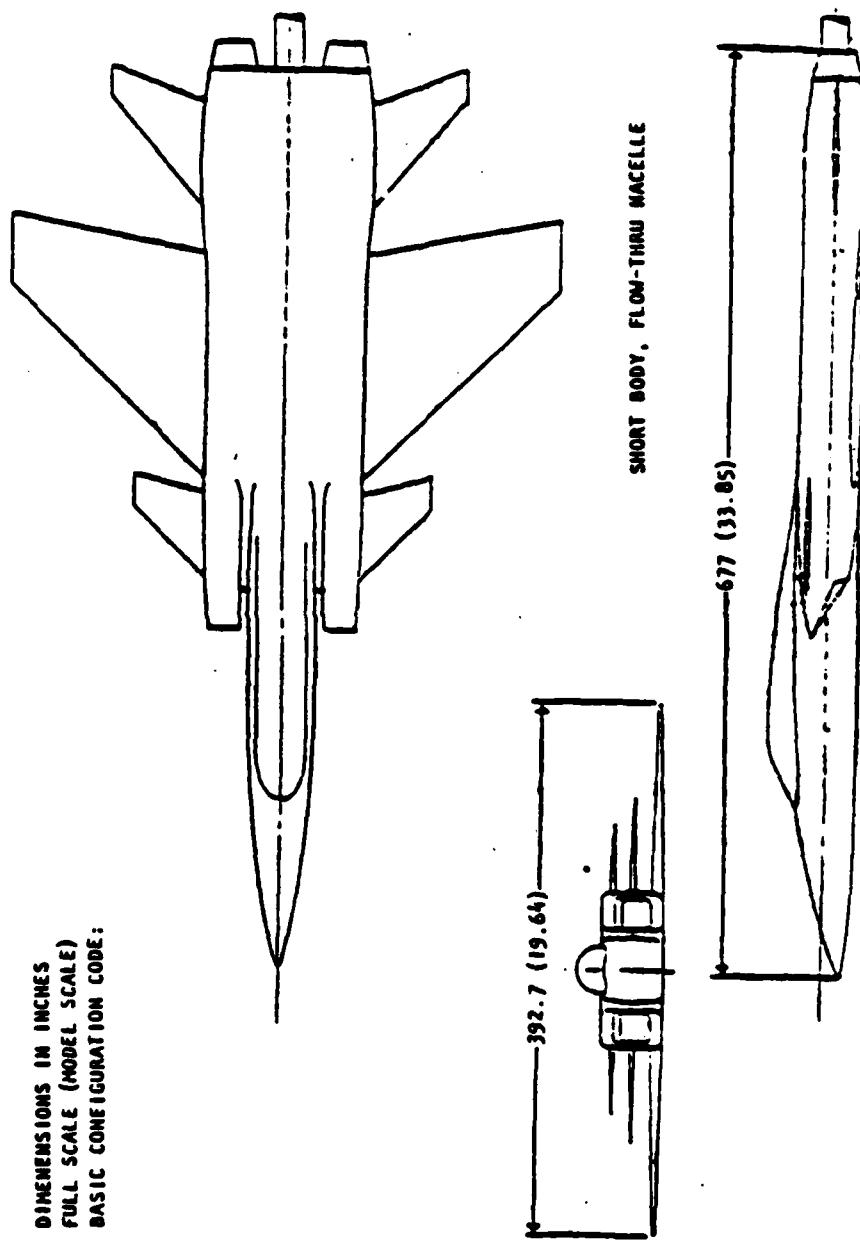
Figure 25. Aircraft Configuration

(Ref 15)

88

Table 2

Fuselage Equivalent Body of Revolution (EBR)

Fuselage Station (inches)		Total Area (in^2) (uncorrected)	Radius EBR (in^2) (corrected)
0 (nose)		0.0	0.0
25		203.14	8.041
50		493.97	12.54
75		801.6	15.97
100		1126.4	18.94
123		1434.7	21.37
130		1580.1	22.43
155		2172.9	26.3
182		2438.9	27.86
209		2445.2	27.9
237		2415.8	27.73
246		2311.3	27.12
267	Corrected	4127.1	31.95
297	Area Reduced by	4390.0	33.23
327	921 in^2	4914.2	35.65
357		5010.0	36.08
417		5000.0	36.03
457		4979.9	35.94
487		4965.7	35.88

Fuselage Station (inches)	Total Area (in^2) (uncorrected)	Radius EBR (in^2) (corrected)
522	5052.1	36.26
556	5131.7	36.61
592	5119.4	36.56
632	4098.8	31.8
657	3821.0	30.38
677	1060.0	6.84

Table 3

Equivalent Body of Revolution - Polynomial Coefficients

		C_1	C_5	C_6
Station	0 - 75	$0.0001497 + 0.355x - 1.279x^2$		
	75 - 155	$0.0098898 + 0.127118x$		
	155 - 246	$0.03729 + 0.007463x$		
	246 - 327	$-0.1122185 + 0.662765x - 0.666058x^2$		
	327 - 592	$0.051765 + 0.002558x$		
	592 - 657	$0.1355 - 0.09326x$		
	657 - 682.8	$1.1766 - 1.1666x$		

Aircraft

Test Conditions

Mach = 0.6

Total Temperature = 100.3°F

Total Pressure   = 1598.2 psi

q_∞ = 314.6 lbf/ft^2

Fuselage angle of attack = 2.5°

Flight path angle   = 0.0°

Mach = 0.9

Total Temperature = 99.6°F

Total Pressure   = 1271.9 psi

q_∞ = 427.1 lbf/ft^2

Run Sequence 1

Mach = 0.6

y_{Ref} = 0

z_{Ref} = 6.07 feet below fuselage reference line (FRL)

x_{Ref} (feet)	C_N	C_m	Part Number
1.51	0.726	-0.160	2393
9	0.795	-0.179	2387
15	0.705	-0.138	2381
21	0.498	-0.105	2375
27	0.743	-0.194	2369
33	0.79	-0.162	2363
39	0.78	-0.176	2354
45	0.911	-0.218	2348
51	1.086	-0.238	2342
54	0.957	-0.174	2339

Note: Part Number refers to an experimental run number.

Run Sequence 2

Mach = 0.6

y_{Ref} = 3.0 feet

z_{Ref} = 6.07 feet below FRL

x_{Ref} (feet)	C_N	C_m	C_Y	C_n	C_ℓ	Part Number
1.51	0.771	-0.165	0.131	-0.227	0.023	2393
9	0.809	-0.182	0.13	-0.201	0.025	2389
15	0.746	-0.15	0.153	-0.289	0.024	2383
21	0.550	-0.112	0.203	-0.346	0.025	2377
27	0.709	-0.181	0.095	-0.034	0.025	2371
33	0.775	-0.169	0.082	-0.173	0.022	2365
39	0.784	-0.177	0.119	-0.182	0.025	2356
45	0.906	-0.214	0.066	-0.04	0.024	2350
51	1.045	-0.229	0.021	-0.001	0.023	2344
54	0.924	-0.172	0.044	-0.097	0.022	2341

Run Sequence 3

Mach = 0.6

$y_{Ref} = 0$

z_{Ref} = 3.82 feet below FRL

x_{Ref} (feet)	C_N	C_m	Part Number
37.22	0.670	-0.167	2357
39	0.724	-0.175	2354
45	0.951	-0.236	2348
51	1.312	-0.294	2342
54	1.045	-0.148	2339

Run Sequence 4

Mach = 0.9

y_{Ref} = 0.0

z_{Ref} = 6.07 feet below FRL

x_{Ref} (feet)	C_N	C_m	Part Number
1.51	.786	-0.184	2616
9	.898	-0.228	2610
15	.860	-0.188	2604
21	.481	-0.084	2598
27	.751	-0.216	2592
33	.896	-0.224	2586
39	.891	-0.213	2580
45	1.024	-0.28	2574
51	1.305	-0.314	2568
54	1.088	-0.198	2565

DIMENSIONS IN INCHES

1.750

0.75D

6.375

1.00

45°
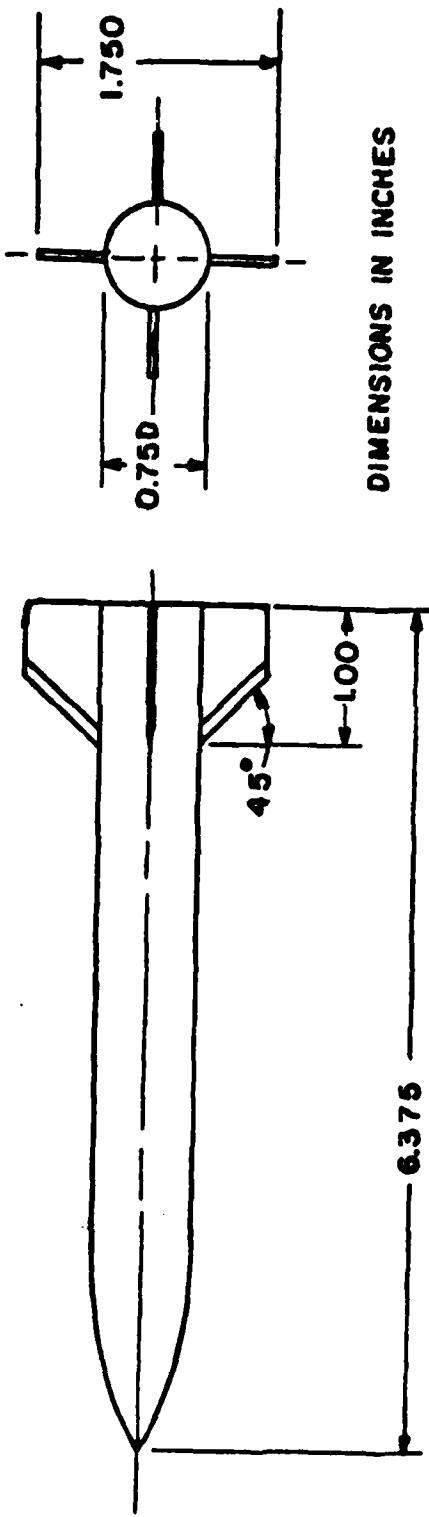
Figure 26. Store Configuration
(Ref 14)

Store

$I_{xx} = 5.4$ slug-ft^2

$I_{yy} = 157.5$ slug-ft^2

$I_{zz} = 157.5$ slug-ft^2

$I_{xy} = I_{xz} = I_{yz} = 0$

CG location (fus. Sta. ft) = 5.3125 ft

Length = 10.625 ft

Body Diameter = 0.625 ft

Fin Semi-Span = 1.45833 ft

Appendix B

Source Program Input, Output

98

Source Input (Ref 5:10-16)

The input deck for the aircraft will be developed. The input for the ogive store is included for reference (figure 27). The program input format is also included (see figure 28).

Item 1 NCARDS=3

Item 2 See figure 27. The data from these cards is not used directly by the program.

Item 3 NSECT=7 $1 < NSECT \leq 7$

Item 4 NSECT values of the end points of the polynomials used.

Item 5 Polynomial coefficients, see figure 27.

Item 6 (listed below)

XSFST = .001, recommended value, x/ℓ

XSLAST = 1.00357 End of body, including wake, x/ℓ

XRMAX = 0.771 point of maximum radius, x/ℓ

XINIT = 0.01 x/ℓ

XFINAL= 1.0 x/ℓ

DELX = 0.02, recommended value

RMAX = 0.54 maximum radius, r/ℓ

Item 7 NRAT=5, $1 < NRAT \leq 5$

This item should not be confused with item 3. NRAT refers

to the number of segments into which the body will be divided for the specification of the source distribution. The segments need not coincide with the NSECT segments except at the end of the body; the segments of NRAT must cover the entire length of the body to be modeled, figure 12.

Item 8　See figure 27.　NRAT values of segment end points

Item 9　NRAT values of PERCR.　PERCR is input as a fraction of the local body radius of the segment.　A value of 0.9 would mean that the source spacing in that segment would be 0.9 times the local radius.

```
3
SOURCE--PROGRAM AWECS
CASE 1   V/(VINLET) = .862
MACH NUMBER    = .6
7   .5
.111      .229     .363    .483    .874    .97      1.0086      ITEM 1
.0001437                           .355    -1.273               ITEM 2
.00989                             .12712                       ITEM 3
.03729                             .007463                      ITEM 4
-.11222                            .66277  -.6651               ITEM 5
.051765                            .002558
.1355                              -.09326
1.1766                             -1.1666
.001      1.00357  .771    .01     1.      .02      .054        ITEM 6
5                                                               ITEM 7
.229      .363     .483    .874    1.00857                      ITEM 8
1.        1.       .9      .3      .4                            ITEM 9
```

(a) Page 1

Figure 27. Source Program Input

101

ITEM 1
ITEM 2
ITEM 3
ITEM 4
ITEM 5

ITEM 6
ITEM 7
ITEM 8
ITEM 9

1
OG:VEC
3   .6
.2353   1.
-.4413   -1.
.C5F72
-.4413   -1.
.C02   1.23

1
1.2353
.7

1.2353
.4706   .1.47

2.   -.7447
.353   .J1   1.23

.J2   1.   1.
.C5342

(b) Page 2

Figure 27. Continued

Figure 28. Source Program Input Format

(a) Page 1

(Ref 5: 61)

Item No. 7 (1 card)

Variable	NRAT
Card Column	5
Format Type	I

Item No. 8 (1 card)

Variable	REND(1)	REND(2)	...	REND(NRAT)	
Card Column	10	20	30	40	50
Format Type	F	F	F	F	F

Item No. 9 (1 card)

Variable	PERCR(1)	PERCR(2)	...	PERCR(NRAT)	
Card Column	10	20	30	40	50
Format Type	F	F	F	F	F

(b) Page 2

Figure 28. Concluded

104

SOURCE-PROGRAM AMECS
CASE 1   V/(VINLET) = .262
MACH NUMBER = .6

X/L OF END POINT OF EACH SECTION OF BODY

SECTION	1	2	3	4	5	6	7
X/L	.11100	.22100	.35300	.43700	.37400	.97000	1.00 60

COEFFICIENTS OF POLYNOMIAL DESCRIBING EACH SECTION

SECTION	C1	C2	C3	C4	C5	C6	C7
1	.00015	0.00000	0.00000	0.00000	.35500	-1.27900	0.00000
2	.00086	0.00000	0.00000	0.00000	.12712	0.00000	0.00000
3	.03725	0.00000	0.00400	0.00000	.00745	0.00000	0.00000
4	-.11022	0.00005	0.07000	0.00000	.66277	-.66610	0.00000
5	.05177	0.00000	0.00000	0.00000	.00256	0.00000	0.00000
6	.13550	0.00000	0.00000	0.00000	-.00326	0.00000	0.00000
7	1.17660	0.00000	0.00000	0.00000	-1.15660	0.00000	0.00000

FIRST SOURCE AT X/L=   .00100

FROM .00100 TO .22100 SOURCE SPACING IS 1.00000 TIMES LOCAL RADIUS
FROM .22100 TO .35300 SOURCE SPACING IS 1.00000 TIMES LOCAL RADIUS
FROM .35300 TO .43700 SOURCE SPACING IS .50000 TIMES LOCAL RADIUS
FROM .43700 TO .87400 SOURCE SPACING IS .30000 TIMES LOCAL RADIUS
FROM .87400 TO 1.00057 SOURCE SPACING IS .40000 TIMES LOCAL RADIUS

(a) Page 1

Figure 29.   Source Program Output

SOURCE LOCATIONS AND BODY RADIUS AND SURFACE SLOPE AT THESE LOCATIONS

X/L	.00130	.00145	.00192	.00255	.00343	.00451	.00556
R/L	.00050	.00065	.00083	.00106	.00135	.00172	.00217
DR/DX	.35244	.35141	.35004	.34543	.34524	.34347	.33995
X/L	.00764	.00947	.01261	.01625	.02072	.02627	.03315
R/L	.00275	.00353	.00445	.00555	.00696	.00860	.01050
DR/DX	.33546	.32575	.32253	.31342	.30200	.26777	.27013
X/L	.04157	.05173	.06330	.07755	.09351	.11166	.13095
R/L	.01270	.01503	.01755	.02004	.02221	.02403	.02654
DR/DX	.24056	.22267	.17173	.15575	.11475	.12712	.12712
X/L	.15217	.17555	.20133	.22571	.25092	.29231	.32387
R/L	.02923	.03221	.03545	.03900	.03924	.03947	.03971
DR/DX	.12712	.12712	.12712	.00746	.00746	.00746	.00746
X/L	.35565	.38751	.41172	.45472	.48175	.50447	.51720
R/L	.03994	.04450	.04461	.05143	.05302	.05306	.05302
DR/DX	.00740	.14640	.10362	.05693	.03255	.00256	.00256
X/L	.32555	.54263	.55545	.56822	.58099	.59377	.60655
R/L	.05312	.05315	.05319	.05322	.05325	.05328	.05332
DR/DX	.00256	.00256	.00256	.00256	.00256	.00256	.00255
X/L	.61935	.63216	.64497	.65777	.67061	.68345	.65627
R/L	.05335	.05338	.05341	.05345	.05349	.05351	.05355
DR/DX	.00256	.00256	.00256	.00256	.00256	.00256	.00256
X/L	.70914	.72200	.73487	.74774	.76063	.77352	.78642
R/L	.05358	.05361	.05364	.05363	.05371	.05374	.05377
DR/DX	.00256	.00256	.00256	.00256	.00256	.00256	.00256
X/L	.79932	.81224	.82516	.83809	.85103	.86397	.87693
R/L	.05381	.05384	.05387	.05391	.05394	.05396	.05372
DR/DX	.00256	.00253	.00256	.00255	.00255	.00256	-.05326
X/L	.88412	.91077	.92697	.94267	.95783	.97267	.98607
R/L	.05211	.05056	.04705	.04755	.04517	.04162	.02627
DR/DX	-.05325	-.05326	-.05326	-.09326	-.05326	-1.16669	-1.16660
X/L	.59447	.99374	1.00303				
R/L	.01645	.01031	.00646				
DR/DX	-1.16660	-1.16662	-1.16660				

(b) Page 2

Figure 29. Continued

106

FOR THIS CASE THERE ARE 73 SOURCES

INCOMPRESSIBLE SOURCE DISTRIBUTION FOR MACH NUMBER .63

| X/L | 1.0000E-03 | 1.4327E-03 | 1.9129E-03 | 2.5795E-03 | 3.4254E-03 | 4.5060F-03 |
| Q | 1.3113F-06 | -1.1440F-06 | 7.5553E-37 | -3.9047E-07 | 3.7451E-37 | 6.4563F-05 |

| X/L | 5.6547E-03 | 7.6403F-03 | 9.6731E-03 | 1.2633E-02 | 1.6253F-02 | 2.0719F-02 |
| Q | 4.2065E-07 | 4.2557E-07 | 3.4777E-07 | 1.2453E-05 | 2.0196F-06 | 3.0673F-06 |

| X/L | 2.6243E-02 | 3.3150E-02 | 4.1573E-02 | 5.1731E-02 | 6.3604E-02 | 7.7978E-02 |
| Q | 4.6365E-06 | 6.7354E-06 | 9.4145E-06 | 1.2410E-05 | 1.5147E-05 | 1.6445E-05 |

| X/L | 9.5310E-02 | 1.1194E-01 | 1.3455E-01 | 1.5217E-01 | 1.7556E-01 | 2.0133F-01 |
| Q | 1.5249E-05 | 3.1104F-06 | 4.0501E-05 | 1.1094E-05 | 4.6308E-05 | 2.9016E-05 |

| X/L | 2.2971E-01 | 2.6152E-01 | 2.9231E-01 | 3.2335F-01 | 3.5565E-01 | 3.8761F-01 |
| Q | 1.2131E-04 | -1.5331E-04 | 1.5332E-04 | -1.3135E-04 | 7.7127E-05 | 1.3654E-04 |

| X/L | 4.1172E-01 | 4.5472E-01 | 4.8175E-01 | 5.0447E-01 | 5.1720E-01 | 5.2995E-01 |
| Q | 1.4433E-05 | 4.7631E-05 | -7.3121E-05 | 4.1321E-05 | 6.0785E-06 | -3.4747F-05 |

| X/L | 5.4259E-01 | 5.5345F-01 | 5.6622E-01 | 5.8033E-01 | 5.9377E-01 | 6.0656F-01 |
| Q | 4.5635E-05 | -5.1226E-05 | 5.3282E-05 | -5.3167E-05 | 5.3446E-05 | -5.2519E-05 |

| X/L | 6.2135E-01 | 6.3216E-01 | 6.4497E-01 | 6.5773E-01 | 6.7061E-01 | 6.8345F-01 |
| Q | 5.2314F-05 | -4.3240F-05 | 4.1641E-05 | -2.0473E-05 | -3.1130E-05 | 1.7284E-04 |

| X/L | 6.9629E-01 | 7.0314E-01 | 7.2200E-01 | 7.3447E-01 | 7.4774E-01 | 7.6063E-01 |
| Q | -5.3512F-04 | 1.4463E-03 | -3.4397E-03 | 7.2574E-03 | -1.1974E-02 | 1.5692E-02 |

| X/L | 7.7352E-01 | 7.4542E-01 | 7.5932E-01 | 8.1224E-01 | 8.2516E-01 | 8.3809E-01 |
| Q | -1.7671E-02 | 1.4516F-02 | -1.6793E-02 | 1.8965E-02 | -1.8613E-02 | 1.7113E-02 |

| X/L | 4.5103E-01 | 5.6357E-01 | 8.7653E-01 | 8.9412E-01 | 9.1079E-01 | 9.2697F-01 |
| Q | -1.5355E-02 | 1.4220E-02 | -9.2335F-03 | 5.4614E-03 | -4.3810E-03 | 5.1440E-03 |

| X/L | 9.4267E-01 | 9.5720E-01 | 9.7267E-01 | 9.8607E-01 | 9.9447E-01 | 9.9974E-01 |
| Q | -5.3044E-03 | 5.3117E-03 | -3.6116E-03 | 1.4390E-03 | -7.0358E-04 | 3.6572E-04 |

| X/L | 1.0036E+00 |
| Q | -2.1207E-04 |

(c) Page 3

Figure 29. Continued

107

SHAPE CALCULATED FROM SOURCE DISTRIBUTION AND POLYNOMIALS

X/L	.01000	.03000	.05000	.07000	.09000	.11000	.13000
R/L(S.D.)	.00422	.00941	.01497	.01989	.02189	.02335	.02631
R/L(POLY)	.00557	.00965	.01470	.01973	.02174	.02372	.02542

X/L	.15000	.17000	.19000	.21000	.23000	.25000	.27000
R/L(S.D.)	.02995	.03143	.03412	.03660	.03902	.03987	.03524
R/L(POLY)	.02996	.03152	.03414	.03655	.03701	.03915	.03731

X/L	.29000	.31000	.33000	.35000	.37000	.39000	.41000
R/L(S.D.)	.03737	.04031	.03945	.03766	.04235	.04567	.04733
R/L(POLY)	.03745	.03984	.03775	.03590	.04192	.04495	.04754

X/L	.43000	.45000	.47000	.49000	.51000	.53000	.55000
R/L(S.D.)	.05014	.05173	.05259	.05329	.05337	.05342	.05347
R/L(POLY)	.04961	.05114	.05214	.05302	.05307	.05312	.05317

X/L	.57000	.59000	.61000	.63000	.65000	.67000	.69000
R/L(S.D.)	.05353	.05358	.05350	.05366	.05371	.05376	.05362
R/L(POLY)	.05322	.05327	.05333	.05338	.05343	.05348	.05353

X/L	.71000	.73000	.75000	.77000	.79000	.81000	.83000
R/L(S.D.)	.05367	.05395	.05305	.05326	.05331	.05324	.05326
R/L(POLY)	.05358	.05363	.05366	.05373	.05373	.05344	.0538

X/L	.85000	.87000	.89000	.91000	.93000	.95000	.97000
R/L(S.D.)	.05342	.05360	.05231	.05049	.04991	.04627	.04503
R/L(POLY)	.05344	.0539	.05250	.05063	.04877	.04690	.04503

X/L	.99000
R/L(S.D.)	.03127
R/L(POLY)	.02167

1

(d) Page 4

Figure 29. Concluded

108

Appendix C

Trajectory Program Input, Output

TRAJECTORY PROGRAM INPUT

The program input consists of 46 items, figure 30. Each item will be listed; however, not all definitions will be included. Reference 5, pages 23-40, must be used along with this report. The program input format is given in figure 31.

Use of the proper coordinate system is critical in this input, and numerous errors are possible. The basic reference frame is the fuselage system, figure 32.

Item 1 NCARDS=3

Item 2 See figure 30. The information from these cards
    is not used directly by the program.

Item 3

ALFAC=2.5 (degrees), GAMF=0 (degrees),

FMACH=0.6, RHO=0.0001397 slugs/ft^3

VINF=671.2 feet/sec

These values were calculated or given in the experimental

data, see Appendix 1.

Item 4 NFU=2, NPY=0, NRACK=0

    NSTRS=2 (0≤NSTRS≤10)

Item 5

    FLTHC=56.4 feet

    FRMAX=3.05 feet

Item 6 Lists the number of sources used to describe the EBR. This number is printed at the top of page 3 of the source distribution output, figure 29, Appendix B.

Item 7 Lists the x/ℓ locations of the sources used to describe the EBR.

Item 8 Lists the non-dimensional source strengths. Item 7 and 8 are printed on page 3 of the source program output, figure 29, Appendix B.

Items 9,10,11 Apply only if NFU=1 (Ref 5:24)

Item 12

NXSTAT=10   NXSTAT$\leq$20

MC=30   MC$\leq$100

VD1NF=0.862 inlet velocity ratio

$0.0 \leq$VDVINF≤ 1.0

NXSTAT is the number of X_B station where polar harmonic solutions are to be generated.

MC is the number of control points to be used, in the range of 0° to 180° to obtain the polar harmonics. The coordinate system is shown in figure 33. Note: the origin of this system is located at the nose of the actual fuselage, see figure 32.

<u>Item 13</u> is repeated for each X_B station, NXSTAT values,

see figure 30.

XSTAT X_B location of crossflow plane

REQ radius of EBR at X_B station

DRDXC dr/dx of EBR at X_B station

MPH number of polar harmonics to be used at each X_B station

MPH$\leq$50

NOPSUR indicates if a portion of the contour is open to the

flow, see figure 34.

THOPB value of θ at which open surface begins

THOPE value of θ at which open surface begins

The values of REQ and DRDXC come from the source program

output for the fuselage.

The locations X_B were chosen by analysis of the fuselage

cross-section. The values of X_B and reasoning for each

are given in Table 4. The values of THOPB and THOPE were

found during calculations for item 14. Selection of MPH

is discussed in Chapter V. The value of MC=30 was chosen

because it gave a good range for the possible values of

MPH, and it gave a reasonable representation of the fuse-

lage cross-section without a large amount of calculations.

A computer program could be written to handle the calcula-

tions required for items 13 and 14, but for this case all

112

calculations were done by hand.

Table 4

X_B Stations for Polar Harmonics

Station (X_B) Inches/Feet	Reasoning
-182/-15.17	highest point on canopy
-246/-20.5	start of inlet
-267/-22.25	center of inlet, open to flow
-297/-24.75	end of inlet open to flow
-327/-27.25	rapidly changing cross-section
-357/-29.75	end of rapid change
-417/-34.75	point over wing
-487/-40.45	point over wing
-522/-43.5	end of wing
-592/-49.33	point aft of wing
-598/-49.83	final position so that harmonics at station 592 will be calculated

<u>Item 14</u> is repeated for each X_B station where data are to
be input. The number of cards is equal to the
number of control points MC.

$$\Delta\theta = \frac{180}{MC} = 6 \text{ degrees}$$

$$\theta_i = \frac{\Delta\theta}{2} + (i-1)\Delta\theta \quad i=1,2,\ldots,MC$$

The value of r_B was determined using the coordinate system
of figure 33 applied to the actual fuselage cross-section
at each X_B station, figure 35. The values of Y_B and Z_B
for each control point were determined from the drawing.
These coordinates were then converted into an $r_B(\theta)$. The
value of $dr_B(\theta)/d\theta$ (feet/radian) were determined from a
plot of r_B versus θ, figure 36.

Analysis of the values given in the example (Ref 5:
125) revealed that the slope at any point was determined
by $\Delta R/\Delta\theta$ applied to the points on either side of the
desired point. This worked for points where the curve
was smooth. At points with sharp corners, $\Delta R/\Delta\theta$ was
applied to the desired point and an adjacent point, see
figure 36. The choice was made to always pick the point
after the desired point as the adjacent point. Judgement

114

was required as to when the two point method was required.

Item 15

XBWOC=-28.88 feet X_B location of the wing leading

edge

ZBWO=0.333 feet Z_B location of the wing leading edge

WIC=0 incidence angle of the wing root chord rela-

tive to fuselage X_B axis.

Careful reference should be made to the algebraic signs of

the input values, figure 32. Values were taken from the

engineering drawing of the wind tunnel model.

Item 16

CRW=+13.67 (feet), SSPAN=+16.42 (feet)

Values are from engineering drawing.

Item 17

NCW=8, MSW=5 (MSW$\leq$30)

The values of NCW and MSW were those recommended (Ref 5:

27-28).

Item 18 numbers and specifies the location of each wing

(left) vortex trailing leg, figure 30. The wing

trailing and leading edge sweep angle as well as

the wing dihedral angle are also specified.

Guidelines are given (Ref 5:27-28) for the proper

positions.

115

Item 19 is associated with the wing twist and camber

NTAC=0 (no twist or camber)

NUNI=1 (omit if NTAC=0)

Item 20 is omitted if NTAC=0

Item 21 specifies the wing thickness distribution

NCWS=12 (NCWS x MSW$\leq$400)

NUNIS=1 (similar thickness distribution at all stations).

The value of NCWS=12 was chosen because data for this item

and item 22 were available, see figure 30.

Item 22 THETAL(J) - slope of the wing thickness distribu-
         tion at the centers of the thickness panels. For
         NUNIS=1 only data for the chordwise row adjacent
         to the root chord is input. The first value is
         for the panel at the leading edge.

The procedure for finding THETAL is given, (Ref 5:30-31).

The airfoil for this report was NACA, 65A005 and the data

for a NACA 65A006 airfoil (Ref 17) were scaled to provide

the required NACA 65A005 airfoil section. This airfoil

was plotted to give the required slope.

Items 23-27 are associated with the pylon if present.
             (Ref 5:31-33)

Items 28-31 are associated with the bomb rack if present.
             (Ref 5:33-34).

<u>Item 32</u>   is a deck of cards, with one card for each store, figure 30.

NUMSTR(J)   store identification number $\leq$ 99

NSHAPE(J)   store, shape identification number $\leq$ 99

SLTHC(J)   length of store, feet

SRMAY(J)   maximum radius of store, feet

XSNC(J) x_{ℓ} location of store nose relative to the wing chord leading edge immediately above the store, feet; positive ahead.

YSN(J) z_w location of the store nose measured from the fuselage centerline, feet; positive to the right.

ZSN(J)   Z location of store nose relative to the wing chord leading edge immediately above the store, feet, positive below.

SIC(J)   store incidence angle measured relative to the wing root chord, degrees; positive nose up.

The store position is input as a function of the store nose with respect to the wing of the aircraft. The incidence angle of the store is then input with respect to incidence angle of the wing. All experimental data were given with the store center of gravity (CG) located with respect to the store nose and fuselage reference line (FRL). The

117

store incidence was given with respect to horizontal. The geometry for the store location is given in figures 37 and 38.

The store was first located at a reference position. From this position the store could be moved without the need to go back through the geometry.

The reference position was chosen to match a position where experimental data were available.

X_B = -33 feet, Z = 6.08 feet (below FRL), y_B=0, α=6° Store dimensions are shown in Appendix A. For this position XSNC(J) = +2.192 feet, ZSN(J) = 4.256 feet. The geometry for ZSN(J) is shown in figure 38. The aircraft is at angle of attack 2.5°, and the wing incidence is 0°. Therefore, the store incidence with respect to the wing is 3.5°.

The calculations can be verified by the trajectory program output which gives the store CG position with respect to the nose of the aircraft.

The directions for calculation of YSN(J) are incorrect (Ref 5:34). YSN(J) is measured from the fuselage centerline. This error was discovered when the program was run with YSN(J)≠0.

<u>Item 33</u> is one card which specifies NSHPT=1, the number
of different shapes for which source distribution
are to be input.

<u>Item 34</u>

MSHAPE=1 shape number of store to be represented
by the following source data; equal to one of the
values of MSHAPE(J), item 32.

MSOR=59 number of sources from page 3 of source
output for the store

<u>Items 35,36</u>

DUMX(J) x/ℓ of store sources

DUMQ(J) source strengths

The data for items 34, 35, 36 come from a source program run
to model the store. The procedure is identical to that for
the fuselage. The complete derivation for the source input
is given in Reference 5, pages 13-13. The input deck is
given in figure 27 of this report.

<u>Item 37</u>

NEJECT=2 identification number of the store being
separated

NSEG=40 number of segments the body is to be
broken into for the force calculations:
NSEG $\leq$ 40. It was found that the best

119

results occurred when NSEG=40.

NSEGXO=40   number of segments to the flow separation loca-
            tion. The recommended value of 40 was used.

NGAM=0   trajectory to simulate a wind tunnel captive
            store

NPOLY=2   number of polynomials representing the store
            shape. The wake can carry no forces, and is
            not included.

NROLL=1   rolling moment to be calculated

NFMP=1   empennage present

NDAMP=0   no damping to be included.

Item 38 (from Ref 15)

SMASS=29.8497 slugs   store mass

FIXX=5.4 slug-ft^3

FIYY=157.5 slug-ft^3

FIZZ=157.5 slug-ft^3

FIYZ=0

FIXZ=0

FIYY=0

Item 39

XMOM=-5.3125 store position where moments are
              to be taken.

XBAR=0 x positive forward of store CG, relative
        to moment center

YBAR=0 y positive right of store CG, relative
        to moment center

ZBAR=0 z positive below of store CG, relative
        to moment center

For this case the moment center and CG are the same point.

Item 40

XEND(J) x/ℓ of end points of the polynomials
         specifying the separated store.

Item 41

COEF(J,K) coefficients of the polynomials
          representing the separated store.

The data for items 40, and 41 come directly from the source
program input, figure 27.

Item 42

CA=0.34 store axial-force coefficient, reference
         area is store cross-sectional area. CA
         was given in the experimental data.

CDC=1.2 crossflow drag coefficient, the recommended
        value was used (Ref 5:33)

Item 43

IPLNR=0   cruciform empennage

MSF=5   number of spanwise control points on each fine

MSF must be odd, $5 \leq MSF \leq 11$. The recommended

value was used.

Item 44

XTAIL=-9.57   x location on the store axis where the

empennage forces act feet, negative

RADAV=0.625   average store radius in empennage region,

feet

FINSS=1.45833 tail fin semispan, feet, positive

PHIROL=0   initial fin orientation $0 \leq PHIROL \leq 90$

CLALPH=3.1   lift-curve slope of two exposed panels

joined together, per radian. The

reference area is the store maximum

cross-sectional area.

RADAV, FIWSS, and PHIROL were taken from the experimental data,

Reference 15. CLALPH was determined using store data and

DATCOM (Ref 18:4.1.3.2-4). The reference area used in DATCOM

is the fin (wing) surface area. This must be redefined using

the store cross-sectional area.

XTAIL   was determined using DATCOM (Ref 18:4.1.4.2-3)

which calculates the aerodynamic-center location.

Item 45

This card specifies initial velocities of the store

relative to the parent aircraft. For this case all

were zero.

Item 46

DTIME = 0.5   integration time, seconds

TIMEI = 0.0   initial time in seconds

TIMEF = 0.0   final time, seconds. With TIMEI,

equal to 0.0, the forces and moments are given for the

initial position of the store.

Item 47   is used when a trajectory is being restarted.

```
         3                                                                    ITEM 1
AWECS1                                                                        ITEM 2
V/VINLET = 0.862
FLIGHT MACH = 0.6
2.5         .0          .6          .0013970   671.2                         ITEM 3
      2     0     0     2                                                     ITEM 4
56.4        3.05                                                             ITEM 5
      73                                                                     ITEM 6
 1.00000E-03 1.40274E-03 1.91886E-03 2.57981E-03 3.42543E-03 4.50600E-03     ITEM 7
 5.88469E-03 7.64027E-03 9.87014E-03 1.26933E-02 1.62531E-02 2.07185E-02
 2.62331E-02 3.31604E-02 4.15726E-02 5.17306E-02 6.38038E-02 7.78784E-02
 9.39093E-02 1.11676E-01 1.30945E-01 1.52174E-01 1.75552E-01 2.01327E-01
 2.29714E-01 2.60917E-01 2.92307E-01 3.23884E-01 3.55550E-01 3.87605E-01
 4.19717E-01 4.54719E-01 4.91745E-01 5.04471E-01 5.17204E-01 5.29945E-01
 5.42694E-01 5.55451E-01 5.63215E-01 5.80988E-01 5.93759E-01 6.06556E-01
 6.19352E-01 6.32156E-01 6.44968E-01 6.57767E-01 6.70615E-01 6.83450E-01
 6.96293E-01 7.09144E-01 7.22003E-01 7.34870E-01 7.47745E-01 7.60628E-01
 7.73513E-01 7.86417E-01 7.99323E-01 8.12237E-01 8.25150E-01 8.38090E-01
 8.51023E-01 8.63974E-01 8.76925E-01 8.94118E-01 9.10794E-01 9.26373E-01
 9.42663E-01 9.57897E-01 9.72670E-01 9.86073E-01 9.94472E-01 9.99736E-01
 1.00303E+00
 1.31125E-06-1.14398E-06 7.58930E-07-3.90870E-07 3.39510E-07 6.45626E-09     ITEM 8
 4.20647E-07 4.25565E-07 8.47773E-07 1.24532E-06 2.01363E-06 3.06734E-06
 4.63943E-06 6.73578E-06 9.41491E-06 1.24099E-05 1.51972E-05 1.64853E-05
 1.52490E-05 3.11043E-08 4.05010E-05 1.10939E-05 4.63076E-05 2.90156E-05
 1.01314E-04-1.33811E-04 1.33325E-04-1.31349E-04 7.71259E-05 1.36544E-04
 1.44325E-05 8.76310E-05-7.31210E-05 4.13205E-05 6.07353E-06-3.47470E-05
 4.66945E-05-5.12255E-05 5.32920E-05-5.31670E-05 5.39455E-05-5.25186E-05
 5.23142E-05-4.82799E-05 4.18405E-05-2.04730E-05-3.11904E-05 1.72843E-04
-5.35122E-04 1.44634E-03-3.49966E-03 7.25740E-03-1.19744E-02 1.56920E-02
-1.76913E-02 1.85182E-02-1.67897E-02 1.88031E-02-1.36129E-02 1.81126E-02
-1.63952E-02 1.42200E-02-9.23352E-03 5.46140E-03-4.98096E-03 5.14399E-03
-5.50035E-03 5.31966E-03-3.81177E-03 1.48898E-03-7.03531E-04 3.65719E-04
-2.12074E-04
     11    30 .362                                                           ITEM 12
-15.17     2.32        .00746      15     0 .0          .0                   ITEM 13
          3.        .672        .037                                         ITEM 14
         9.        .677        .113
        15.        .699        .204
        21.        .723        .276
        27.        .754        .366
        33.        .806        .550
        39.        .870        .764
        45.        .961        .971
        51.       1.069       1.377
        57.       1.246       1.517
        63.       1.407       1.455
        69.       1.529       1.12
        75.       1.645       1.010
        81.       1.751        .94
        87.       1.833        .636
        93.       1.884        .277
        99.       1.942        .565
       105.       2.006        .713
       111.       2.091        .985
       117.       2.205       1.213
       123.       2.348       1.430
       129.       2.491       1.55
       135.       2.729       2.077
       141.       2.952       1.613
       147.       3.108       1.243
       153.       3.208       5.67
       159.       3.792       4.691
       165.       4.165       2.957
       171.       4.494       1.703
       177.       4.521        .611
```

(a)   Page 1

Figure 30.   Trajectory Program Input

-20.5	2.26	.00746	15	0	.0	.9	ITEM 13
3.	.669	.0131					ITEM 14
9.	.677	.104					
15.	.691	.156					
21.	.714	.245					
27.	.743	.341					
33.	.786	.502					
39.	.845	.653					
45.	.937	.923					
51.	1.049	1.304					
57.	1.196	1.852					
63.	1.425	2.472					
69.	1.73	1.931					
75.	1.847	.766					
81.	1.874	.105					
87.	1.863	-.024					
93.	1.869	.096					
99.	1.889	.292					
105.	1.932	.526					
111.	2.001	.78					
117.	2.095	1.074					
123.	2.219	1.454					
129.	2.404	1.947					
135.	2.626	2.665					
141.	2.949	2.618					
147.	3.215	1.744					
153.	3.317	1.981					
159.	3.631	2.42					
165.	3.898	2.452					
171.	4.146	1.455					
177.	4.202	.435					
-22.25	2.66	.13769	15	1	99.00	104.3	ITEM 13
3.	.667	.007					ITEM 14
9.	.674	.112					
15.	.691	.167					
21.	.715	.27					
27.	.745	.389					
33.	.795	.517					
39.	.854	.7					
45.	.937	.949					
51.	1.054	1.316					
57.	1.212	1.913					
63.	1.452	2.535					
69.	1.752	2.264					
75.	1.941	.712					
81.	1.9	-.267					
87.	1.886	-.065					
93.	1.886	-.098					
99.	1.907	24.7°1					
105.	4.634	2.242					
111.	4.856	2.437					
117.	5.136	-7.069					
123.	4.415	-6.353					
129.	3.821	-4.873					
135.	3.421	-2.954					
141.	3.099	1.51					
147.	3.25	1.124					
153.	3.325	1.557					
159.	3.587	2.235					
165.	3.801	1.776					
171.	3.951	1.042					
177.	4.023	.304					

(b) Page 2

Figure 30.   Continued

125

-24.73	2.77	.0783	15	0 .0	.3	ITEM 1
3.	.669	.023				ITEM 1
9.	.676	.109				
15.	.691	.193				
21.	.715	.293				
27.	.753	.397				
33.	.804	.539				
39.	.865	.74				
45.	.955	.985				
51.	1.067	1.375				
57.	1.23	1.985				
63.	1.476	2.262				
69.	1.696	1.549				
75.	1.795	.766				
81.	1.856	13.065				
87.	3.254	12.5				
93.	4.456	1.013				
99.	4.565	1.443				
105.	4.762	1.902				
111.	4.953	3.115				
117.	5.277	-2.113				
123.	5.053	-4.332				
129.	4.337	-5.573				
135.	3.877	-3.324				
141.	3.509	-2.305				
147.	3.264	.645				
153.	3.332	.971				
159.	3.467	1.153				
165.	3.574	.938				
171.	3.663	.621				
177.	3.705	.231				
-27.25	2.37	.0193	15	0 .0	.3	ITEM 1
3.	.668	.027				ITEM 1
9.	.675	.106				
15.	.691	.191				
21.	.715	.2F3				
27.	.753	.3=4				
33.	.799	.536				
39.	.864	.737				
45.	.956	1.015				
51.	1.076	1.42				
57.	1.247	1.986				
63.	1.491	2.317				
69.	1.715	3.786				
75.	2.26	2.346				
81.	3.476	11.729				
87.	4.723	.327				
93.	4.756	.407				
99.	4.806	.754				
105.	4.912	1.423				
111.	5.139	1.943				
117.	5.322	1.245				
123.	5.368	-6.525				
129.	4.709	-5.744				
135.	4.184	-4.315				
141.	3.79	-3.18				
147.	3.513	-2.158				
153.	3.339	-.735				
159.	3.346	.034				
165.	3.346	.233				
171.	3.395	.234				
177.	3.397	-.013				

(c) Page 3

Figure 30. Continued

-29.75	3.007	.00256	15	0 .0	.0	ITEM 13
3.	.667	0.0				ITEM 14
9.	.675	.11				
15.	.691	.191				
21.	.718	.264				
27.	.75	.355				
33.	.795	.533				
39.	.864	.705				
45.	.943	.985				
51.	1.067	1.347				
57.	1.23	1.96				
63.	1.461	3.077				
69.	1.873	5.21				
75.	2.555	15.32				
81.	4.154	5.743				
87.	4.757	-.00				
93.	4.756	.235				
99.	4.806	.757				
105.	4.915	1.305				
111.	5.08	1.536				
117.	5.308	1.409				
123.	5.377	-5.654				
129.	4.789	-5.349				
135.	4.243	-4.368				
141.	3.863	-3.152				
147.	3.583	-2.369				
153.	3.375	-1.438				
159.	3.293	-.729				
165.	3.222	-.644				
171.	3.159	-.401				
177.	3.139	-.153				
-34.75	3.003	.00256	15	0 .0	.0	ITEM 13
3.	.651	.02				ITEM 14
9.	.656	.009				
15.	.673	.154				
21.	.696	.255				
27.	.728	.338				
33.	.769	.475				
39.	.824	.662				
45.	.91	.974				
51.	1.011	1.291				
57.	1.17	1.404				
63.	1.386	3.496				
69.	1.752	4.608				
75.	2.349	9.925				
81.	3.817	11.582				
87.	4.758	-.029				
93.	4.755	.227				
99.	4.806	.76				
105.	4.92	1.321				
111.	5.086	1.971				
117.	5.322	1.789				
123.	5.46	-6.273				
129.	4.839	-5.643				
135.	4.278	-4.443				
141.	3.897	-3.217				
147.	3.612	-2.393				
153.	3.392	-1.779				
159.	3.242	-1.274				
165.	3.127	-.66				
171.	3.057	-.49				
177.	3.021	-.245				

(d) Page 4

Figure 30. Continued

```
-40.59    2.99     .00256     15    0  .0        .0                    ITEM 13
 3.        .651     .02                                                ITEM 14
 5.        .658     .009
15.        .673     .184
21.        .696     .256
27.        .728     .338
33.        .769     .475
39.        .824     .652
45.        .91      .974
51.       1.011    1.231
57.       1.17     1.404
63.       1.386    3.446
69.       1.752    4.606
75.       2.349    9.928
81.       3.817   11.562
87.       4.758    -.029
93.       4.755     .227
99.       4.806     .76
105.      4.92     1.321
111.      5.086    1.571
117.      5.322    1.79
123.      5.46    -6.273
129.      4.839   -5.6?3
135.      4.278   -4.443
141.      3.897   -3.217
147.      3.612   -2.3?3
153.      3.392   -1.77?
159.      3.242   -1.274
165.      3.127    -.56
171.      3.057    -.4?
177.      3.021    -.245
-43.5     3.022     .00256     15    0  .0        .)                    ITEM 13
 3.        .65      .06                                                 ITEM 14
 9.        .66      .09
15.        .67      .2
21.        .7       .3
27.        .73      .38
33.        .78      .51
39.        .841     .6?
45.        .?19     .96
51.       1.044    1.33
57.       1.207    1.97
63.       1.44     3.45
69.       1.82     5.29
75.       2.55    11.75
81.       4.17     5.9
87.       4.76     3.25
93.       4.82      .5
99.       4.87      .77
105.      4.99     1.33
111.      5.15     1.62
117.      5.33     1.15
123.      5.38    -5.45
129.      4.78    -5.3?
135.      4.25    -4.33
141.      3.87    -3.05
147.      3.58    -2.38
153.      3.37    -1.76
159.      3.21    -1.24
165.      3.11     -.85
171.      3.04     -.52
177.      3.       -.25
```

(e) Page 5

Figure 30. Continued

```
-49.33    3.047    -.09326    15    0 .0      .0                              ITEM 13
3.        .67      0.0                                                        ITEM 14
9.        .68      .09
15.       .69      .15
21.       .71      .32
27.       .75      .41
33.       .8       .48
39.       .86      .67
45.       .94      .95
51.       1.05     1.4
57.       1.22     2.0
63.       1.45     2.76
69.       1.8      4.55
75.       2.45     12.9
81.       3.73     10.95
87.       4.64     6.14
93.       5.02     2.62
99.       5.19     1.57
105.      5.35     .91
111.      5.39     .1
117.      5.37     -.66
123.      5.21     -4.70
129.      4.74     -4.85
135.      4.24     -4.35
141.      3.87     -3.1?
147.      3.57     -2.43
153.      3.36     -1.76
159.      3.2      -1.29
165.      3.09     -.86
171.      3.02     -.48
177.      2.99     -.25
-49.53    3.047    -.09326    15    0 .0      .0                              ITEM 13
3.        .67      0.0                                                        ITEM 14
9.        .68      .09
15.       .69      .15
21.       .71      .32
27.       .75      .41
33.       .8       .48
39.       .66      .67
45.       .94      .95
51.       1.05     1.4
57.       1.22     2.0
63.       1.45     2.76
69.       1.8      4.55
75.       2.45     12.9
81.       3.73     10.95
87.       4.64     6.14
93.       5.02     2.62
99.       5.19     1.57
105.      5.35     .91
111.      5.39     .1
117.      5.37     -.86
123.      5.21     -4.70
129.      4.74     -4.85
135.      4.24     -4.35
141.      3.87     -3.19
147.      3.57     -2.43
153.      3.36     -1.76
159.      3.2      -1.29
165.      3.09     -.66
171.      3.02     -.43
177.      2.99     -.25
```

(f) Page 6

Figure 30. Continued

```
-29.83      .333        .0                                                              ITEM 15
13.67       16.42                                                                       ITEM 16
     8        5                                                                         ITEM 17
     1 -0.333      .0          .0          .0                                           ITEM 18
     2 -7.15      45.         11.          .0
     3 -9.47      45.         11.          .C
     4 -11.73     45.         11.          .C
     5 -14.1      45.         11.          .0
     6 -16.42     45.         11.          .0
     0                                                                                  ITEM 19
    12        1                                                                         ITEM 21
.0872       .0593       .0436       .0218       .0          -.025       -.0392  -.0392  ITEM 22
-.0332      -.0392      -.03°2      -.0352
     2    1 10.625      .625        2.192       .0          4.256       3.5             ITEM 32
     8    1 10.625      .625        8.d375      .0          .953        .0
     1                                                                                  ITEM 33
     1       59                                                                         ITEM 34
2.00003E-03 2.56501E-03 3.29665E-03 4.24330E-03 5.46696E-03 7.04621E-03                ITEM 35
9.08123E-03 1.16977E-02 1.50519E-02 1.93364E-02 2.47335E-02 3.16694E-02
4.03092E-02 5.10518E-02 6.42597E-02 8.02789E-02 9.33922E-02 1.21760F-01
1.47355E-01 1.75900E-01 2.06827E-01 2.39281E-01 2.71985E-01 3.04488E-01
3.37091E-01 3.69694E-01 4.02297E-01 4.54901E-01 4.67504E-01 5.00107F-01
5.32713E-01 5.65313E-01 5.97917E-01 6.30520E-01 6.63123E-01 6.95726E-01
7.28329E-01 7.60933E-01 7.93536E-01 8.26139E-01 8.58742E-01 8.91345F-01
9.23943E-01 9.56552E-01 9.89155E-01 1.02176E+00 1.05442E+00 1.08569F+00
1.11447F+00 1.13997E+00 1.16173E+00 1.17953F+00 1.19383E+08 1.20487F+00
1.21322E+00 1.21942E+00 1.22395E+00 1.22723E+00 1.22958E+00
5.52307E-06-5.24710E-06 3.05297E-06-1.33409E-06 1.23479E-06 2.81412E-07                ITEM 36
1.44612E-06 1.91947E-06 3.46467E-06 5.55270E-06 3.09092E-06 1.44075E-05
2.24017E-05 3.36919E-05 4.86576E-05 6.64669E-05 8.50761E-05 9.56485E-05
1.15161E-04 3.05698E-05 1.04260E-04-1.26905E-04 3.11739E-05-9.44446E-05
9.06413E-05-9.28368E-05 9.13533E-05-9.23778E-05 9.16563E-05-9.21635F-05
9.18163E-05-9.20356E-05 9.19258E-05-9.19357E-05 9.20249E-05-9.18293E-05
9.21479E-05-9.16771E-05 9.23483E-05-9.13974E-05 9.27639E-05-9.07454E-05
9.39791E-05-8.93356E-05 1.04210E-04-3.86997E-05-7.97454E-05-1.08728E-04
-1.11593E-04-9.59665E-05-7.18790E-05-4.85464F-05-2.37963E-05-1.76253E-05
-9.01843E-06-6.03434E-06-7.96050E-07-4.89273E-06 3.63033E-06
     2       40       40        1        2        1        1        3                   ITEM 37
24.8447     5.4         157.5       157.5       .0          .0          .0             ITEM 38
-5.3125     .0          .0          .0                                                  ITEM 39
.2353       1.1                                                                         ITEM 40
-.4413      -1.         .4706       .1;47       .0          .0          1.             ITEM 41
.05882      .0          .0          .0          .0          .0          .3
.34         1.2                                                                         ITEM 42
     0        5                                                                         ITEM 43
-9.578      .625        1.45-33     .0          3.10                                    ITEM 44
.0          .0          .0          .0          .0          .0                          ITEM 45
.05         .0          .0                                                              ITEM 46
```

(g) Page 7

Figure 30. Concluded

130

Item No. 1 (1 card)

Variable	NCARDS
Card Column	5
Format Type	I

Item No. 2 (NCARDS cards)

Variable	HEAD	
Card Column		80
Format Type	A	

Item No. 3 (1 card)

Variable	ALFAC	GAMF	FMACH	RHO	VINF
Card Column	10	20	30	40	50
Format Type	F	F	F	F	F

Item No. 4 (1 card)

Variable	NFU	NPY	NRACK	NSTRS
Card Column	5	10	15	20
Format Type	I	I	I	I

Item No. 5 (1 card, omit if NFU = 0)

Variable	FLTHC	FRMAX
Card Column	10	20
Format Type	F	F

Item No. 6 (1 card, omit if NFU = 0)

Variable	NFSOR
Card Column	5
Format Type	I

Item No. 7 (NFSOR values, six to a card. Omit if NFU = 0)

Variable	FXL(1)	FXL(2)	FXL(3)	...	FXL(NFSOR)
Card Column	12	24	36	48	60	72
Format Type	E	E	E	E	E	E

(a) Page 1

Figure 31. Trajectory Program Input Format

(Ref 5:105)

131

Item No. 8 (NFSOR values, six to a card. Omit if NFU = 0)

Variable	FSOR(1)		FSOR(2)		FSOR(3)		...		FSOR(3)		...		FSOR(NFSOR)
Card Column		12		24		36				48		60		72
Format Type	E		E		E		E		E		E		E

Item No. 9 (1 card. Omit if NFU = 0 or 2)

Variable	NFPOLY
Card Column	5
Format Type	I

Item No. 10 (1 card. Omit if NFU = 0 or 2)

Variable	FXEND(1)		FXEND(2)		FXEND(3)		...		FXEND(NFPOLY)
Card Column		10		20		30		40		50
Format Type	F		F		F		F		F

Item No. 11 (J = 1 to NFPOLY; NFPOLY cards. Omit if NFU = 0 or 2)

Variable	FCOEF(J,1)		FCOEF(J,2)		FCOEF(J,3)		FCOEF(J,4)		FCOEF(J,5)		FCOEF(J,6)		FCOEF(J,7)
Card Column		10		20		30		40		50		60		70
Format Type	F		F		F		F		F		F		F

Item No. 12 (1 card. Omit if NFU = 0 or 1)

Variable	NXSTAT		VDVTNF
Card Column	5		10		20
Format Type	I		I		F

Item No. 13* (1 card. Omit if NFU = 0 or 1)

Variable	XSTAT		REQ		DRDXC		MPH		NOPSUR		THOPB		THOPE
Card Column		10		20		30	35		40		50		60
Format Type	F		F		F	I		I		F		F

Item No. 14* (J = 1 to MC; MC cards. Omit if NFU = 0 or 1)

Variable	THRTF(J)		RBF(J)		DRBDT(J)
Card Column		10		20		30
Format Type	F		F		F

*Repeat items 13 and 14, in sequence, NXSTAT times.

(b) Page 2

Figure 31. Continued

132

Item No. 15 (1 card)

Variable	XBWOC	ZBWO	WIC
Card Column	10	20	30
Format Type	F	F	F

Item No. 16 (1 card)

Variable	CRW	SSPAN
Card Column	10	20
Format Type	F	F

Item No. 17 (1 card)

Variable	NCW	MSW
Card Column	5	10
Format Type	I	I

Item No. 18 (I = 1 to MSW+1; MSW+1 cards)

Variable	I	Y(I)	PSIMLE(I)	PSIWTE(I)	PHIO(I)
Card Column	5	15	25	35	45
Format Type	I	F	F	F	F

Item No. 19 (1 card)

Variable	NTAC	NUNI
Card Column	5	10
Format Type	I	I

Item No. 20 (NCW values, eight to a card. Omit if NTAC = 0. One set of cards if NUNI = 1; MSW sets if NUNI = 0.)

Variable	ALPHAL(1)	ALPHAL(2)	...	ALPHAL(NCW)				
Card Column	10	20	30	40	50	60	70	80
Format Type	F	F	F	F	F	F	F	F

(c) Page 3

Figure 31. Continued

133

Item No. 21 (1 card)

Variable	NCNS	NUMIS
Card Column	5	10
Format Type	I	I

Item No. 22 (NCNS values, eight to a card. One set of cards if NUMIS = 1; NSW sets if NUMIS = 0.)

Variable	THETAL(1)	THETAL(2)	...	THETAL(NCNS)				
Card Column	10	20	30	40	50	60	70	80
Format Type	F	F	F	F	F	F	F	F

Item No. 23 (1 card. Omit if NPY = 0.)

Variable	IP	PSIPLE	PSIPTE	CRP	H	XPLE
Card Column	5	15	25	35	45	55
Format Type	I	F	F	F	F	F

Item No. 24 (1 card. Omit if NPY = 0.)

Variable	NCP	MSP
Card Column	5	10
Format Type	I	I

Item No. 25 (K = 1 to MSP+1; MSP+1 cards. Omit if NPY = 0.)

Variable	K	Z(K)
Card Column	5	15
Format Type	I	F

Item No. 26 (1 card. Omit if NPY = 0.)

Variable	NCPS	NUMIP
Card Column	5	10
Format Type	I	I

Item No. 27 (NCPS values, eight to a card. Omit if NPY = 0. One set of cards if NUMIP = 1; MSP sets if NUMIP = 0.)

Variable	THETPL(1)	THETPL(2)	...	THETPL(NCPS)				
Card Column	10	20	30	40	50	60	70	80
Format Type	F	F	F	F	F	F	F	F

(d) Page 4

Figure 31. Continued

134

Item No. 28 (1 card. Omit if NRACK = 0.)

Variable	RLTIC	RHMAX	XRMC	ZRN	RIC
Card Column	10	20	30	40	50
Format Type	F	F	F	F	F

Item No. 29 (1 card. Omit if NRACK = 0.)

Variable	NRSOR
Card Column	5
Format Type	I

Item No. 30 (NRSOR values, six to a card. Omit if NRACK = 0.)

Variable	RXL(1)	RXL(2)	...	RXL(NRSOR)		
Card Column	12	24	36	48	60	72
Format Type	E	E	E	E	E	E

Item No. 31 (NRSOR values, six to a card. Omit if NRACK = 0.)

Variable	RSOR(1)	RSOR(2)	...	RSOR(NRSOR)		
Card Column	12	24	36	48	60	72
Format Type	E	E	E	E	E	E

Note: If NSTRS = 0, this completes the input data. Since no stores are present, NSTRS = 0, a trajectory cannot be run.

Item No. 32 (J = 1 to NSTRS; NSTRS cards)

Variable	NUMSTR(J)	NSHAPE(J)	SLTIC(J)	RNMAX(J)	XSNC(J)	YSN(J)	ZSN(J)	SIC(J)
Card Column	5	10	20	30	40	50	60	70
Format Type	I	I	F	F	F	F	F	F

Item No. 33 (1 card)

Variable	NSHPT
Card Column	5
Format Type	I

(e) Page 5

Figure 31. Continued

135

Item No. 34* (1 card)

Variable	NSHAPE	MSOR
Card Column	5	10
Format Type	I	I

Item No. 35* (MSOR values, six to a card)

Variable	DUMX(1)	DUMX(2)	...	DUMX(MSOR)		
Card Column	12	24	36	48	60	72
Format Type	E	E	E	E	E	E

Item No. 36* (MSOR values, six to a card)

Variable	DUMQ(1)	DUMQ(2)	...	DUMQ(MSOR)		
Card Column	12	24	36	48	60	72
Format Type	E	E	E	E	E	E

Item No. 37 (1 card)

Variable	NEJECT	NSEG	NSEGKO	NGAM	NPOLY	NROLL	NENP	NDAMP
Card Column	5	10	15	20	25	30	35	40
Format Type	I	I	I	I	I	I	I	I

Item No. 38 (1 card)

Variable	SMASS	FIXX	FIYY	FIZZ	FIYZ	FIXZ	FIXY
Card Column	10	20	30	40	50	60	70
Format Type	F	F	F	F	F	F	F

Item No. 39 (1 card)

Variable	XNUM	XBAR	YBAR	ZBAR
Card Column	10	20	30	40
Format Type	F	F	F	F

*If NSHPT > 1, repeat items 34 through 36, in sequence, NSHPT times.

(f) Page 6

Figure 31. Continued

136

Item No. 40 (1 card)

Variable	XEND(1)	XEND(2)	...	XEND(NPOLY)			
Card Column	10	20	30	40	50	60	70
Format Type	F	F	F	F	F	F	F

Item No. 41 (J = 1 to NPOLY; NPOLY cards)

Variable	COEF(J,1)	COEF(J,2)	COEF(J,3)	COEF(J,4)	COEF(J,5)	COEF(J,6)	COEF(J,7)
Card Column	10	20	30	40	50	60	70
Format Type	F	F	F	F	F	F	F

Item No. 42 (1 card)

Variable	CA	CDC
Card Column	10	20
Format Type	F	F

Item No. 43 (1 card. Omit if NEMP = 0)

Variable	IPLNR	MSF
Card Column	5	10
Format Type	I	I

Item No. 44 (1 card. Omit if NEMP = 0)

Variable	XTAIL	RADAV	FINSS	PHIROL	C1ALPH
Card Column	10	20	30	40	50
Format Type	F	F	F	F	F

Item No. 45 (1 card)

Variable	VXZERO	VYZERO	VZZERO	VAR(4)	VAR(5)	VAR(6)
Card Column	10	20	30	40	50	60
Format Type	F	F	F	F	F	F

(g) Page 7

Figure 31. Continued

137

Item No. 46 (1 card)

Variable	DTIME	TIMEI	TIMEF
Card Column	10	20	30
Format Type	F	F	F

Item No. 47 (2 cards. Omit if TIMEI = 0)

Variable	VAR(1)	VAR(2)	...	VAR(12)				
Card Column	10	20	30	40	50	60	70	80
Format Type	F	F	F	F	F	F	F	F

(h) Page 8

Figure 31. Concluded

138
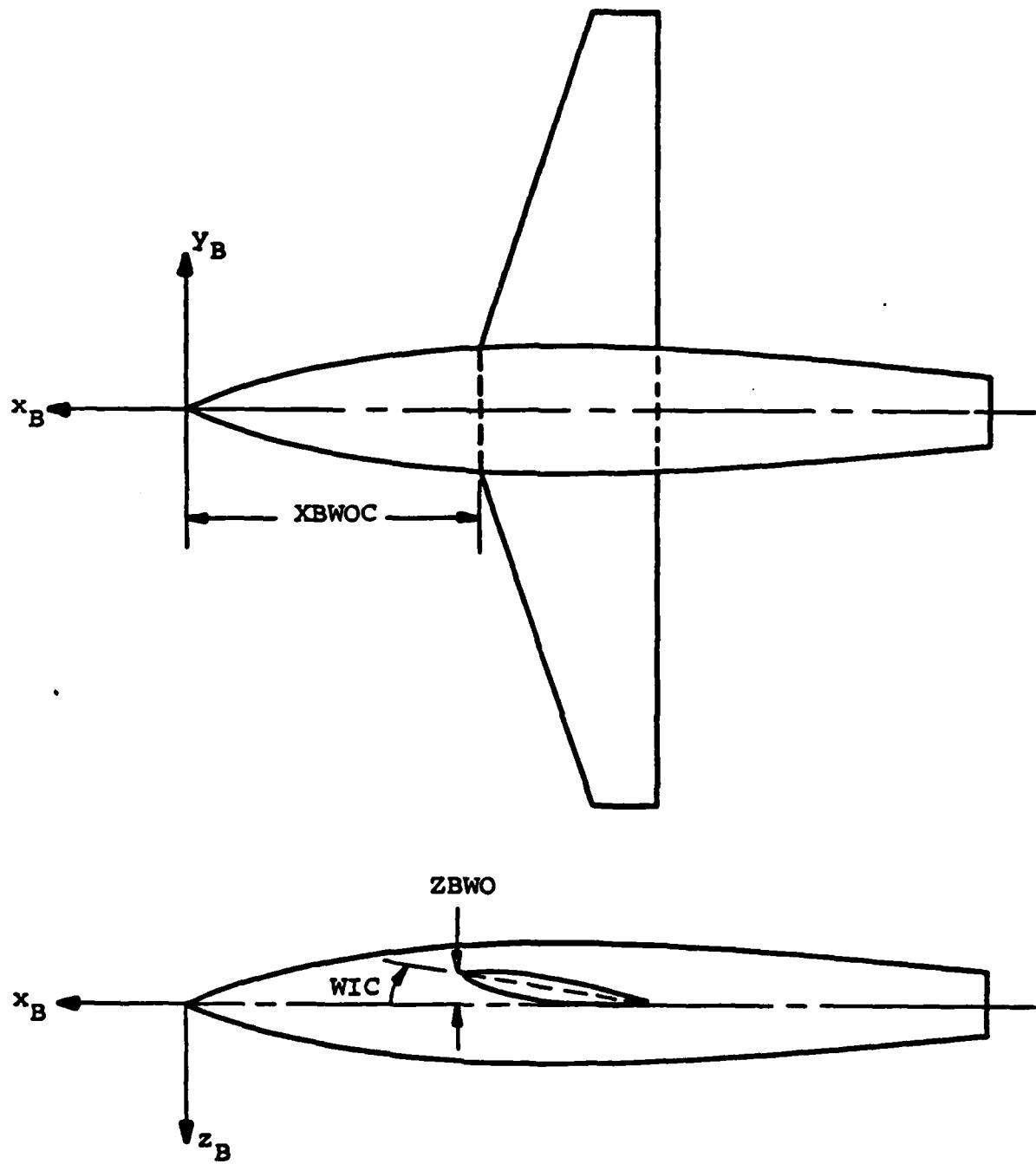
Figure 32. Fuselage Coordinate System

(Ref 5: 13)

139
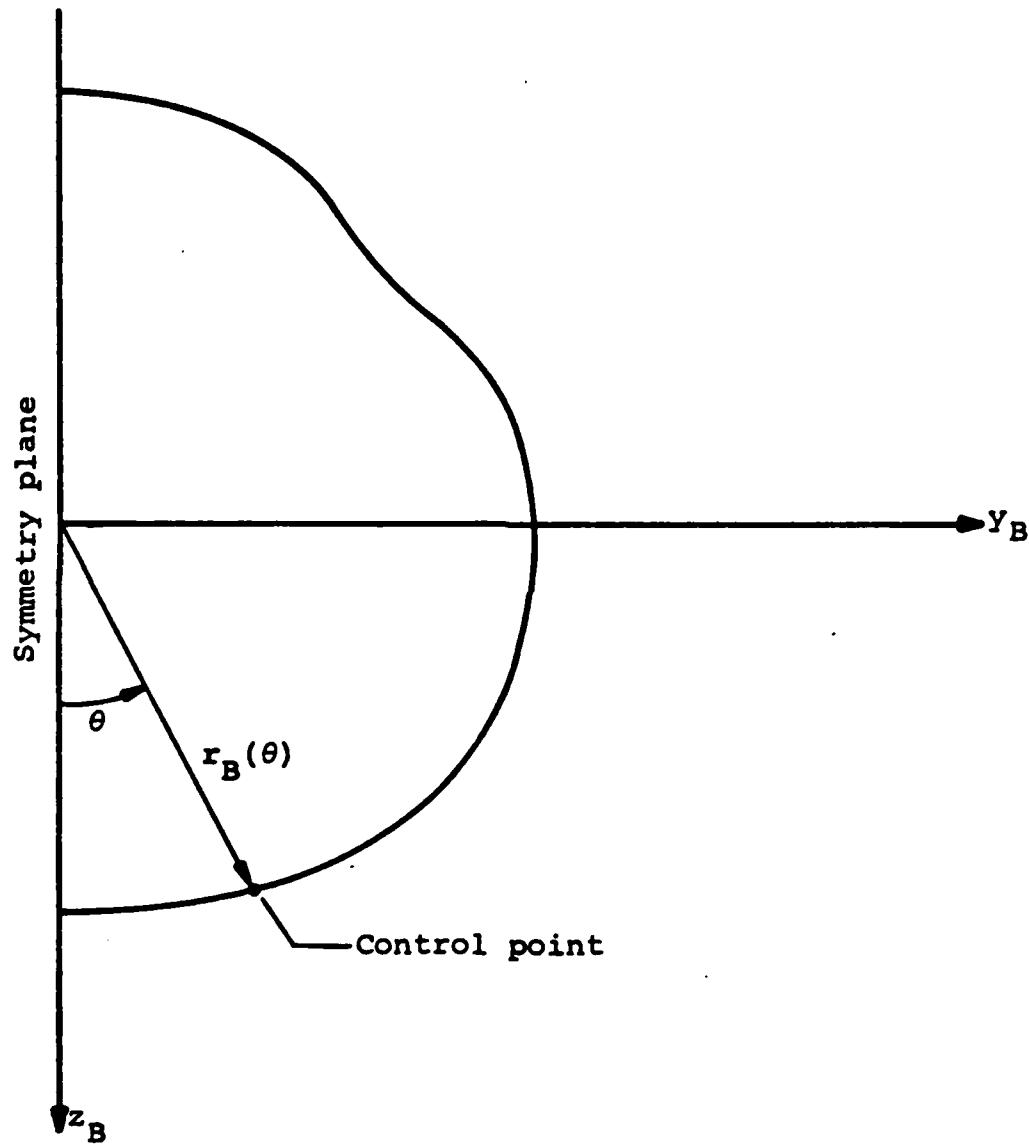
Figure 33. Coordinate System in Crossflow Plane

140
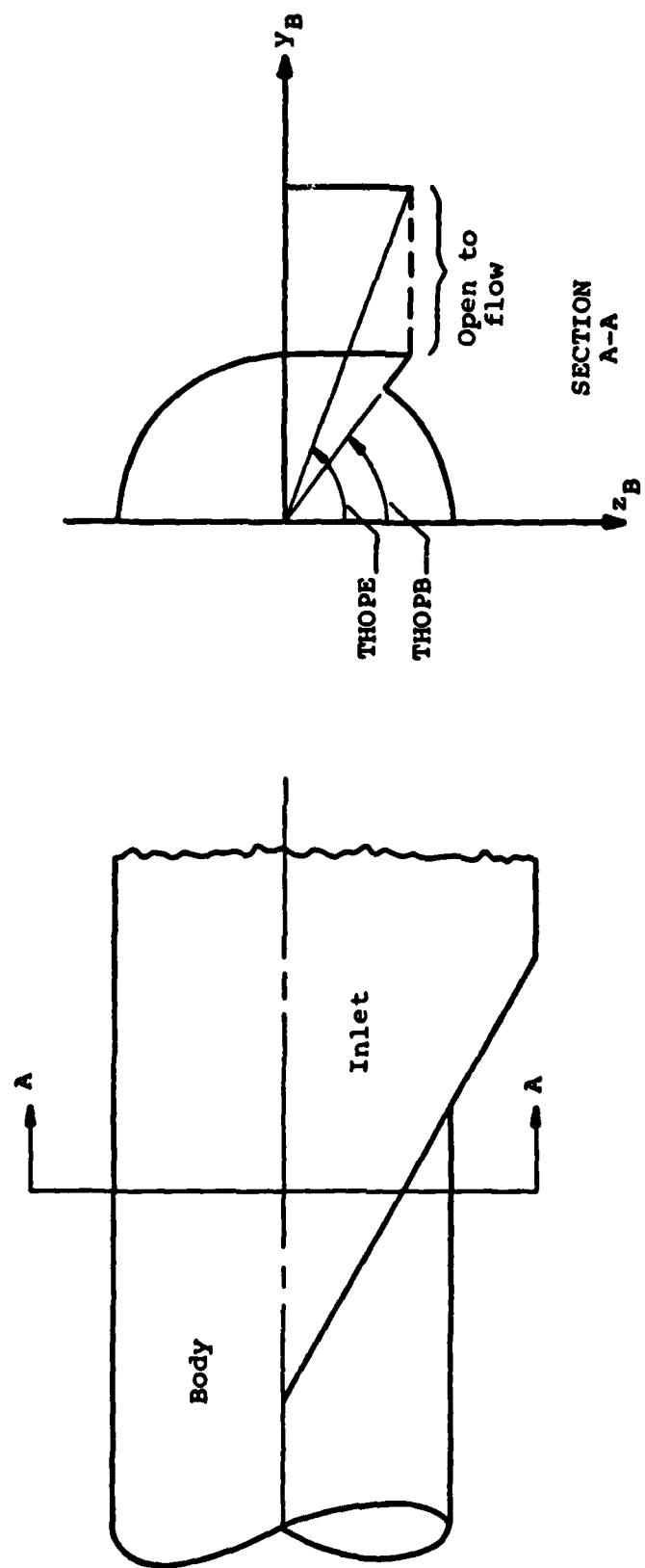
Figure 34. Crossflow Plane Contour With Non-Solid Boundary
(Ref 5: 115)

141
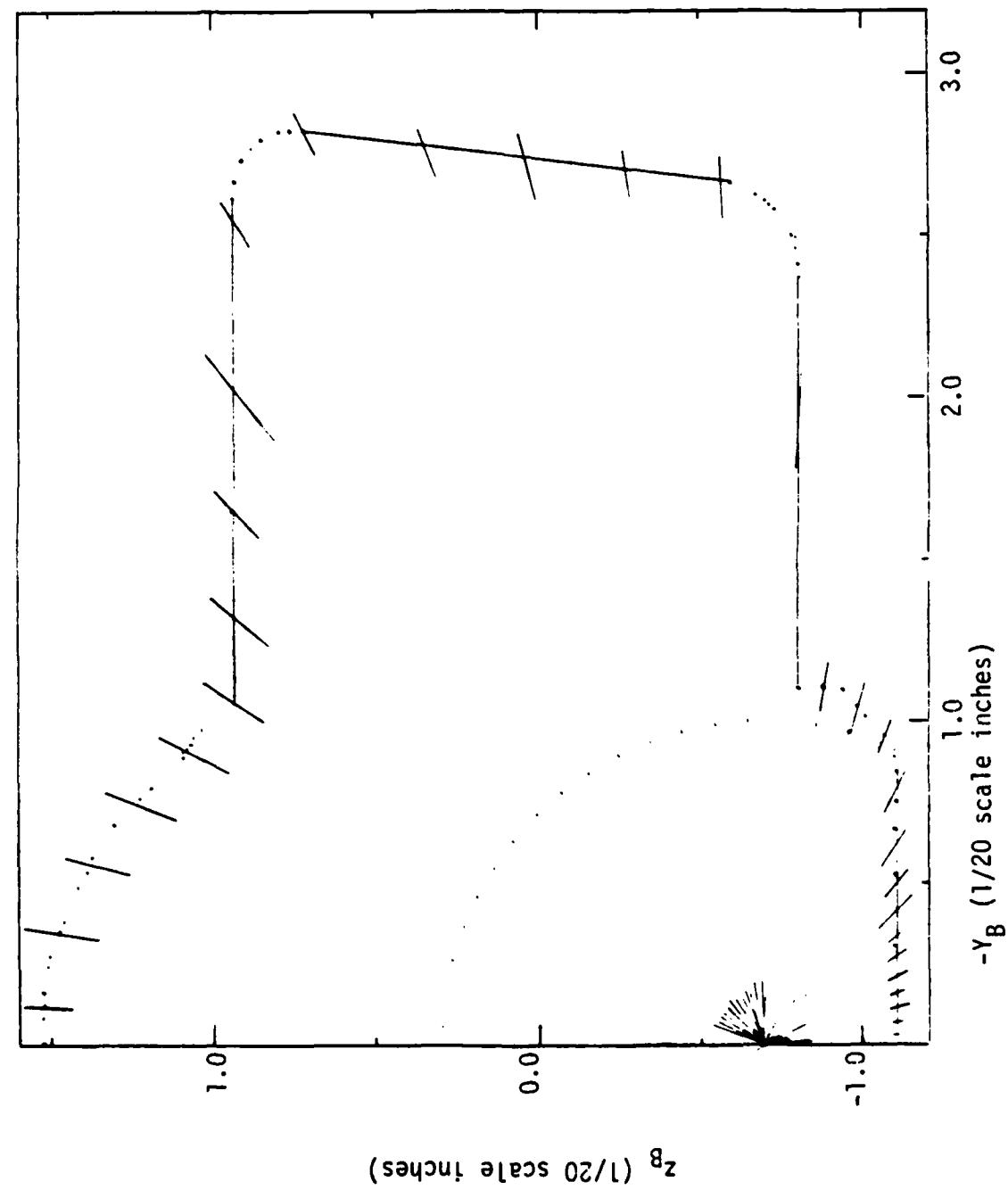
Figure 35. Fuselage Crossflow Section

-Y_B (1/20 scale inches)

z_B (1/20 scale inches)
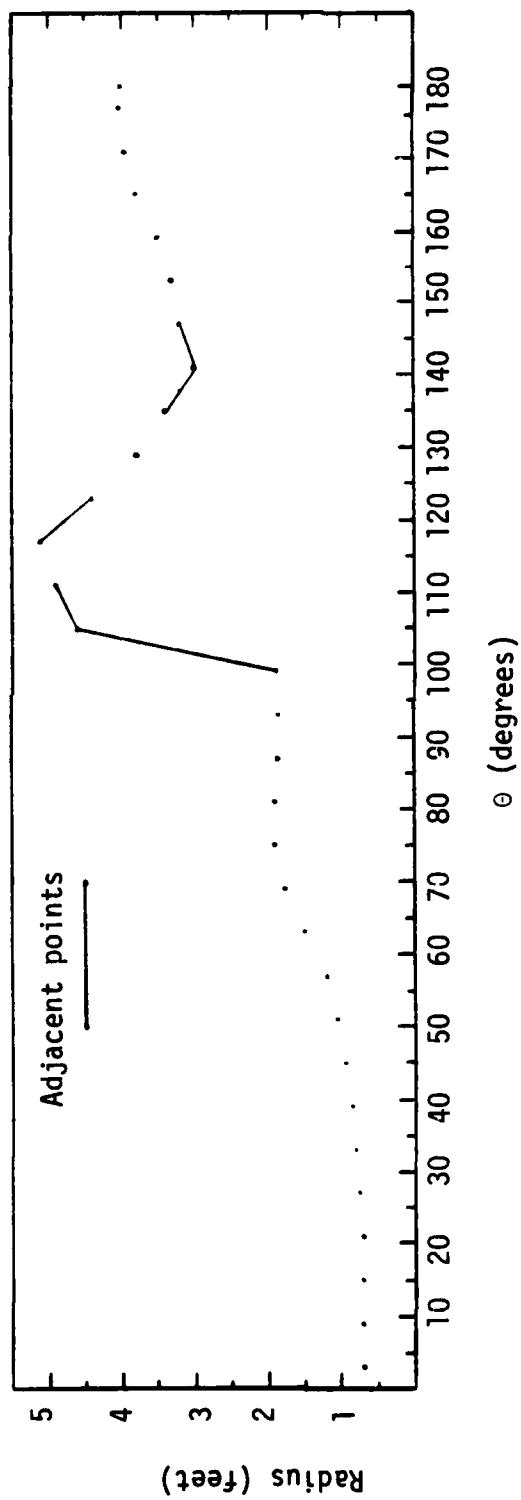
Figure 36. Trajectory Program Input Item 14, r_B vrs θ

143

Fuselage

WING

Store length
10.625 feet

5.3125 feet

(+ Forward)
XSN(J)

29.88 feet

STORE

CG

$x_B = -33$ feet
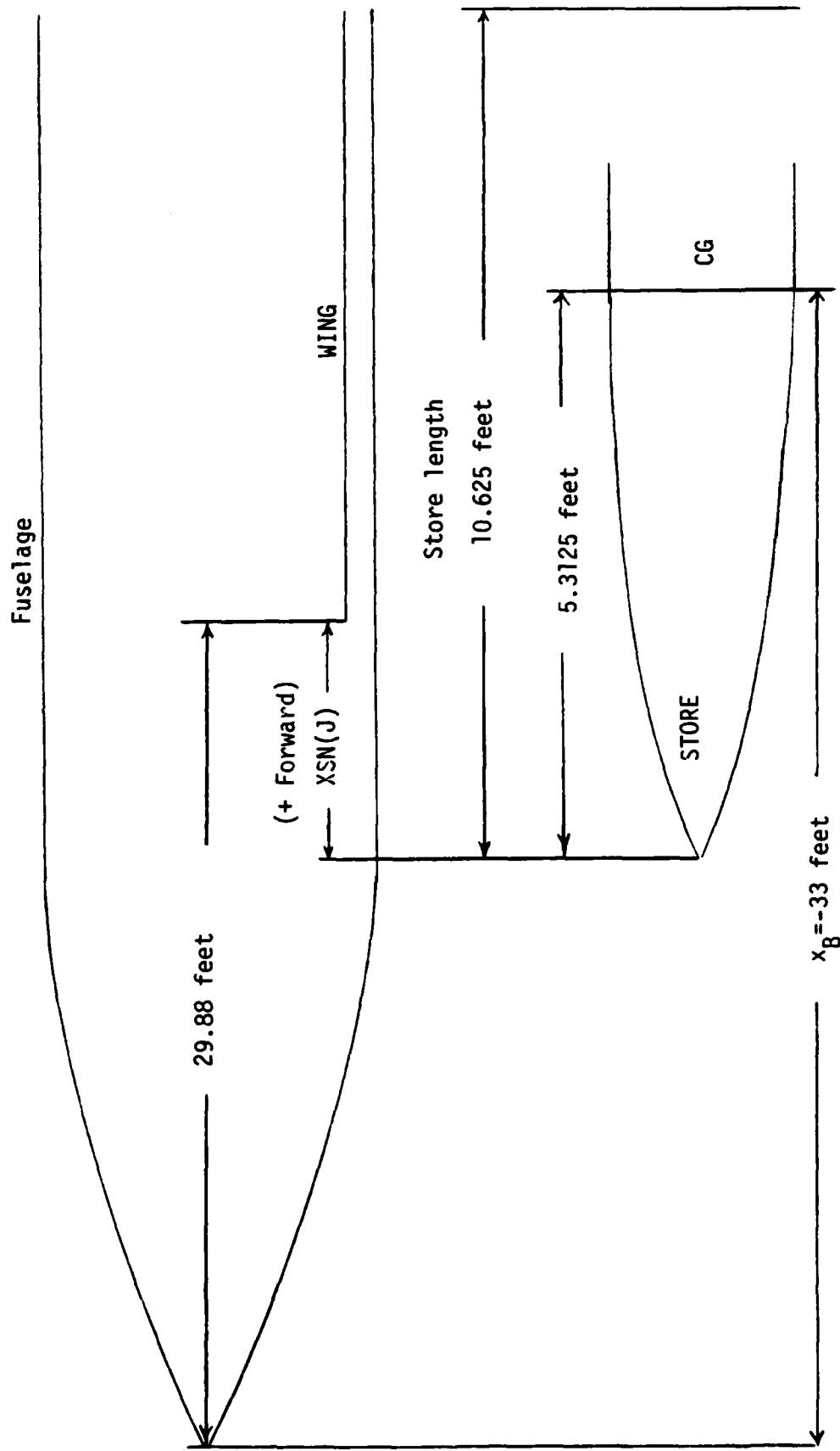
Figure 37. Store Position-x

144
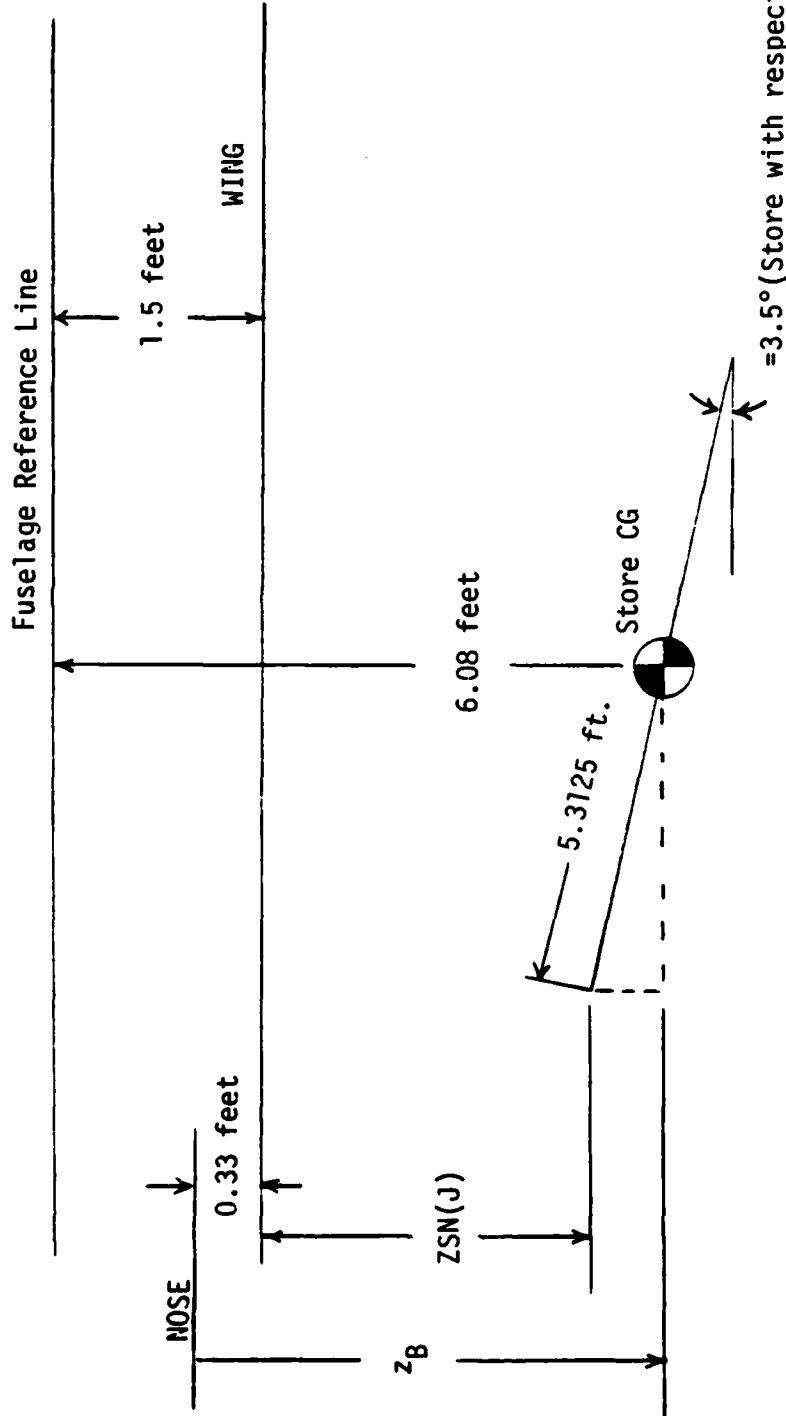
$ZSN(J)=6.08 - 1.5 - 5.3125(\sin 3.5°)=4.256$

$z_B=ZSN(J) + 0.33 + 5.3125(\sin 3.5°)=4.91$ feet

Figure 38. Store Position z

SIX-DEGREE-OF-FREEDOM TRAJECTORY PROGRAM

AMECS1
V/VINLE = 0.962
FLIGHT MACH = 0.6

AIRCRAFT FLIGHT CONDITIONS
    ANGLE OF ATTACK = 2.50 DEGREES
    FLIGHT PATH ANGLE = 0.00 DEGREES
    MACH NUMBER = .60
    FREE STREAM MASS DENSITY =   .0013370 SLUGS PER CUBIC FOOT
    FREE STREAM VELOCITY = 671.20 FEET PER SECOND

FUSELAGE INPUT DATA

    EQUIVALENT BODY OF REVOLUTION
        FUSELAGE LENGTH = 56.40003 FEET
        MAXIMUM RADIUS = 3.05600 FEET

INCOMPRESSIBLE SOURCE DISTRIBUTION

```
X/L   1.00080E-03 1.40274E-03 1.91086E-03 2.57981E-03 3.42543E-03 4.50688E-03 5.84969E-03 7.64027E-03
Q+(K) 1.31126E-06-1.14398E-06 7.58930E-07-3.98078E-07 3.98518E-07 6.45626E-09 4.20647E-07 4.25565E-07

X/L   9.57014E-03 1.26733E-02 1.62531E-02 2.07105E-02 2.62031E-02 3.31604E-02 4.15726E-02 5.17306E-02
Q+(K) 8.47773E-07 1.24532E-06 2.81363E-06 3.06734E-06 4.63049E-06 6.73570E-06 9.41491E-06 1.24099E-05

X/L   6.38036E-02 7.78764E-02 9.39099E-02 1.11676E-01 1.30945E-01 1.52174E-01 1.75362E-01 2.01327E-01
Q+(K) 1.51472E-05 1.64453E-05 1.52450E-05 3.11043E-08 4.05010E-05 1.10939E-05 4.63076E-05 2.90156E-05

X/L   2.29714E-01 2.60417E-01 2.92387E-01 3.23044E-01 3.55650E-01 3.87665E-01 4.19717E-01 4.54719E-01
Q+(K) 1.01314E-04-1.33611E-04 1.33325E-04-1.31349E-04 7.71269E-05 1.36544E-04 1.44326E-05 8.76310E-05

X/L   4.91745E-01 5.04471E-01 5.17204E-01 5.29945E-01 5.42694E-01 5.55051E-01 5.68215E-01 5.80980E-01
Q+(K)-7.31210E-05 6.13209E-05 6.87053E-06-3.47470E-05 4.66940E-05-5.12255E-05 5.32020E-05-5.31670E-05

X/L   5.93768E-01 6.06556E-01 6.19352E-01 6.32156E-01 6.44960E-01 6.57717E-01 6.70615E-01 6.13450E-01
Q+(K) 5.39465E-05-5.25156E-05 5.23142E-05-4.82799E-05 4.18005E-05-2.60730E-05-3.11804E-05 1.72043E-04

X/L   6.96293E-01 7.09144E-01 7.22003E-01 7.34878E-01 7.47749E-01 7.60628E-01 7.73510E-01 7.86417E-01
Q+(K)-5.35122E-04 1.44634E-03-3.49966E-03 7.25740E-03-1.19744E-02 1.56928E-02-1.76810E-02 1.85182E-02

X/L   7.94323E-01 8.12237E-01 8.25160E-01 8.38090E-01 8.51020E-01 8.63974E-01 8.76926E-01 8.94110E-01
Q+(K)-1.87947E-02 1.86031E-02-1.86129E-02 1.81126E-02-1.60953E-02 1.42200E-02-9.23352E-03 5.46140E-03

X/L   9.10754E-01 9.26973E-01 9.42663E-01 9.57847E-01 9.72670E-01 9.86075E-01 9.94472E-01 9.99736E-01
Q+(K)-4.98036E-03 5.14359E-03-5.50036E-03 5.31966E-03-3.81177E-03 1.40898E-03-7.03501E-04 3.65719E-04

X/L   1.00383E+00
Q+(K)-2.12074E-04
```

(a)   Page 1

Figure 39.   Trajectory Program Output

146

NON-CIRCULAR FUSELAGE DATA

THE NON-CIRCULAR FUSELAGE CONTOUR WILL BE SPECIFIED AT 11 STATIONS
30 CONTROL POINTS WILL BE USED IN DETERMINING THE POLAR HARMONICS AT EACH STATION
THE INLET VELOCITY RATIO IS .66

STATION NO. 1   15 POLAR HARMONIC COEFFICIENTS

	EQUIVALENT BODY		THETA RANGE WHERE THE	
XF, FT	RADIUS, FT	DR/DX	BODY CONTOUR IS NOT SOLID	
-15.17000	2.32000	.00746	0.000 DEG. TO 0.000 DEG.	

SHAPE OF CONTOUR

THETA	RADIUS	DR/DTHETA	SLOPE OF CONTOUR	
DEG.	FT.	FT/RAD	DEG.	DNU/DX
3.00000	.67200	.03700	99.84950	-.00045
9.00000	.67700	.11800	89.11276	0.00000
15.00000	.69700	.20400	83.73035	-.00115
21.00000	.72300	.27600	90.10601	-.00126
27.00000	.75400	.35600	83.85044	-.00147
33.00000	.80600	.56000	89.20895	-.00247
39.00000	.87000	.76400	87.71166	-.00282
45.00000	.96100	.57100	83.70344	-.00253
51.00000	1.06500	1.37700	89.62310	-.00184
57.00000	1.24600	1.56700	95.13649	-.00463
63.00000	1.40700	1.45900	106.96055	.00188
69.00000	1.52500	1.12800	122.59243	.02428
75.00000	1.64500	1.01800	133.24891	.02578
81.00000	1.75100	.94000	142.77149	.01627
87.00000	1.83300	.63600	157.86465	.00510
93.00000	1.88400	.27700	174.63586	-.00223
99.00000	1.94200	.56500	172.77632	-.00764
105.00000	2.00600	.71300	175.43307	-.01047
111.00000	2.09100	.58500	175.77645	-.01222
117.00000	2.20500	1.21200	178.20417	-.01447
123.00000	2.34600	1.43000	181.65737	-.01654
129.00000	2.49100	1.65000	192.39970	-.01048
135.00000	2.72900	2.07700	187.72579	-.01230
141.00000	2.95200	1.81300	199.44342	-.00039
147.00000	3.10800	1.24300	215.20177	.01461
153.00000	3.20500	5.67000	182.50052	.00906
159.00000	3.79200	4.69100	197.95056	-.01519
165.00000	4.16500	2.95700	219.62662	-.03266
171.00000	4.40400	1.70300	239.85882	-.03612
177.00000	4.52100	.61100	259.30327	-.04745

POLAR HARMONIC
COEFFICIENTS

K	A(K)
1	-.24777E-01
2	.11933E-01
3	-.72327E-02
4	.74668E-02
5	-.71430E-02
6	.56469E-02
7	-.40513E-02
8	.26542E-02
9	-.14631E-02
10	.62846E-03
11	-.20047E-03
12	.45612E-04
13	-.69946E-05
14	.64871E-06
15	-.27533E-07

(b)   Page 2

Figure 39.   Continued

147

STATION NO. 2   15 POLAR HARMONIC COEFFICIENTS

	EQUIVALENT BODY		THETA RANGE WHERE THE	
XF, FT	RADIUS, FT	DR/DX	BODY CONTOUR IS NOT SOLID	
-20.50000	2.26000	.00745	0.000 DEG. TO	0.000 D:

SHAPE OF CONTOUR

THETA	RADIUS	DR/DTHETA	SLOPE OF CONTOUR	
DEG.	FT.	FT/RAD	DEG.	DNU/D>
3.00000	.66500	.01910	91.36465	-.000
9.00000	.67700	.10800	89.93613	-.001
15.00000	.69100	.15600	89.93449	0.000
21.00000	.71400	.24500	92.06100	.000
27.00000	.74300	.34100	92.34723	.000
33.00000	.78600	.50200	90.43457	.002
39.00000	.84500	.66300	90.05194	.003
45.00000	.93700	.92300	90.43125	0.000
51.00000	1.04900	1.30800	89.72919	.001
57.00000	1.19600	1.:5200	89.85390	.003
63.00000	1.42500	2.47200	92.96157	.006
69.00000	1.73000	1.58100	110.13059	.006
75.00000	1.84700	.70600	144.08107	.040
81.00000	1.87400	.10500	167.79308	.011
87.00000	1.86900	-.02400	177.73570	.007
93.00000	1.86900	.09600	180.05762	.007
99.00000	1.88900	.29200	180.21292	.009
105.00000	1.93200	.52600	179.76998	1.191
111.00000	2.00100	.78000	179.70391	1.216
117.00000	2.09500	1.07400	179.85809	1.237
123.00000	2.21500	1.46400	179.58490	.8379
129.00000	2.40400	1.94700	179.99598	.5033
135.00000	2.62600	2.68500	179.36353	.2541
141.00000	2.94500	2.81800	187.30127	.0495
147.00000	3.21500	1.74400	203.52206	.0140
153.00000	3.31700	1.98100	212.15323	.0031
159.00000	3.63100	2.62000	211.16546	-.0156
165.00000	3.89800	2.45200	222.82844	-.0375
171.00000	4.14600	1.45500	241.66195	-.0841
177.00000	4.20200	.43800	261.04920	-.0813

POLAR HARMONIC
COEFFICIENTS

K	A(K)
1	-.18712E+00
2	.28371E+00
3	-.25804E+00
4	.16789E+00
5	-.92550E-01
6	.56304E-01
7	-.41268E-01
8	.28955E-01
9	-.16257E-01
10	.68681E-02
11	-.21291E-02
12	.47055E-03
13	-.70359E-04
14	.63934E-05
15	-.26714E-06

(c)   Page 3

Figure 39.   Continued

	EQUIVALENT BODY		THETA RANGE WHERE THE
XF, FT	RADIUS, FT	DR/DX	BODY CONTOUR IS NOT SOLID
-22.25000	2.66000	.13789	99.900 DEG. TO 104.000 DEG.

		SHAPE OF CONTOUR		
THETA	RADIUS	DR/DTHETA	SLOPE OF CONTOUR	
DEG.	FT.	FT/RAD	DEG.	DNU/DX
3.00000	.66700	.00700	92.35372	.00032
9.00000	.67400	.11200	89.56525	.00063
15.00000	.69100	.18700	89.85720	0.00000
21.00000	.71500	.27000	90.31234	0.00000
27.00000	.74500	.38800	89.46926	.00227
33.00000	.79500	.51700	89.96347	.00241
39.00000	.85400	.70000	89.65948	.00272
45.00000	.93700	.94800	89.56565	.00405
51.00000	1.05400	1.31600	89.69165	.00260
57.00000	1.21200	1.91300	89.35671	.00308
63.00000	1.45200	2.53500	92.80326	.00382
69.00000	1.75200	2.26400	105.73455	-.01097
75.00000	1.94100	.71200	144.85599	-.04386
81.00000	1.90000	-.26700	179.39912	-.01304
87.00000	1.86600	-.06500	179.97389	.43750
93.00000	1.86600	-.09800	135.97452	.82125
99.00000	1.90700	24.79100	103.39870	.00900
105.00000	4.63400	2.24200	163.18159	.03607
111.00000	4.85600	2.43700	174.35006	.02774
117.00000	5.13600	-7.06900	260.95962	.02652
123.00000	4.41500	-6.35300	263.20274	.11651
129.00000	3.82100	-4.87300	270.89942	.10165
135.00000	3.42100	-2.95400	265.91029	.11044
141.00000	3.09500	1.51000	205.02216	.11794
147.00000	3.25000	1.12400	217.92225	.00423
153.00000	3.32500	1.56700	217.76652	.00203
159.00000	3.58700	2.23500	217.07365	-.03259
165.00000	3.80100	1.77600	229.95599	-.06531
171.00000	3.95100	1.04200	246.22575	-.08311
177.00000	4.02300	.30400	262.67563	-.10147

POLAR HARMONIC
COEFFICIENTS

K	A(K)
1	-.83303E-02
2	.77467E-01
3	-.55936E-01
4	.34117E-01
5	-.26176E-01
6	.17893E-01
7	-.74845E-02
8	.50629E-03
9	.10435E-02
10	-.74006E-03
11	.26263E-03
12	-.58377E-04
13	.82515E-05
14	-.68471E-06
15	.25579E-07

(d) Page 4

Figure 39. Continued

149

STATION NO. 4   15 POLAR HARMONIC COEFFICIENTS

XF, FT	EQUIVALENT BODY RADIUS, FT	DR/DX	THETA RANGE WHERE THE BODY CONTOUR IS NOT SOLID
-24.75000	2.77000	.07830	0.000 DEG. TO 0.000 DEG.

SHAPE OF CONTOUR

THETA DEG.	RADIUS FT.	DR/DTHETA FT/RAD	SLOPE OF CONTOUR DEG.	DNU/DX
3.00000	.66600	.02300	91.02302	0.00000
9.00003	.67600	.10900	89.94032	-.00032
15.00000	.69100	.19300	89.39467	0.00000
21.00000	.71500	.29800	89.06056	0.00000
27.00000	.75300	.39700	89.20071	0.00000
33.00000	.80400	.53800	89.21137	-.00133
39.00000	.86500	.74000	89.45330	-.00024
45.00000	.95500	.96500	89.11405	.00022
51.00000	1.06700	1.37500	88.81146	.00177
57.00000	1.23600	1.98500	89.76432	.00227
63.00000	1.47600	2.26200	96.12525	.00262
69.00000	1.69600	1.54900	116.59375	.00449
75.00000	1.79500	.76600	141.89007	.13646
81.00000	1.85600	13.06500	89.99529	.07291
87.00000	3.25400	12.50000	101.59133	.11342
93.00000	4.45600	1.01900	170.11906	.09358
99.00000	4.56500	1.44300	171.45921	.07353
105.00000	4.76200	1.90200	173.22764	.04455
111.00000	4.95300	3.11500	168.83373	.05038
117.00000	5.27700	-2.11300	229.32200	.01337
123.00000	5.05300	-4.33200	253.60630	.07653
129.00000	4.33700	-5.57300	271.10936	.07311
135.00000	3.87700	-3.92400	270.34519	.06505
141.00000	3.50500	-2.90500	270.62038	.06926
147.00000	3.26400	.64800	225.77111	.07215
153.00000	3.33200	.97100	226.75300	.00215
159.00000	3.46700	1.16300	230.45635	-.03671
165.00000	3.57400	.93800	240.29432	-.07057
171.00000	3.66300	.62100	251.37795	-.08455
177.00000	3.70500	.23100	263.43233	-.09837

POLAR HARMONIC COEFFICIENTS

K	A(K)
1	-.16694E-01
2	.52443E-01
3	-.42120E-01
4	.24854E-01
5	-.12288E-01
6	.51739E-02
7	-.18115E-02
8	.51793E-03
9	-.12269E-03
10	.25423E-04
11	-.48470E-05
12	.81637E-06
13	-.10577E-06
14	.87529E-08
15	-.33577E-09

(e) Page 5

Figure 39. Continued

150

STATION NO. 5   15 POLAR HARMONIC COEFFICIENTS

	EQUIVALENT BODY		THETA RANGE WHERE THE	
XF, FT	RADIUS, FT	DR/DX	BODY CONTOUR IS NOT SOLID	
-27.25000	2.97000	.01930	0.000 DEG. TO	0.000 DEG.

SHAPE OF CONTOUR

THETA	RADIUS	DR/DTHETA	SLOPE OF CONTOUR	
DEG.	FT.	FT/RAD	DEG.	DNU/DX
3.00000	.66900	.02700	90.68541	-.00032
9.00000	.67500	.10600	90.07533	C.00000
15.00000	.69100	.19100	89.54362	-0.00000
21.00000	.71500	.28800	89.06056	.00089
27.00000	.75300	.39400	89.37962	-.00095
33.00000	.79300	.53600	89.14477	-.00106
39.00000	.86400	.73700	88.53551	0.00000
45.00000	.95600	1.01900	89.17296	-.00295
51.00000	1.07600	1.42000	89.15290	-.00174
57.00000	1.24700	1.98600	89.12452	-.00294
63.00000	1.49100	2.31700	95.76146	-.00519
69.00000	1.71500	3.78900	93.35843	.02095
75.00000	2.26000	8.34600	90.15167	.02457
81.00000	3.47600	11.72500	97.50763	.06165
87.00000	4.72300	.32700	173.03941	.01035
93.00000	4.75600	.40700	179.10577	0.00000
99.00000	4.80600	.75400	180.08370	0.00000
105.00000	4.91200	1.42300	179.84377	.00092
111.00000	5.13900	1.94300	180.28894	-.01766
117.00000	5.32200	1.24500	193.93331	-.00436
123.00000	5.36800	-6.52500	263.55648	.00183
129.00000	4.70900	-5.74800	263.67424	.01622
135.00000	4.18400	-4.31500	270.89306	.01314
141.00000	3.79000	-3.16000	270.99633	.01790
147.00000	3.51300	-2.15800	269.56198	.01909
153.00000	3.33900	-.79500	256.39250	.01121
159.00000	3.34600	.03400	248.41781	-.01696
165.00000	3.34600	.23300	251.01562	-.03958
171.00000	3.39500	.23600	257.02354	-.07534
177.00000	3.39700	-.01800	267.30359	-.08256

POLAR HARMONIC
COEFFICIENTS

K	A(K)
1	-.51833E-01
2	.32952E-01
3	-.63105E-02
4	-.33093E-02
5	.18753E-03
6	.36152E-02
7	-.41863E-02
8	.25561E-02
9	-.10656E-02
10	.32119E-03
11	-.70727E-04
12	.11175E-04
13	-.12058E-05
14	.79805E-07
15	-.24494E-08

(f) Page 6

Figure 39. Continued

151

STATION NC. 6   15 POLAR HARMCNIC COEFFICIENTS

XF, FT	EQUIVALENT BODY RADIUS, FT	DR/DX	THETA RANGE WHERE THE BODY CONTOUR IS NOT SOLID
-23.75300	5.00700	.00256	0.300 DEG. TO 0.000 DEG.

SHAPE OF CONTOUR

THETA DEG.	RADIUS FT.	DR/DTHETA FT/RAD	SLOPE OF CONTOUR DEG.	DNU/DX
3.00030	.66700	0.00000	93.30000	-.00256
9.0C000	.67500	.11000	89.74427	-.00268
15.30C00	.69100	.19100	89.54862	-.00278
21.00003	.71900	.29400	89.41906	-.00327
27.00000	.75000	.39500	89.22572	-.00311
33.00000	.79500	.53300	89.16051	-.00346
39.30000	.86400	.70800	89.66729	-.00495
45.03000	.94300	.98500	89.75205	-.00365
51.C3000	1.06700	1.34700	89.38392	-.00556
57.30000	1.23000	1.96000	89.11037	-.00510
63.00000	1.46100	3.07700	88.39838	-.00515
69.30000	1.87300	5.21000	88.77356	-.00655
75.03000	2.55500	15.52000	84.34854	-.00535
91.30000	4.15400	5.74300	116.87573	-.03160
97.00000	4.75700	-.30900	177.10940	.00016
93.00000	4.75600	.23600	180.15923	-.00016
99.30000	4.80630	.75700	180.34890	0.00000
105.30000	4.91500	1.30500	180.13027	.00077
111.00000	5.08000	1.93600	180.13404	.00090
117.00000	5.30530	1.40800	192.14395	.00217
123.30000	5.37730	-5.65400	259.43845	.00915
129.00000	4.78930	-5.34900	267.16167	.00534
135.3C000	4.24300	-4.36800	270.83166	.00390
141.00000	3.86300	-3.18800	270.53167	.00420
147.00000	3.58300	-2.36900	270.47179	.00397
153.00000	3.37500	-1.40800	265.64517	.00251
159.00000	3.29300	-.72900	261.48274	-.00767
165.00000	3.22200	-.64400	266.30309	-.01401
171.00000	3.15900	-.40100	268.23437	-.01619
177.00000	3.13900	-.15800	269.88152	-.01886

POLAR HARMONIC
COEFFICIENTS

K	A(K)
1	-.41210E-01
2	.17688E-01
3	.17111E-02
4	-.68442E-02
5	.32077E-02
6	.72438E-03
7	-.18679E-02
8	.13139E-02
9	-.57593E-03
10	.17707E-03
11	-.39218E-04
12	.61832E-05
13	-.66239E-06
14	.43390E-07
15	-.13153E-08

(g)   Page 7

Figure 39.   Continued

152

STATION NC. 7   15 POLAR HARMONIC COEFFICIENTS

	EQUIVALENT BODY		THETA RANGE WHERE THE
XF, FT	RADIUS, FT	DR/DX	BODY CONTOUR IS NCT SOLID
-34.75000	3.00300	.00255	0.000 DEG. TO 0.000 DEG.

SHAPE OF CONTOUR

THETA	RADIUS	DR/DTHETA	SLOPE OF CONTOUR	
DEG.	FT.	FT/RAD	DEG.	DNU/DX
3.00000	.65100	.02000	91.24031	0.00000
9.00000	.65600	.00900	99.21637	0.00000
15.00000	.67300	.18400	89.70887	0.00000
21.00000	.69600	.25600	90.90567	0.00000
27.00000	.72300	.33800	92.09523	0.00000
33.00000	.76900	.47500	91.29638	0.00000
39.00000	.82400	.66200	90.22167	0.00000
45.00000	.91000	.67400	91.15604	0.00000
51.00000	1.01100	1.28100	89.29146	0.00000
57.00000	1.17000	1.40400	95.80557	C.00000
63.00000	1.38600	3.48600	84.68225	0.00000
69.00000	1.75200	4.60800	83.81722	0.00000
75.00000	2.34900	9.92600	93.31159	0.00000
81.00000	3.81700	11.58200	93.24031	0.00000
87.00000	4.75800	-.02900	177.34921	0.00000
93.00000	4.75500	.22700	180.26682	0.00000
99.00000	4.80600	.76000	180.01390	0.00000
105.00000	4.92000	1.32100	179.97079	0.00000
111.00000	5.08600	1.97100	179.81694	0.00000
117.00000	5.32200	1.78500	189.41593	0.00000
123.00000	5.46000	-6.27300	261.96373	0.00000
129.00000	4.83900	-5.63300	268.59604	0.00000
135.00000	4.27600	-4.44300	271.08390	0.00000
141.00000	3.89700	-3.21700	270.53990	0.00000
147.00000	3.61200	-2.39300	270.52502	0.00000
153.00000	3.39200	-1.77900	270.67563	0.00000
159.00000	3.24200	-1.27400	270.45320	0.00000
165.00000	3.12700	-.86000	270.37753	0.00000
171.00000	3.05700	-.49000	270.10636	0.00000
177.00000	3.02100	-.24500	271.63643	0.00000

POLAR HARMONIC
COEFFICIENTS

K	A(K)
1	-.39204E-01
2	.13867E-01
3	.45069E-02
4	-.78955E-02
5	.33636E-02
6	.65971E-03
7	-.17084E-02
8	.11594E-02
9	-.4696CE-03
10	.14501E-33
11	-.30935E-04
12	.46979E-05
13	-.48477E-06
14	.30590E-07
15	-.89342E-09

(h)   Page 8

Figure 39.   Continued

153

STATION NO. 8   15 POLAR HARMONIC COEFFICIENTS

	EQUIVALENT BODY		THETA RANGE WHERE THE
XF, FT	RADIUS, FT	DR/DX	BODY CONTOUR IS NOT SOLID
-40.58000	2.99000	.00256	0.000 DEG. TO 0.000 DEG.

SHAPE OF CONTOUR

THETA DEG.	RADIUS FT.	DR/DTHETA FT/RAD	SLOPE OF CONTOUR DEG.	DNU/DX
3.00000	.65100	.02000	91.24031	-.00027
9.00000	.65800	.00900	93.21637	.00055
15.00000	.67300	.16400	89.70387	-.00079
21.00000	.69600	.25600	90.80567	.00103
27.00000	.72800	.33800	92.09523	.00050
33.00000	.76900	.47500	91.29698	.00256
39.00000	.82400	.66200	90.22167	.00363
45.00000	.91000	.87400	91.15604	.00178
51.00000	1.01100	1.29100	89.28146	.00560
57.00000	1.17000	1.40400	96.80557	.00649
63.00000	1.38600	3.46600	84.68229	.00547
69.00000	1.75200	4.60800	89.81722	.00662
75.00000	2.34900	9.92800	88.31159	.01268
81.00000	3.81700	11.56200	93.24031	.03027
87.00000	4.75000	-.02900	177.34921	.00055
93.00000	4.75500	.22700	199.26692	.01779
99.00000	4.80600	.76000	190.01390	.01732
105.00000	4.92000	1.32100	179.97078	.01652
111.00000	5.08600	1.97100	179.81694	.01635
117.00000	5.32200	1.78900	189.41983	.00208
123.00000	5.46300	-6.27300	261.96379	-.01439
125.00000	4.83900	-5.68300	268.58604	-.01049
135.00000	4.27500	-4.44300	271.08390	-.00532
141.00000	3.89700	-3.21700	270.53990	-.00570
147.00000	3.61200	-2.39300	270.52502	-.00731
153.00000	3.39200	-1.77900	270.67563	-.00534
159.00000	3.24200	-1.27400	270.45320	-.00916
165.00000	3.12700	-.86000	270.37753	-.00449
171.00000	3.05700	-.45000	270.10636	-.00460
177.00000	3.02100	-.24500	271.63649	-.00573

POLAR HARMONIC
COEFFICIENTS

K	A(K)
1	-.46237E-01
2	.17611E-01
3	.47747E-02
4	-.56546E-02
5	.44861E-02
6	.51305E-03
7	-.19735E-02
8	.13977E-02
9	-.60256E-03
10	.18095E-03
11	-.39015E-04
12	.59773E-05
13	-.62154E-06
14	.39490E-07
15	-.11606E-08

(i)   Page 9

Figure 39.   Continued

154

STATION NC. 9   15 POLAR HARMONIC COEFFICIENTS

XF, FT	EQUIVALENT BODY RADIUS, FT	DR/DX	THETA RANGE WHERE THE BODY CONTOUR IS NOT SOLID
-43.50000	3.02200	.00256	0.000 DEG. TO 0.000 DEG.

SHAPE OF CONTOUR

THETA DEG.	RADIUS FT.	DR/DTHETA FT/RAD	SLOPE OF CONTOUR DEG.	DNU/DX
3.00000	.65000	.06000	87.72610	.00273
9.00000	.66000	.09000	91.23483	.00272
15.00000	.67000	.20000	93.37924	.00263
21.00000	.70000	.30000	87.90141	.00126
27.00000	.73000	.38000	89.50086	.00243
33.00000	.78000	.51000	99.82149	.00230
39.00000	.84100	.68000	90.04234	.00203
45.00000	.91900	.96000	89.75000	.00199
51.00000	1.04400	1.33000	99.13058	.00051
57.00000	1.20700	1.97000	86.49540	.00053
63.00000	1.44000	3.45000	85.65523	.00053
69.00000	1.82000	5.25000	97.98554	-.00085
75.00000	2.55000	11.75000	87.24453	-.00201
81.00000	4.17000	5.90000	116.25189	-.03455
87.00000	4.76000	3.25000	142.67579	-.01360
93.00000	4.82000	.50000	177.07764	.02730
99.00000	4.97000	.77000	190.01529	.04337
105.00000	4.99000	1.33000	180.07573	.04773
111.00000	5.15000	1.62000	183.53835	.03142
117.00000	5.33000	1.15000	194.82451	.00537
123.00000	5.38000	-5.45000	258.37033	-.01639
129.00000	4.78000	-5.39000	267.37969	-.00365
135.00000	4.25000	-4.33000	278.53421	-.00056
141.00000	3.87000	-3.05000	263.24213	0.00000
147.00000	3.56000	-2.38000	270.61614	-.00114
153.00000	3.37000	-1.76000	270.57605	-.00122
159.00000	3.21000	-1.24000	270.12119	-.00128
165.00000	3.11000	-.85000	270.28629	-.00265
171.00000	3.04000	-.52000	270.70665	-.00271
177.00000	3.00000	-.25000	271.76364	-.00137

POLAR HARMONIC
COEFFICIENTS

K	A(K)
1	-.19226E-01
2	.50772E-02
3	-.37020E-02
4	.46463E-02
5	-.15185E-02
6	-.23542E-02
7	.34597E-02
8	-.23985E-02
9	.10816E-02
10	-.34286E-03
11	.77841E-04
12	-.12489E-04
13	.13521E-05
14	-.68948E-07
15	.26932E-08

(j) Page 10

Figure 39. Continued

155

STATION NO. 10   15 POLAR HARMONIC COEFFICIENTS

XF, FT	EQUIVALENT BODY RADIUS, FT	DR/DX	THETA RANGE WHERE THE BODY CONTOUR IS NOT SOLID
-49.33000	3.04700	-.09326	0.000 DEG. TO 0.000 DEG.

SHAPE OF CONTOUR

THETA DEG.	RADIUS FT.	DR/DTHETA FT/RAD	SLOPE OF CONTOUR DEG.	DNU/DX
3.00000	.67000	0.00000	93.00000	0.00000
9.00000	.68000	.09000	91.46055	0.00000
15.00000	.69000	.15000	92.73523	0.00000
21.00000	.71000	.32000	86.73571	0.00000
27.00000	.75000	.41000	93.33604	0.00000
33.00000	.80000	.48000	92.03624	0.00000
39.00000	.86000	.67000	91.97892	0.00000
45.00000	.94000	.95000	89.69695	0.00000
51.00000	1.05000	1.40000	97.96990	0.00000
57.00000	1.22000	2.00000	88.38313	0.00000
63.00000	1.45000	2.76000	90.71574	0.00000
69.00000	1.80000	4.55000	90.58397	0.00000
75.00000	2.45000	12.60000	85.93571	0.00000
81.00000	3.73000	10.95000	93.81086	0.00000
87.00000	4.64000	6.14000	124.07535	0.00000
93.00000	5.02000	2.62000	155.43935	0.00000
99.00000	5.19000	1.57000	172.16919	0.00000
105.00000	5.35000	.91000	185.34675	0.00000
111.00000	5.39000	.10000	199.93712	0.00000
117.00000	5.37000	-.86000	216.09860	0.00000
123.00000	5.21000	-4.79000	255.05399	0.00000
129.00000	4.74000	-4.85000	264.65717	0.00000
135.00000	4.24000	-4.35000	270.73366	0.00000
141.00000	3.87000	-3.19000	270.49840	0.00000
147.00000	3.57000	-2.43000	271.24203	0.00000
153.00000	3.36000	-1.76000	270.64597	0.00000
159.00000	3.20000	-1.29000	270.95559	0.00000
165.00000	3.09000	-.86000	270.55290	0.00000
171.00000	3.02000	-.43000	270.03107	0.00000
177.00000	2.99000	-.25000	271.77950	0.00000

POLAR HARMONIC
COEFFICIENTS

K	A(K)
1	-.62456E-01
2	-.13760E-01
3	.21067E-01
4	-.73246E-02
5	-.22153E-02
6	.38650E-02
7	-.22629E-02
8	.82247E-03
9	-.20086E-03
10	.31725E-04
11	-.25102E-05
12	-.11319E-06
13	.52209E-07
14	-.53801E-08
15	.20777E-09

(k) Page 11

Figure 39. Continued

156

STATION NO. 11   O POLAR HARMONIC COEFFICIENTS

	EQUIVALENT BODY		THETA RANGE WHERE THE
XF, FT	RADIUS, FT	DR/DX	BODY CONTOUR IS NOT SOLID
-49.83000	3.04700	-.09326	0.300 DEG. TO 0.000 DFG.

SHAPE OF CONTOUR

THETA DEG.	RADIUS FT.	DR/DTHETA FT/RAD	SLOPE OF CONTOUR DEG.	DNU/DX
3.00000	.67000	0.00000	93.00000	
9.00000	.66000	.09000	91.46055	
15.00000	.69000	.15000	92.73523	
21.00000	.71000	.32000	86.73871	
27.00000	.75000	.41000	68.33604	
33.00000	.80000	.48000	92.03624	
39.00000	.86000	.67000	91.07692	
45.00000	.94000	.55000	89.69685	
51.00000	1.05000	1.40000	87.86990	
57.00000	1.22000	2.00000	89.38319	
63.00000	1.45000	2.76000	90.71574	
69.00000	1.60000	4.55000	90.58397	
75.00000	2.45000	12.80000	65.93571	
81.00000	3.73000	10.95000	99.81086	
87.00000	4.64000	6.14000	124.07835	
93.00000	5.02000	2.62000	155.43939	
99.00000	5.19000	1.57000	172.16918	
105.00000	5.35000	.91000	185.34675	
111.00000	5.39000	.10000	199.33712	
117.00000	5.37000	-.86000	216.89860	
123.00000	5.21000	-4.70000	255.05398	
129.00000	4.74000	-4.85000	264.65717	
135.00000	4.24000	-4.35000	270.73366	
141.00000	3.87000	-3.19000	273.45840	
147.00000	3.57000	-2.43000	271.24203	
153.00000	3.36000	-1.76000	270.64537	
159.00000	3.20000	-1.29000	270.95553	
165.00000	3.09000	-.66000	270.55290	
171.00000	3.02000	-.49000	270.03107	
177.00000	2.99000	-.25000	271.77950	

LOCATION OF WING ROOT CHORD LEADING EDGE RELATIVE TO FUSELAGE NOSE
        XF = -29.98000 FEET
        ZF =   .33300 FEET
INCIDENCE ANGLE OF WING ROOT CHORD RELATIVE TO FUSELAGE AXIS
        IW =   0.00 DEGREES

(1) Page 12

Figure 39. Continued

157

WING INPUT DATA
LENGTH OF WING ROOT CHORD
    CRW = 13.67000 FEET

WING SEMISPAN
    S'PAN = 16.42000 FEET

40 VORTICES ARE TO BE LAID OUT ON EACH WING PANEL.
    5 CHORDWISE ROWS WITH 8 IN EACH ROW

SPANWISE LOCATIONS OF TRAILING VORTEX LEGS AND SWEEP ANGLES AND
DIHEDRAL ANGLE OF WING SECTION TO THE RIGHT

I	SPANWISE LOCATION FEET	LE SWEEP DEGREES	TE SWEEP DEGREES	DIHEDRAL DEGREES
1	-4.3300	0.00000	0.00000	0.00000
2	-7.15000	45.00000	11.00000	0.00000
3	-9.47000	45.00000	11.00000	0.00000
4	-11.79000	45.00000	11.00000	0.00000
5	-14.10000	45.00000	11.00000	0.00000
6	-16.42000	45.00000	11.00000	0.00000

60 THICKNESS PANELS ARE TO BE LAID OUT ON EACH WING PANEL
   5 CHORDWISE ROWS WITH 12 IN EACH ROW
   THE CHORDWISE ROWS COINCIDE WITH THOSE USED
   IN THE VORTEX LATTICE

(m) Page 13

Figure 39. Continued

158

VORTEX LATTICE COORDINATES, SWEEP AND DIHEDRAL ANGLES,
AND INPUT TWIST AND CAMBER DISTRIBUTION
AT CONTROL POINTS
(WING COORDINATE SYSTEM)

WING VORTICES

ROW	VORTEX	CONTROL POINT X,FT	BOUND LEG MID POINT X,FT	Y,FT	Z,FT	SWEEP DEG	DIHEDRAL DEG	CAMBER SLOPE
1	1	-2.35256	-1.55652	-5.93150	0.00000	44.26962	0.00000	0.00000
1	2	-3.34465	-3.14d61	-5.93150	0.00000	41.15742	0.00000	0.00000
1	3	-5.53674	-4.74069	-5.93150	0.00000	37.71906	0.00000	0.00000
1	4	-7.12882	-6.33278	-5.93150	0.00000	33.92939	0.00000	0.00000
1	5	-8.72091	-7.92467	-5.93150	0.00000	29.77019	0.00000	0.00000
1	6	-10.31300	-9.51635	-5.93150	0.00000	25.23507	0.00000	0.00000
1	7	-11.90508	-11.10904	-5.93150	0.00000	20.33519	0.00000	0.00000
1	8	-13.49717	-12.70112	-5.93150	0.00000	15.10462	0.00000	0.00000
2	1	-4.49594	-3.81665	-8.31000	0.00000	44.26962	0.00000	0.00000
2	2	-5.85456	-5.17526	-8.31000	0.00000	41.15742	0.00000	0.00000
2	3	-7.21317	-6.53397	-8.31000	0.00000	37.71906	0.00000	0.00000
2	4	-8.57178	-7.89247	-8.31000	0.00000	33.92939	0.00000	0.00000
2	5	-9.93039	-9.25108	-8.31000	0.00000	29.77019	0.00000	0.00000
2	6	-11.26899	-10.60969	-8.31000	0.00000	25.23507	0.00000	0.00000
2	7	-12.64760	-11.96830	-8.31000	0.00000	20.33519	0.00000	0.00000
2	8	-14.00621	-13.32630	-8.31000	0.00000	15.10462	0.00000	0.00000
3	1	-6.64073	-6.07824	-10.63000	0.00000	41.15742	0.00000	0.00000
3	2	-7.76571	-7.20322	-10.63000	0.00000	37.71906	0.00000	0.00000
3	3	-8.89069	-8.32820	-10.63000	0.00000	33.92939	0.00000	0.00000
3	4	-10.01567	-9.45310	-10.63000	0.00000	29.77019	0.00000	0.00000
3	5	-11.14064	-10.57816	-10.63000	0.00000	25.23507	0.00000	0.00000
3	6	-12.26562	-11.70313	-10.63000	0.00000	20.33519	0.00000	0.00000
3	7	-13.39060	-12.82811	-10.63000	0.00000	15.10462	0.00000	0.00000
4	1	-8.78089	-8.33436	-12.94500	0.00000	44.26962	0.00000	0.00000
4	2	-9.67274	-9.22681	-12.94500	0.00000	41.15742	0.00000	0.00000
4	3	-10.56459	-10.11867	-12.94500	0.00000	37.71906	0.00000	0.00000
4	4	-11.45644	-11.01052	-12.94500	0.00000	33.92939	0.00000	0.00000
4	5	-12.34830	-11.90237	-12.94500	0.00000	29.77019	0.00000	0.00000
4	6	-13.24015	-12.79422	-12.94500	0.00000	25.23507	0.00000	0.00000
4	7	-14.13200	-13.68607	-12.94500	0.00000	20.33519	0.00000	0.00000
4	8	-15.02385	-14.57732	-12.94500	0.00000	15.10462	0.00000	0.00000
5	1	-10.32189	-10.59169	-15.26000	0.00000	44.26962	0.00000	0.00000
5	2	-11.57977	-11.25001	-15.26000	0.00000	41.15742	0.00000	0.00000
5	3	-12.23849	-11.90913	-15.26000	0.00000	37.71906	0.00000	0.00000
5	4	-12.89722	-12.56796	-15.26000	0.00000	33.92939	0.00000	0.00000
5	5	-13.55595	-13.22658	-15.26000	0.00000	29.77019	0.00000	0.00000
5	6	-14.21467	-13.88531	-15.26000	0.00000	25.23507	0.00000	0.00000
5	7	-14.87340	-14.54403	-15.26000	0.00000	20.33519	0.00000	0.00000
5	8	-15.53212	-15.20276	-15.26000	0.00000	15.10462	0.00000	0.00000

(n) Page 14

Figure 39. Continued

159

WING IMAGE VORTICES

ROW	VORTEX	BOUND LEG MID POINT X, FT	Y, FT	Z, FT	SWEEP DEG	DIHEDRAL DEG
1	1	-1.55652	-1.60636	-.23677	-74.61299	-6.60806
1	2	-3.14861	-1.60696	-.23677	-72.93842	-6.60806
1	3	-4.74069	-1.60636	-.23677	-70.87004	-6.60806
1	4	-6.33278	-1.60636	-.23677	-68.25833	-6.60806
1	5	-7.92487	-1.60636	-.23677	-64.87353	-6.60806
1	6	-9.51695	-1.60636	-.23677	-60.35122	-6.60806
1	7	-11.10904	-1.60636	-.23677	-54.10031	-6.60806
1	8	-12.70112	-1.60696	-.23677	-45.17391	-6.60806
2	1	-3.81665	-1.13967	-.28552	-81.99134	-4.68043
2	2	-5.17526	-1.13967	-.28552	-81.08279	-4.68043
2	3	-6.53387	-1.13967	-.28552	-79.94418	-4.68043
2	4	-7.89247	-1.13967	-.28552	-78.47653	-4.68043
2	5	-9.25108	-1.13967	-.28552	-76.51664	-4.68043
2	6	-10.60969	-1.13967	-.28552	-73.77489	-4.68043
2	7	-11.96830	-1.13967	-.28552	-69.69182	-4.68043
2	8	-13.32690	-1.13967	-.28552	-63.86268	-4.68043
3	1	-6.07824	-.88474	-.30462	-85.11979	-3.63175
3	2	-7.20322	-.88474	-.30462	-84.56077	-3.63175
3	3	-8.32820	-.88474	-.30462	-83.85766	-3.63175
3	4	-9.45318	-.88474	-.30462	-82.94685	-3.63175
3	5	-10.57816	-.88474	-.30462	-81.72110	-3.63175
3	6	-11.70313	-.88474	-.30462	-79.98494	-3.63175
3	7	-12.82811	-.88474	-.30462	-77.34234	-3.63175
3	8	-13.95309	-.88474	-.30462	-72.86151	-3.63175
4	1	-8.33496	-.72389	-.31408	-86.71683	-2.97075
4	2	-9.22681	-.72389	-.31408	-86.33957	-2.97075
4	3	-10.11867	-.72389	-.31408	-85.86453	-2.97075
4	4	-11.01052	-.72389	-.31408	-85.24812	-2.97075
4	5	-11.90237	-.72389	-.31408	-84.41645	-2.97075
4	6	-12.79422	-.72389	-.31408	-83.23355	-2.97075
4	7	-13.68607	-.72389	-.31408	-81.41946	-2.97075
4	8	-14.57792	-.72389	-.31408	-78.29479	-2.97075
5	1	-10.59168	-.61294	-.31947	-87.64089	-2.51471
5	2	-11.25041	-.61284	-.31947	-87.36948	-2.51471
5	3	-11.90913	-.61294	-.31947	-87.02755	-2.51471
5	4	-12.56786	-.61294	-.31947	-86.58357	-2.51471
5	5	-13.22659	-.61294	-.31947	-85.98394	-2.51471
5	6	-13.88531	-.61284	-.31947	-85.12962	-2.51471
5	7	-14.54403	-.61294	-.31947	-83.81540	-2.51471
5	8	-15.20276	-.61284	-.31947	-81.53668	-2.51471

(o) Page 15

Figure 39. Continued

160

INPUT VALUES OF THE LOCAL SURFACE SLOPE OF THE THICKNESS
DISTRIBUTION. FOR EACH CHORDWISE ROW THE FIRST VALUE
IS FOR THE PANEL NEAREST THE LEADING EDGE

WING THICKNESS DATA
ROW   SLOPES
1   .02720   .05930   .04360   .02120   0.00000   -.02600   -.03920   -.03920
      -.03920   -.03920   -.03920   -.03920   0.00000
2   .08720   .05930   .04360   .02130   0.00000   -.02600   -.03920   -.03920
      -.03920   -.03920   -.03920   -.03920   0.00000
3   .08720   .05930   .04360   .02130   0.00000   -.02600   -.03920   -.03920
      -.03920   -.03920   -.03920   -.03920   0.00000
4   .08720   .05930   .04360   .02130   0.00000   -.02600   -.03920   -.03920
      -.03920   -.03920   -.03920   -.03920   0.00000
5   .08720   .05930   .04360   .02130   0.00000   -.02600   -.03920   -.03920
      -.03920   -.03920   -.03920   -.03920

(p) Page 16

Figure 39. Continued

161

STORE INPUT DATA

STORE SHAPE NO	NO	LENGTH FT	MAXIMUM RADIUS FT	STORE LOCATION RELATIVE TO LOCAL WING CHORD LEADING EDGE			INCIDENCE ANGLE DEG
				X, FT	Y, FT	Z, FT	
2	1	10.62500	.62500	2.13200	0.0000	4.25600	3.50000
9	1	10.62500	.62500	9.33750	0.00000	.95800	0.00000

SOURCE DISTRIBUTION FOR SHAPE NO 1

INCOMPRESSIBLE SOURCE DISTRIBUTION

X/L   0.00000E-03 2.56501E-03 3.29665E-03 6.24130E-03 5.46606E-03 7.04621E-03 9.09120E-03 1.16977E-02
Q.(K) 5.32307E-06-5.24710E-06 3.05297E-06-1.33409E-06 1.23479E-06 2.81012E-07 1.44612E-06 1.91907E-06

X/L   1.50519E-02 1.93364E-02 2.47833E-02 3.16694E-02 4.03092E-02 5.10518E-02 6.42597E-02 8.02789E-02
Q.(K) 3.46467E-06 5.55270E-06 9.08092E-06 1.40075E-05 2.24017E-05 3.36919E-05 4.86576E-05 6.64669E-05

X/L   9.93922E-02 1.21760E-01 1.47356E-01 1.75900E-01 2.06827E-01 2.39281E-01 2.71845E-01 3.04088E-01
Q.(K) 8.50761E-05 9.56405E-05 1.15161E-04 3.05098E-05 1.04260E-04 9.11703E-05-9.44446E-05

X/L   3.37391E-01 3.69694E-01 4.02297E-01 4.30901E-01 4.67500E-01 5.00107E-01 5.32710E-01 5.65313E-01
Q.(K) 9.06410E-05-9.28360E-05 9.13533E-05-9.23778E-05 9.16563E-05-9.21635E-05 9.10160E-03-9.20356E-05

X/L   5.97317E-01 6.30520E-01 6.63125E-01 6.95726E-01 7.28329E-01 7.60933E-01 7.93536E-01 8.26139E-01
Q.(K) 9.19259E-05-9.19357E-05 9.20249E-05-9.18293E-05 9.21479E-05-9.16771E-05 9.23483E-05-9.13974E-05

X/L   8.58742E-01 5.91345E-01 9.23949E-01 9.56552E-01 9.89155E-01 1.02176E+00 1.05442E+00 1.08569E+00
Q.(K) 9.27639E-05-9.07454E-05 9.39791E-05-8.93336E-05 1.04218E-04-3.06997E-05-7.97454E-05-1.00720E-04

X/L   1.11447E+00 1.13997E+00 1.16170E+00 1.17959E+00 1.19369E+00 1.20407E+00 1.21322E+00 1.21942E+00
Q.(K)-1.11599E-04-9.59665E-05-7.18790E-05-4.05564E-05-2.97969E-05-1.76253E-05-9.01840E-06-6.03434E-06

X/L   1.22395E+00 1.22723E+00 1.22950E+00
Q.(K)-7.96050E-07-4.09273E-06 3.63053E-06

(q) Page 17

Figure 39. Continued

162

VORTEX LATTICE CONTROL POINT COORDINATES
INTERFERENCE VELOCITIES INDUCED AT THESE POINTS
CALCULATED VORTEX STRENGTHS
(WING COORDINATE SYSTEM)

WING CONTROL POINTS ROW VORTEX		X_0 FT	Y_0 FT	Z_0 FT	U/VINF	V/VINF	W/VINF	GAMMA/VINF
1	1	-2.35256	-5.59150	0.00000	-.01736	-.00855	-.01175	.18031
1	2	-3.94465	-5.59150	0.00000	-.01449	-.00655	-.01142	.08072
1	3	-5.53674	-5.59150	0.00000	-.01347	-.00531	-.01134	.05536
1	5	-7.12862	-5.59150	0.00000	-.01325	-.00594	-.01162	.04250
1	6	-8.72091	-5.59150	0.10000	-.01372	-.00533	-.01190	.03296
1	6	-10.31300	-5.59150	0.00000	-.01427	-.00403	-.01239	.02407
1	7	-11.90508	-5.59150	0.00000	-.01341	-.00054	-.01234	.00145
1	8	-13.49717	-5.59150	0.00000	-.01356	.00391	-.00516	-.00041
2	1	-4.49596	-8.31000	0.00000	-.01275	-.00271	-.00619	.22577
2	2	-5.65456	-8.31000	0.00000	-.01229	-.00185	-.00623	.10307
2	3	-7.21317	-8.31000	0.00000	-.01197	-.00115	-.00636	.07059
2	4	-8.57178	-8.31000	0.00000	-.01195	-.00042	-.00652	.05263
2	5	-9.93039	-8.31000	0.00000	-.01204	.00040	-.00674	.03932
2	6	-11.28899	-8.31000	0.00000	-.01216	.00172	-.00601	.02612
2	7	-12.64760	-8.31000	0.00000	-.01251	.00356	-.00403	.01420
2	8	-14.00621	-8.31000	0.00000	-.01351	.00522	-.00327	.00867
3	1	-6.60073	-10.63000	0.00000	-.01056	-.00042	-.00393	.23002
3	2	-7.76571	-10.63000	0.00000	-.01047	.00021	-.00402	.10667
3	3	-8.89069	-10.63000	0.00000	-.01045	.00047	-.00412	.07245
3	4	-10.01567	-10.63000	0.00000	-.01050	.00151	-.00424	.05300
3	5	-11.14064	-10.63000	0.00000	-.01063	.00233	-.00392	.03818
3	6	-12.26562	-10.63000	0.00000	-.01074	.00365	-.00290	.02593
3	7	-13.39060	-10.63000	0.00000	-.01124	.00465	-.00190	.01725
3	8	-14.51558	-10.63000	0.00000	-.01170	.00500	-.00259	.01211
4	1	-8.78069	-12.94500	0.00000	-.00908	.00186	-.00282	.21300
4	2	-9.67274	-12.94500	0.00000	-.00909	.00155	-.00289	.07863
4	3	-10.56659	-12.94500	0.00000	-.00913	.00200	-.00296	.06566
4	5	-11.45644	-12.94500	0.00000	-.00920	.00271	-.00258	.04614
4	5	-12.34830	-12.94500	0.00000	-.00930	.00344	-.00196	.03277
4	6	-13.24015	-12.94500	0.00000	-.00944	.00421	-.00143	.02301
4	7	-14.13200	-12.94500	0.00000	-.00959	.00438	-.00151	.01627
4	8	-15.02385	-12.94500	0.00000	-.00775	.00510	-.00205	.01019
5	1	-10.72109	-15.26000	0.00000	-.00743	.00220	-.00207	.17223
5	2	-11.57977	-15.26000	0.00000	-.00745	.00262	-.00178	.07649
5	3	-12.23849	-15.26000	0.00000	-.00746	.00306	-.00149	.04723
5	4	-12.43722	-15.26000	0.00000	-.00748	.00352	-.00121	.03064
5	5	-13.55595	-15.26000	0.00300	-.00749	.00000	-.00092	.02041
5	6	-14.21467	-15.26000	0.00300	-.00790	.00465	-.00115	.01417
5	7	-14.73400	-15.26000	0.10000	-.00789	.00533	-.00142	.00955
5	8	-15.53212	-15.26000	0.00000	-.00787	.00543	-.00170	.00559

(r) Page 18

Figure 39. Continued

163

STORE NUMBER   2 IS THE STORE EJECTED

ADDITIONAL INPUT FOR THIS STORE
STORE MASS =   24.845 SLUGS
MOMENTS AND PRODUCTS OF INERTIA, SLUG - SQ FT
        IXX =   5.40
        IVV =   157.50
        IZZ =   157.50
        IVZ =   0.00
        IXZ =   0.00
        IXY =   0.00
STORE MOMENT CENTER IS -5.31250 FEET BEHIND NOSE
STORE CENTER OF GRAVITY OFFSET FROM MOMENT CENTER, FEET
    XBAR = 0.00000
    YBAP = 0.00000
    ZBAR = 0.00000
POLYNOMIALS SPECIFYING COMPRESSIBLE STORE SHAPE
    X/L OF END OF EACH SECTION
    SECTION   X/L
        1   .23530
        2   1.10000
    COEFFICIENTS OF POLYNOMIALS DESCRIBING EACH SECTION

SECTION	C1	C2	C3	C4	C5	C6	C7
1	-.44130	-1.00000	.47060	.19470	0.00000	0.00000	1.00000
2	.05802	0.00000	0.00000	0.00000	0.00000	0.00000	0.00000

SEPARATION ASSUMED 10.62500 FEET FROM NOSE
AXIAL-FORCE COEFFICIENT IS .34300
CROSSFLOW-DRAG COEFFICIENT IS 1.20000

THIS STORE HAS A CRUCIFORM EMPENNAGE
THE EMPENNAGE FORCES ACT -9.57300 FEET BEHIND NOSE
THE AVERAGE BODY RADIUS IN THE EMPENNAGE REGION IS .62500 FEET
THE TAIL FIN SEMISPAN MEASURED FROM THE BODY AXIS IS 1.45833 FEET
THE FINS ARE INITIALLY ROLLED 0.00 DEGREES FROM THE VERTICAL AND HORIZONTAL
THE FIN LIFT-CURVE SLOPE IS 3.10000 PER RADIAN

(s) Page 19

Figure 39. Continued

164

TIME = 0.00300 SECONDS

FORCE AND MOMENT COEFFICIENTS

	CN	CY	CLM	CLN	CLL
BUOYANCY	.01382	-.00000	.05494	.00003	
SLENDER BODY	.19258	-.00300	.44937	.03003	
CROSSFLOW	0.00000	0.00000	0.00000	0.03003	
EMPENNAGE	.60029	.00300	-2.04457	-.03000	-.0008:
TOTAL	.40661	.00300	-1.33967	-.00000	-.0000:

LOAD AND VELOCITY DISTRIBUTION:

X, FT	X/L	DCN/DX	DCY/DX	U/VS	V/VS	W/VS
.13281	.01250	.02953	-.00000	1.02752	-.00000	.08434
.39844	.03750	.07474	-.00000	1.02565	-.00000	.08612
.66406	.06250	.10267	-.00000	1.02337	-.00000	.08758
.92969	.08750	.11534	-.00000	1.02222	-.00000	.08840
1.19531	.11250	.11544	.00000	1.02373	-.00300	.08543
1.46094	.13750	.10549	-.00000	1.01998	-.00000	.09073
1.72656	.16250	.0873	-.00000	1.01923	-.00000	.09153
1.99219	.18750	.06475	.00000	1.01721	-.00000	.09227
2.25781	.21250	.03552	-.00000	1.01631	-.00000	.09304
2.52344	.23750	.01147	.00000	1.01552	-.00000	.09352
2.78906	.26250	.01212	-.00000	1.01479	-.00000	.09462
3.05469	.28750	.01246	-.00000	1.01411	-.00000	.09543
3.32031	.31250	.01273	.00000	1.01344	-.00000	.09627
3.58594	.33750	.01275	-.00000	1.01274	-.00000	.09712
3.85156	.36250	.01235	-.0000C	1.01197	-.00000	.09796
4.11719	.38750	.01137	-.00000	1.01111	-.00000	.09875
4.38281	.41250	.00973	.00000	1.01015	-.00000	.09946
4.64844	.43750	.00746	-.00000	1.00911	-.00000	.10003
4.91406	.46250	.00472	.03000	1.03301	-.00000	.10044
5.17969	.48750	.00175	-.00000	1.00670	-.00000	.10066
5.44531	.51250	-.00116	-.00000	1.00534	-.00000	.10067
5.71094	.53750	-.00374	-.00000	1.00437	-.00000	.10051
5.97656	.56250	-.00576	-.00000	1.00405	-.00000	.10019
6.24219	.58750	-.00713	.00000	1.00340	-.00000	.09975
6.50781	.61250	-.00782	.00000	1.00294	-.00000	.09925
6.77344	.63750	-.00789	-.00000	1.00256	-.00000	.09872
7.03906	.66250	-.00779	.00000	1.00254	-.00000	.09821
7.30469	.68750	-.00759	-.00000	1.00256	-.00000	.09769
7.57031	.71250	-.00657	.00000	1.00278	-.00000	.09722
7.83594	.73750	-.00550	-.00000	1.00291	-.00000	.09672
8.10156	.76250	-.00442	-.00000	1.00313	-.00000	.09649
8.36719	.78750	-.00332	-.00000	1.00351	-.00000	.09623
8.63281	.81250	-.00241	.00000	1.00395	-.00000	.09604
8.89844	.83750	-.00152	.00000	1.00420	-.00000	.09591
9.16406	.86250	-.00071	-.00000	1.00455	-.00030	.09584
9.42969	.88750	.00001	-.00000	1.00490	-.0000C	.09551
9.69531	.91250	.00068	.00000	1.00524	-.00000	.09594
9.96094	.93750	.00130	.00000	1.00551	-.00000	.09590
10.22656	.96250	.00170	-.00000	1.00551	-.00000	.09601
10.49219	.98750	.00240	.00000	1.00623	-.00000	.09616

LOCATION OF STORE IN FUSELAGE COORDINATE SYSTEM, DIMENSIONS OF FEET

	RELATIVE TO FUSELAGE NOSE			RELATIVE TO INITIAL POSITION		
	XF	YF	ZF	DEL XF	DEL YF	DEL ZF
NOSE	-27.69098	0.00003	4.59980	.03000	0.00000	-.00000
MOM	-32.99059	0.00000	4.51332	0.03000	0.00000	0.00000
BASE	-36.29318	0.00030	5.23764	.03000	0.00000	0.00000

TRANSLATIONAL VELOCITIES AND ACCELERATIONS OF STORE IN FUSELAGE COORDINATE SYSTEM
RELATIVE TO FUSELAGE MOTION

DXF	DYF	DZF	D2XF	D2YF	D2ZF
0.00030	0.00000	0.00000	-7.04371	.03000	19.95142

ROTATIONAL VELOCITIES AND ACCELERATIONS OF STORE IN STORE COORDINATE SYSTEM

P	Q	R	PDOT	QDOT	RDOT
0.00000	0.00000	0.00000	-.00003	-4.13589	-.00000

STORE ANGULAR ORIENTATION IN FUSELAGE COORDINATE SYSTEM AND RATES OF CHANGE OF THESE ANGLES
ANGLES IN DEGREES, RATES OF CHANGE IN RADIANS PER SECOND

PSI	THETA	PHI	DPSI	DTHETA	DPHI
0.00000	3.50000	0.00000	0.00000	0.03000	0.00000

(t) Page 20

Figure 39. Concluded

165

VITA

Arthur C. Powell was born on 29 July 1949 in Okarche, Oklahoma. He attended Oklahoma State University from September 1967 to May 1972, receiving his Bachelor of Science in Mechanical and Aerospace Engineering. Upon graduation, he received a commission in the USAF through the ROTC program, and completed pilot training in May 1973. During the period May 1973 through May 1981, he served as an F-4 aircraft commander and OV-10A aircraft commander and Forward Air Controller. In June 1981, he entered the Graduate Aeronautical Engineering program at the Air Force Institute of Technology.

Permanent address: 1435 Bills Dr.

Xenia, OH 45385

REPORT DOCUMENTATION PAGE	READ INSTRUCTIONS BEFORE COMPLETING FORM

1. REPORT NUMBER	2. GOVT ACCESSION NO.	3. RECIPIENT'S CATALOG NUMBER
AFIT/GAE/AA/82D-22	AD A124473	

4. TITLE (and Subtitle)	5. TYPE OF REPORT & PERIOD COVERED
COMPUTER PREDICTION OF STORE AERODYNAMIC LOADING DURING SEPARATION	MS Thesis
	6. PERFORMING ORG. REPORT NUMBER

7. AUTHOR(s)	8. CONTRACT OR GRANT NUMBER(s)
Arthur C. Powell Capt USAF	

9. PERFORMING ORGANIZATION NAME AND ADDRESS	10. PROGRAM ELEMENT PROJECT, TASK AREA & WORK UNIT NUMBERS
Air Force Institute of Technology (AFIT-EN) Wright-Patterson AFB, Ohio 45433	

11. CONTROLLING OFFICE NAME AND ADDRESS	12. REPORT DATE
Air Force Institute of Technology (AFIT-EN) Wright-Patterson AFB, Ohio 45433	December 1982
	13. NUMBER OF PAGES
	178

14. MONITORING AGENCY NAME & ADDRESS(if different from Controlling Office)	15. SECURITY CLASS. (of this report)
	Unclassified
	15a. DECLASSIFICATION DOWNGRADING SCHEDULE

16. DISTRIBUTION STATEMENT (of this Report)

Approved for public release; distribution unlimited

17. DISTRIBUTION STATEMENT (of the abstract entered in Block 20, if different from Report)

18. SUPPLEMENTARY NOTES

Approved for public release: IAW AFR 190-17.

LYNN E. WOLAVER
Dean for Research and Professional Development
Air Force Institute of Technology (ATC)
Wright Patterson AFB OH 45433

19 JAN 1983

19. KEY WORDS (Continue on reverse side if necessary and identify by block number)

Potential Flow
Store Trajectory Simulation
Subcritical Flow
Store Separation
Computer Prediction

Off-Body Loading
Nielsen Program

20. ABSTRACT (Continue on reverse side if necessary and identify by block number)

An advanced fighter design is modeled using the Nielsen store separation and trajectory program with the nonlinear nonplanar cross section option. The data required to run the computer model is consolidated for better understanding, with the major points referenced to the appropriate report. The theory and programming behind the computer model are described. The methods by which the aerodynamics given store is used to predict store forces and moments are compared with experimental results on the same configuration at a fixed Mach number of 0.9, at a store position

20. Abstract (continued)

of three store diameters away from the aircraft, is within ten percent of experiment in the region of interest, which is the area under that portion of the fuselage occupied by the wing.

END

FILMED

3-83

DTIC